The Institute of Paper Science and Technology

Atlanta, Georgia

Doctoral Dissertation Reprint

AN EXPERIMENTAL INVESTIGATION OF THE IN-PLANE ELASTIC MODULI OF PAPER

A thesis submitted by

Alan R. Jones
B.S. (Ch.E.) 1962, The University of Colorado
M.S. 1964, Lawrence College

in partial fulfillment of the requirements
of The Institute of Paper Chemistry
for the degree of Doctor of Philosophy
from Lawrence University,
Appleton, Wisconsin

June, 1967

TABLE OF CONTENTS

SUMMARY

A knowledge of the elastic properties of paper and the relationships between these moduli should benefit two areas of research. With such information, a strength of materials approach to the design of paper containers and the associated converting equipment can be made, and the elastic moduli of the sheet can be compared with the several theories available which relate the mechanical properties of paper to the mechanical properties of the component fibers.

Workers in the field of paper mechanics have felt that paper behaves mechanically as an orthotropic material. Recently, Campbell (10) proposed a different set of equations to describe the elastic response of paper.

It was the hypothesis of this thesis that paper may be described by the orthotropic model when force is applied parallel to the plane of the sheet. Measurements of Young's modulus, the shear modulus, and Poisson's ratio were made at several directions on six different paper samples. These results were compared to the behavior predicted by the orthotropic model and by Campbell's proposal.

Young's modulus was calculated from the initial slope of the load-elongation curve obtained with a Table Model Instron.

Poisson's ratio was measured by taking photographs at three different stress levels of a tensile specimen on which an array of small glass beads were glued. The strains required to calculate Poisson's ratio were obtained from measurements of the bead spacings on the three photographs.

To determine the shear modulus, paper cylinders were formed from sheets of the material to be tested. The cylinder was used as the elastic element in a torsion pendulum, and the resonance frequency of the pendulum was determined

by varying the sinusoidal driving frequency of the system. Corrections were made for the cylinder seam width and for nonideal end effects before the shear modulus of the material was calculated from the resonance frequency.

The paper samples tested included a kraft sheet formed on a laboratory fourdrinier, two regular kraft sack papers, an extensible kraft sack paper, and a kraft linerboard.

It was found that the measured value of Poisson's ratio increased with tensile strain. This was attributed to a stress-induced wrinkling observed on the paper surface. The magnitude of the increase was found to be related to the sheet formation of the tensile specimen. The effect of the stress-induced wrinkling was removed by extrapolating measured values of Poisson's ratio to zero stress.

It was found that the orthotropic model describes the mechanical behavior of paper for stresses parallel to the plane of the sheet. The equations proposed by Campbell (10) were found to describe approximately the variations of Young's modulus and the shear modulus with direction in the sheet, but the Poisson's ratios predicted by the Campbell equations were much too low.

The fact that paper behaves as an orthotropic material for stresses parallel to the plane of the sheet is a necessary condition for paper to be an orthotropic material. However, measurements of elastic moduli must be made in other planes to confirm this model for paper.

INTRODUCTION AND OBJECTIVE

The mechanical behavior of paper and paperboard has been of interest to both the manufacturer and the consumer for many years. More recently, the elastic response of paper to load has been an active topic for investigation. Two questions arise: what are the magnitudes of shear moduli and Poisson's ratios, as well as Young's moduli, and what relationships exist between these quantities?

The elastic behavior of paper is of importance for several reasons. In many cases paperboard is used as the structural material in a container which must hold and protect its contents. If the elastic nature of this structural material is known, it will be possible to use the theories of strength of materials when designing containers. This will abet the more empirical approach used at the present time.

In paper converting operations the entering material is subjected to a variety of loading conditions. Again, if the mechanical constants of the sheet are known, it should be possible to understand anomalous behavior.

Yet another related area of interest is the relationship between wood pulp fiber mechanical properties and the mechanical constants of a sheet of paper. Van den Akker (1) among others (2, 3) has published a theory to relate fiber and sheet elastic moduli. The successful establishment of a theory of this type should lead to a much better understanding of the response of paper to load. However, to establish such a theory, experimental data as to the magnitude of and the relations between the elastic moduli of paper must be available.

The objective of this thesis was, therefore, twofold. First, techniques for the measurement of shear moduli and Poisson's ratios were developed. Then,

with these techniques and an existing method for the measurement of Young's moduli, the relationships between the elastic moduli for stress in the plane of the sheet were determined.

HISTORICAL REVIEW

Until recently, research investigations of the mechanical behavior of paper have been primarily concerned with the response of a specimen to tensile loads. It has been recognized for a number of years that paper, in certain instances, may be considered to be a viscoelastic material. When a load is placed on a paper sample, the specimen undergoes an immediate elastic deformation which is then followed by a time-dependent deformation. As long as the specimen remains loaded, the deformation increases and eventually failure will occur.

In early attempts to describe this behavior, mathematical models consisting of spring and dashpot elements were devised which produced an approximately similar form of time-dependent-deformation with load. Ivarsson and Steenberg (4) published an investigation of this type. Although a spring and dashpot model exhibits a similar time-dependent behavior to that noted for paper, it is difficult to visualize the physical significance of spring and dashpot elements in relation to the structure of paper.

Brezinski (5) studied the viscoelastic properties of paper by means of tensile creep tests. Three types of deformations were observed. These were the immediate elastic deformation, the delayed elastic deformation, and non-recoverable deformation. With application of the load an immediate deformation occurred. This deformation was almost entirely recovered upon removal of the load. If the load was not removed shortly after it was applied, additional deformation was observed. When the load was removed, some of the elongation was recovered immediately, and an additional amount was recovered with time. The rate of elongation was found to depend upon the initial stress and upon the time elapsed following application of the load.

Hill (6) has shown that individual pulp fibers exhibit tensile creep behavior similar to that noted by Brezinski (5) for paper.

The viscoelastic nature of paper may also be demonstrated by the technique of stress relaxation. Johanson and Kubat (7), for example, have reported a study in which paper specimens were given an initial tensile strain and held at that point. It was found that the stress in the sample decayed with time. The magnitude of relaxation was found to depend upon the magnitude of the initial stress.

ANISOTROPIC BEHAVIOR

It is a well-established fact that the mechanical behavior of paper is dependent upon the direction in which load is applied. Horio and Onogi (8) used a vibrating reed technique to measure Young's modulus in the plane of the sheet. They found for the several machine-made papers they examined that the variation of Young's modulus with angle fit the following relationship:

$$1/E_\theta = (\cos^2\theta)/E_x + (\sin^2\theta)/E_y, \qquad (1)$$

where E_θ is Young's modulus at direction θ, E_x and E_y are Young's moduli in the machine and cross-machine directions, respectively, and θ is the angle measured from the machine direction.

Riemen and Kurath (9) made a more detailed study of the vibrating reed method. Their findings indicate that the measurements made by Horio and Onogi (8) are inaccurate. However, Campbell (10) reported that Donaldson also obtained Young's modulus data which fit the above equation.

Craver and Taylor (11, 12) describe apparatus for measuring the velocity of propagation of a mechanical pulse in a paper sample. The apparatus is designed

so that the initial stress may be either a longitudinal stress or a shear stress. The time required for the initial stress to travel a known distance in the material is measured.

Craver and Taylor assume that paper meets the requirements of an orthotropic material. Based on this assumption, they discuss relationships between the elastic moduli in the plane of the sheet and the sonic velocities of propagation in the sheet.

Experimentally, the sonic velocity of a longitudinal pulse was found to vary as a function of direction in the plane of the sheet. In their first publication (11) they report the velocity of propagation of a shear wave as a function of direction for one grade of paper. The velocity measurements, taken at 0°, 30°, 60°, and 90° to the machine direction, show no variation with direction. In the second publication (12), the shear wave velocity for four grades of paper is shown to be constant as a function of direction in the sheet. No data points are given. This information indicates that the shear modulus in the plane of the sheet does not vary with direction.

Kubat and Lindbergson (13) have published an article describing a dynamic method for determining the shear modulus in the plane of the sheet. The technique involves determination of the resonance frequency of a torsion pendulum in which a strip of paper is the elastic element.

They point out that shear stresses will not be confined to the plane of the sheet in this method, but that there will be shear stresses in both the plane of sheet and in a plane at right angles to the plane of the sheet. A stress analysis is presented to estimate the order of magnitude of errors caused by this. Assuming that the ratio of the shear moduli for the two planes is $G_{xy}/G_{xz} = 2$, they estimate that the true in-plane shear modulus will be overstated by 2%.

Experimental data reported by Kubat and Lindbergson for a spinning paper show a variation of shear modulus with a direction in the sheet. A maximum value is reported for shear stresses parallel to the machine and cross-machine directions, and the shear modulus is a minimum at 45° to the machine direction.

FACTORS CONTRIBUTING TO THE MECHANICAL BEHAVIOR OF PAPER

The elastic behavior of paper is felt to depend upon the sheet structure and its strain history as well as the nature of the fibers.

PAPER STRUCTURE

For further discussion a rectangular coordinate system will be defined in which the x-axis corresponds to the machine direction, the y-axis denotes the cross-machine direction, and the z-axis is the direction perpendicular to the plane of the sheet.

The angular orientation of the fibers in the sheet is the most conspicuous cause contributing to anisotropy in the mechanical behavior of the sheet. In the forming process, fibers are deposited with their axes roughly parallel to the xy-plane of the sheet. Aaltio (14) has used x-ray diffraction to estimate the z-direction orientation of fibers in the sheet. He found deviations of the fiber axes from orientation parallel to the xy-plane to be small, and to decrease as the pulp was refined.

In the xy-plane of the sheet there is an angular distribution of fiber orientation. Danielsen and Steenberg (15) have developed a technique for measuring this distribution. For machine-made paper they find that the fiber axes are preferentially aligned in the machine direction of the sheet. Van den Akker (1) has presented a theory for the quantitative estimation of the elastic anisotropy of paper produced by the angular distribution of fiber orientation.

During the initial formation of the sheet, it is probable that short fibers and fiber fragments will pass through the forming septum. After deposition of some fiber, however, fragments of the same size are more likely to be retained. This process will produce a variation in structure from the wire-side to the top-side of the sheet. Van den Akker (16) has suggested that a theoretical description of two-sided paper could be accomplished by considering a sheet composed of many layers, each of which is an orthotropic material.

WET-STRAINING

A second mechanism attributed to sheet directionality is the amount of wet-straining the sheet receives during drying. Edge (17, 18) found that, if a laboratory handsheet is stretched during drying, the tensile strength in the direction of the drying stress is much greater than the strength in the direction perpendicular to the drying stress.

Schulz (19) studied the effect of wet-straining on handsheets. He found Young's modulus, in the direction of the wet-strain, to reach maximum values at an optimum degree of wet-straining. At least a portion of this effect is due to increases in the modulus of elasticity of fibers during drying under load. This was established by Jentzen (20).

Van den Akker (21) gives an excellent review of the subject of mechanisms of anisotropy of paper. He points out that during wet-straining a redistribution of stress among the fibers will contribute to mechanical directionality in the sheet. Steenberg (22) has proposed that directionality in strength is introduced during wet-straining at the fiber-to-fiber bonds due to a preferential alignment of bonded fibrils.

STRESS HISTORY

A third factor which can influence the mechanical properties of paper is the stress history of the sample. Paper which has been subjected to strains greater than about 0.5% undergoes a phenomenon known as strain-hardening. The result of this change is observed by an increase in the Young's modulus of the material. Kubat, et al. (23) applied low-frequency sinusoidal tensile stresses to paper specimens. They first strained the sample to a given level, and then varied the strain about this value.

With each of the initial strain cycles, the slope of the stress-strain curve increased. After a number of cycles, the response of the sample became essentially constant. The amount of increase in the Young's modulus of the sample was found to depend upon the magnitude of the prestrain and upon the amplitude of the sinusoidal strain. At higher values of prestrain greater increases in Young's modulus were noted.

ORTHOTROPIC BEHAVIOR

The contention of most investigators (11, 12, 13, 24) of the mechanical behavior of paper has been that the orthotropic model should describe the elastic behavior of paper. Love (25) and March (26) discuss the physical requirements of an orthotropic material. There are two basic criteria.

First, the material must obey the generalized Hooke's Law. That is, each of the six components of stress at a given point is a linear function of each of the six components of strain at the point. Secondly, the material must have three mutually perpendicular planes of mechanical symmetry at all points.

A material which satisfies the above conditions can be described by nine independent elastic moduli. These are the three Young's moduli for the three principal directions, the three shear moduli for each of the three principal planes, and three of the six Poisson's ratios associated with stress in a principal direction. Knowledge of these nine elastic constants then allows the prediction of Young's modulus, shear modulus, and Poisson's ratio in an arbitrary direction having cosines ($\underline{\ell}$, $\underline{m}$, $\underline{n}$),*

$$1/E = \ell^4/E_x + m^4/E_y + n^4/E_z + \ell^2m^2\left[(1/G_{xy}) - (2\,\nu_{xy}/E_x)\right] + m^2n^2\left[(1/G_{yz}) - (2\,\nu_{yz}/E_y)\right] + n^2\ell^2\left[(1/G_{xz}) - (2\,\nu_{xz}/E_x)\right] , \tag{2}$$

$$1/G = 4\left[(\ell^2\ell_1^2/E_x) + (m^2_1/E_y) + (n^2n^2_1/E_z) + 2(mm_1nn_1)(\nu_{yz}/E_y) + 2\,(nn_1\ell\ell_1)\,(\nu_{xz}/E_x) + 2(\ell\ell_1mm_1)\,(\nu_{xy}/E_x)\right] + (mn_1 + m_1n)^2/G_{yz} + (n\ell_1 + n_1\ell)^2/G_{xz} + (\ell m_1 + \ell_1 m)^2/G_{xy} , \tag{3}$$

$$\nu_{xy}/E_x = \nu_{yx}/E_y \quad , \tag{4}$$

$$\nu_{xz}/E_x = \nu_{zx}/E_z \quad , \tag{5}$$

$$\nu_{yz}/E_y = \nu_{zy}/E_z \quad , \tag{6}$$

The quantities $\underline{E}$ and $\underline{G}$ are Young's modulus and shear modulus in the direction $\underline{\ell}$, $\underline{m}$, $\underline{n}$. The terms $\underline{\ell}$, $\underline{m}$, $\underline{n}$, are direction cosines for the direction of the tensile stress, and $\underline{\ell}_1$, $\underline{m}_1$, $\underline{n}_1$ are direction cosines perpendicular to $\underline{\ell}$, $\underline{m}$, $\underline{n}$ in the plane of the shear stress. Young's moduli in the $\underline{x}$-, $\underline{y}$-, and $\underline{z}$-directions are $\underline{E}_x$, $\underline{E}_y$, and $\underline{E}_z$, respectively. Principal shear moduli for the

---

*$\underline{\ell} = \cos\alpha$, $\underline{m} = \cos\beta$, $\underline{n} = \cos\gamma$.

xy, xz, and yz planes are G_{xy}, G_{xz}, and G_{yz}, respectively. Poisson's ratio for tensile strain in the x-direction and contraction in the y-direction is denoted by ν_{xy}. The remaining Poisson's symbols, ν_{ij}, are subscripted similarly.

March (26) discusses the case of stress confined to one plane of an orthotropic material. If stress acts only in the xy-plane of the material, the direction cosine n becomes zero, and the terms ℓ and m may be expressed in terms of θ, the angle measured from x-axis: $\ell = \cos\theta$ and $m = \sin\theta$. Then

$$1/E_\theta = (\cos\theta)^4/E_x + (\sin\theta)^4/E_y + \sin^2\theta\cos^2\theta\ [(1/G_{xy}) - 2(\nu_{xy}/E_x)] \qquad (7)$$

$$1/G_\theta = 4\sin^2\theta\cos^2\theta\ [(1 + 2\nu_{xy})/E_x + (1/E_y)] + (\cos^2\theta - \sin^2\theta)^2/G_{xy} \qquad (8)$$

$$\nu_{xy}/E_x = \nu_{yx}/E_y \quad . \qquad (9)$$

For this case there are four independent elastic moduli required to describe the elastic behavior of the material for stress in one plane.

Campbell (10) has proposed different relationships to express the variation of the elastic moduli in the plane of the sheet. Using the expression which Horio and Onogi (8) found to fit their data, Equation (1), he combined this expression and Equation (7) to arrive at the following relationship

$$1/G_{xy} = (1 + 2\nu_{xy})/E_x + (1/E_y) \quad . \qquad (10)$$

If this relation holds for paper, only three independent elastic moduli exist when describing the elastic behavior for stress in the plane of the sheet.

If the right-hand side of Equation (10) is substituted for $1/G_{xy}$ in Equation (8), it is found that $1/G_\theta = 1/G_{xy}$. Therefore, Campbell's proposal predicts that the shear modulus will not vary with direction in the plane of the sheet.

The above relationships, Equations (2), (3), (7), (8), and (10), all reduce to the well-known expression relating the elastic constants of an isotropic material.

APPROACH TO THE PROBLEM

The hypothesis of this thesis was that paper behaves as an orthotropic material. Because of the experimental difficulty in the measurement of strains in the z-direction due to the short gage length available, it was decided to limit the investigation to the case of stress in the xy-plane of the sheet.

In order to study the elastic behavior of paper it was necessary to develop techniques for the measurement of in-plane shear moduli and Poisson's ratios. The load-elongation recordings from a Table Model Instron were used to evaluate Young's moduli.

The in-plane moduli, E_θ and G_θ, were measured at 15° intervals on five machine-made paper samples. The Poisson's ratios, ν_{xy} and ν_{yx}, were measured for these samples. These data were examined as to their agreement with the behavior expected of an orthotropic material.

The five paper samples tested were of different density and mechanical directionality. With respect to the fiber mechanical properties and fiber structure of the sheet, these two variables were expected to be important in the elastic behavior of paper.

Four of these samples were commercially produced sack paper and linerboard. The commercial papers were selected because the in-use requirements of such grades are of a mechanical nature and because tests on such materials will be of immediate value. The fifth sample was formed on a laboratory fourdrinier. This sample was expected to offer a more nearly ideal sheet structure.

EXPERIMENTAL APPARATUS AND PROCEDURES

All paper samples were tested at 73 ± 2°F. and 50 ± 2% relative humidity. Wink (27) and Crook and Bennett (28) have investigated the effects of temperature and humidity on the physical properties of paper. To reduce the effect of moisture sorption hysteresis, all samples were preconditioned at roughly 20% relative humidity for 24 hours before final conditioning at test conditions.

YOUNG'S MODULUS

Young's modulus measurements were made using load-elongation curves obtained with a Table Model Instron. Line-type specimen clamps described by Wink, et al. (29) were used to grip the test sample.

For all determinations the recording chart speed was 50.80 cm./minute, and the crosshead speed was 1.270 cm./minute. The test sample width was 2.54 cm., and the initial span was between 15.24 cm. and 25.4 cm.

The full-scale load on the recorder was adjusted for the particular sample tested so that full-scale pen deflection occurred in from 7 to 18 seconds. This rate of loading allowed precise estimation of specimen elongation, and was much lower than the maximum response rate of the instrument chart recorder.

The following procedure was used to calculate Young's modulus:

A line was drawn tangent to the initial slope of the load-elongation curve using a steel straight-edge. The elongation axis dimension, e, of this line was measured at the full-scale load with an engineering scale graduated in 1/40's of an inch.

The elongation recorded by the Instron includes instrumental strain as well as the strain of the test specimen (30, 31). A linear correction factor equal to 0.006 inch at 100 pounds load was applied to this elongation measurement when computing the sample strain:

$$\epsilon = [(e/40)(0.5/20) - (P/100)(0.006)]/S \qquad (11)$$

where ϵ is the sample strain at full-scale load, P pounds, S is the initial span length in inches, and (0.5/20) is a factor to convert e to actual elongation.

Young's modulus, E, in dynes/cm.^{2} was then computed from the following relation:

$$E = P(6.894 \times 10^4)/(\epsilon t) \quad , \qquad (12)$$

where t is the specimen thickness in inches.

SHEAR MODULUS

There are several ways to induce shear stress in a material and relate the response to the shear modulus. Paper presents a problem with respect to some of these techniques because of its small dimension in the z-direction. For example, the shear modulus in the xy-plane of the sheet could be measured by applying shear stresses to the edge of a flat sample. However, it was felt that the lack of stability to buckling of such a sample would make precise measurement of the shear strain difficult.

TORSION PENDULUM

The most commonly used technique for determining shear modulus involves the application of torque to one end of a cylinder while holding the opposing end fixed. The angular deflection of the cylinder is measured.

With the same cylindrical geometry, the material can also serve as the elastic element of a torsion pendulum. In this case, the resonance frequency of the pendulum is related to the shear modulus of the cylinder material. This technique was applied to paper by forming a cylinder from a sheet of the paper to be tested.

If an elastic cylinder is rigidly clamped at one end, and an initial shear strain applied at the free end, the cylinder will undergo torsional oscillation when the free end is released. If frictional and inertial damping can be neglected, the equation which describes this motion is given, for example, by Constant (32):

$$I(d^2\phi/dt^2) = - k\phi \quad , \tag{13}$$

where I is the moment of inertia of the system, ϕ is the angle of twist at the free end, t is the time, and k is the torsional stiffness of the cylinder. The constant k is related to the properties and dimensions of the cylinder in the following manner:

$$k = G(\pi/32L)(d_o^4 - d_i^4) \quad , \tag{14}$$

where G is the shear modulus of the material, L is the cylinder length, and d_o and d_i are the outer and inner diameters of the cylinder, respectively.

Equation (13) represents simple harmonic motion. The solution of this equation relates the resonance frequency, ω_o to the torsional stiffness and moment of inertia:

$$\omega_o = 2\pi f_o = \sqrt{k/I} \quad . \tag{15}$$

Therefore, by measuring the resonance frequency of a cylinder, the shear modulus of the cylinder material may be calculated.

CYLINDER FORMATION TECHNIQUES

Paper cylinders were formed by rolling a sheet of paper back upon itself and gluing the overlapped edges of the sheet to make a seam which ran parallel to the axis of the cylinder.

Paper blanks for cylinders were cut with a razor blade and steel straight-edge. The width of each blank was measured with an engineering scale graduated in 1/50's inch. The width was equal to the desired cylinder circumference plus the desired seam width of the cylinder. The length of each blank was equal to the desired cylinder length.

Cylinder Gluing Jig

A jig was built to hold the paper blank in proper alignment during the gluing operation. This jig is pictured in Fig. 1.

The jig was constructed from four pieces of flat ground steel. Each of the pieces is eighteen inches in length. The pieces (A) and (A') are 3/4 by 3/8 inch and 3/16 by 3/16 inch in cross section, respectively. The pieces labeled (B) and (B') measure 3/4 by 1/4 inch and 5/32 by 5/32 inch, respectively.

The two large pieces, (A) and (B), were drilled and tapped at one and one-half inch intervals along one side of the largest surface. Mating clearance holes were drilled in pieces (A') and (B') so that (A) and (A') as well as (B) and (B') could be screwed together. One end of the blank was clamped between (A) and (A') and the other end between (B) and (B'). These parts were then placed together as shown in Fig. 1 to hold the sheet in cylindrical form while gluing.

Reference marks were scribed on pieces (A) and (B) so that the blank could be aligned to give a cylinder of the desired diameter and seam width. The

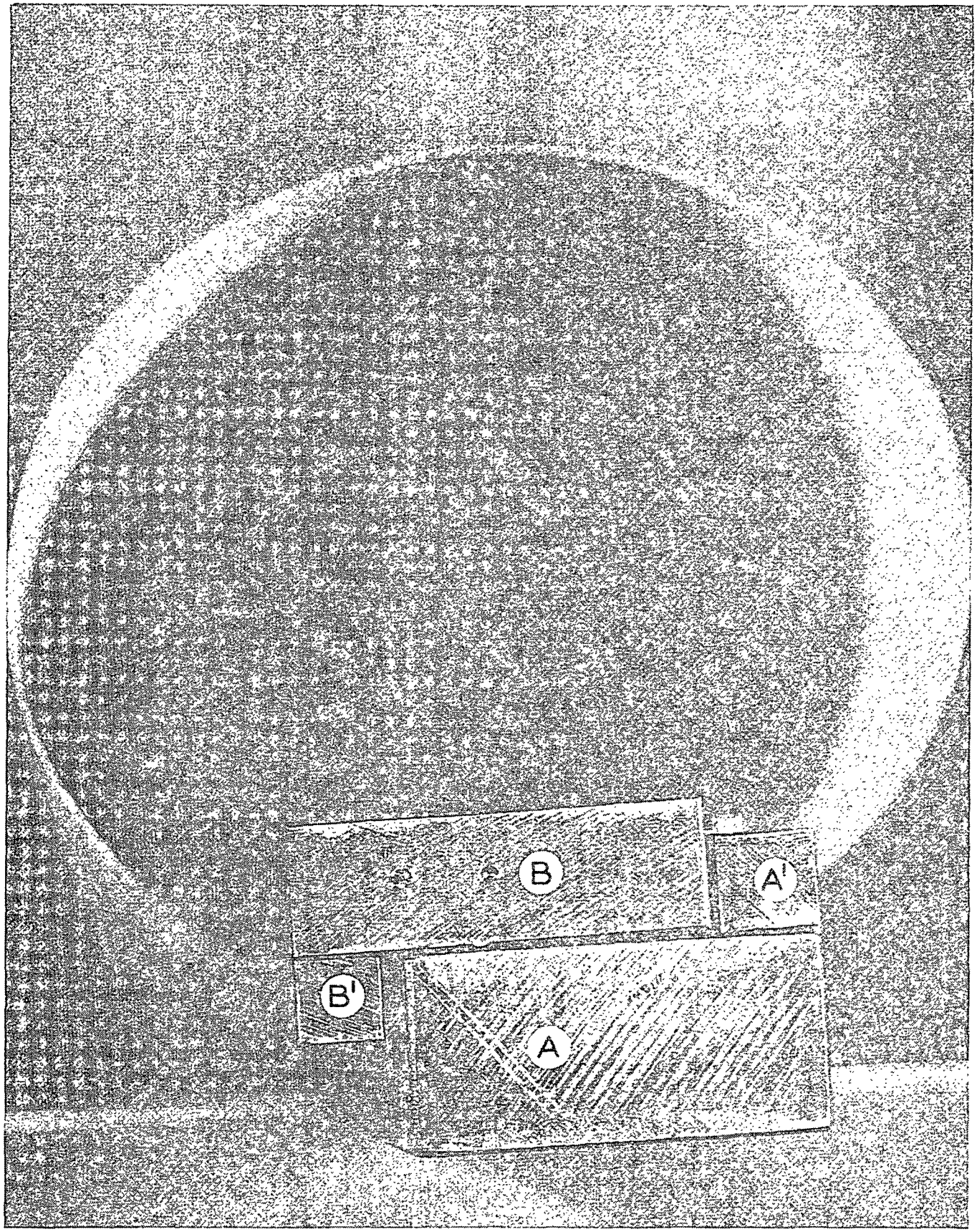

Figure 1. Cylinder Gluing Jig

pieces (A) and (B) had been sprayed with a fluorohydrocarbon to prevent adhesion of the paper to the jig.

Cylinder Gluing

The adhesive used on the seam was Duco cement, a cellulose derivative in a solvent of ethyl acetate or methyl ethyl ketone.

A spreading bar was made to apply an even film of adhesive along the seam area. The bar consisted of a one-eighth inch diameter glass rod which was elevated above the paper by wrapping No. 28 A.W.G. wire around the bar circumference.

After each end of the paper blank was clamped in the gluing jig, an excess of adhesive was applied to one end of the sheet and spread along the seam length with the spreading bar. The parts of the jig were then mated to form the cylinder. The glue was allowed to set for about fifteen minutes before disassembling the jig and removing the cylinder.

BENDING STRESSES

A stress analysis of a cylinder formed by the above procedure was made to determine whether the bending stresses resulting from formation of the cylinder are likely to have an effect on the torsional stiffness of the structure. This derivation is presented in Appendix I.

The analysis indicates that the bending stresses in the wall of the tube have negligible effect on the torsional behavior of the cylinder.

A second consideration is the magnitude of the bending strain in the cylinder wall. The concern with bending strain is that large initial strain will introduce a high stress which would cause internal structural changes in the test.

material. The maximum bending strain, ϵ, is given by the following relationship (33): $\epsilon = t/2r$, where t is the paper thickness and r_m is the mean cylinder radius. If t = 0.01 inch and r = 1.0 inch, the bending strain is 0.5%. Experiments, discussed below, were performed to estimate the effect of bending stress relaxation.

TORSION APPARATUS

The purpose of the torsion apparatus was to apply a sinusoidal torque to one end of a paper cylinder while holding the opposite end fixed. The frequency of this torque could be varied, as will be described, and by doing so the resonance frequency of the cylinder determined.

The torsion apparatus consisted of four major parts: the apparatus frame, the coils, the oscillator, and the cylinder mounts.

Frame

The frame supported the paper cylinder and its mounts in vertical alignment as well as providing mountings for the driving coils. The frame, as pictured in Fig. 2, was composed of the base plate, (A); the right- and left-hand vertical members, (B) and (C); the movable cross plate, (D); the stationary moment arm, (F); and the upper plate, (H).

The base plate, (A), was one-inch brass plate cut to ten by twelve inches. The plate was drilled with clearance holes at either side to accommodate the studs extending from the uprights.

The uprights, (B) and (C), were cut out from one-half inch brass plate, and were nineteen inches in length. Upright (B) was four inches in width, and uprights (C) were one and three-fourths inch in width. Each upright had a series of

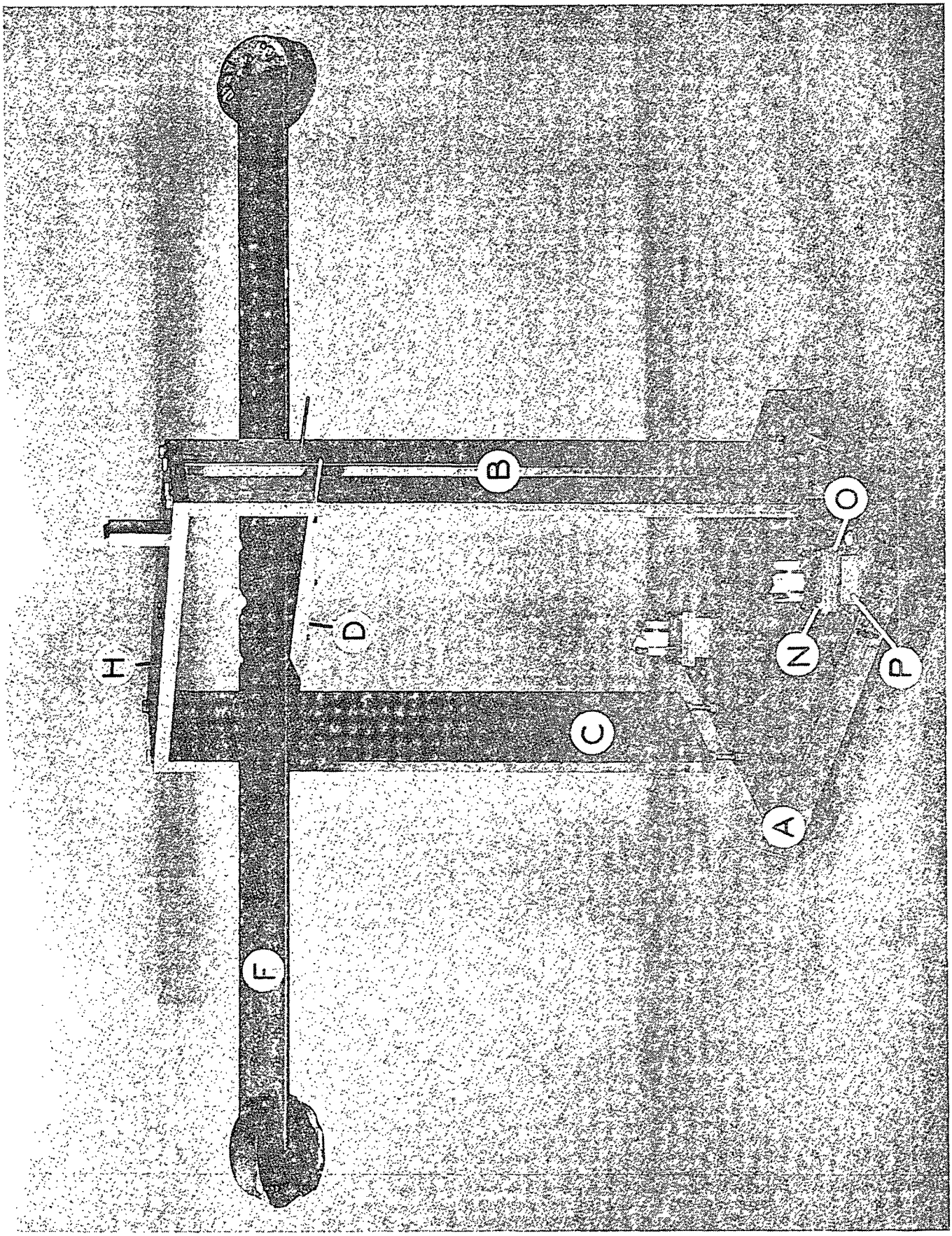

Figure 2. Frame and Coils for Torsion Apparatus

one-eighth inch diameter holes spaced at one-half inch intervals vertically along the upright. These holes served to position the movable cross member, (D), which was held in position by steel pins passing through each upright.

Threaded studs were screwed into the lower end of each upright. These were locked in place with nuts tightened flush with the upright. A second nut screwed onto each stud served as the resting surface on the base plate for the upper portion of the frame.

The upper plate, (H), and the movable cross member, (D), were also cut from one-half inch brass plate. The upper plate measured four by eleven inches, and was bolted to the top of each upright. The movable plate was four by ten inches and contained holes at either end to accommodate the steel pins which provide its support.

The stationary moment arm, (F), was constructed from a 40-inch length of 2-inch steel angle. Five-pound lead blocks were clamped onto either end of this angle. The bar was centered on the movable plate, and rigidly attached to the movable plate with bolts.

Driving Coils

The driving coils provided the magnetic field which produced the sinusoidal torque applied to the cylinder. Each coil consisted of the spool and its winding, and a three-part mounting. The coils are shown in Fig. 2.

The coils were located eleven inches apart on a diagonal joining the corners of the base plate with the coil axis perpendicular to this diagonal. The coils and their mountings were constructed of brass.

Plate (N) was two inches in length by one and three-eighths inches in width. Oversize clearance holes were located at each corner to allow adjustment of the coil position in the horizontal plane.

Part (O), the elevator, consisted of a plate rigidly connected to a one-half inch diameter rod. This rod extended downward into the mounting block, (P), and was held at a given elevation by means of a set screw located in the mounting block.

Coil Winding

The carrying surface of each spool was covered with glass insulating tape. Each spool was wound with 4250 turns of No. 36 A.W.G. copper wire. The direct current resistance of each coil was determined to be 280 ohms, or a circuit resistance of 560 ohms when the coils were wired in series. Including the coil inductance, this impedance allowed maximum power to be drawn from the oscillator used to drive the system.

Oscillator

The oscillator used was model 512F sine wave generator manufactured by Waveforms, Inc. of New York, New York. The frequency range was from one-half cycle/second to 500 kilocycles/second. Output power of the oscillator was two watts into a 600-ohm impedance.

Cylinder Mounts

The cylinder mounts were attached to the paper cylinder by gluing. The upper mount was then bolted to the movable plate in the apparatus frame. The lower mount provided a means for transmitting torsional vibration to the specimen, and it also served as a means for varying the moment of inertia of the vibrating system. The mounts are shown in Fig. 3, and positioned in a cylinder in Fig. 4.

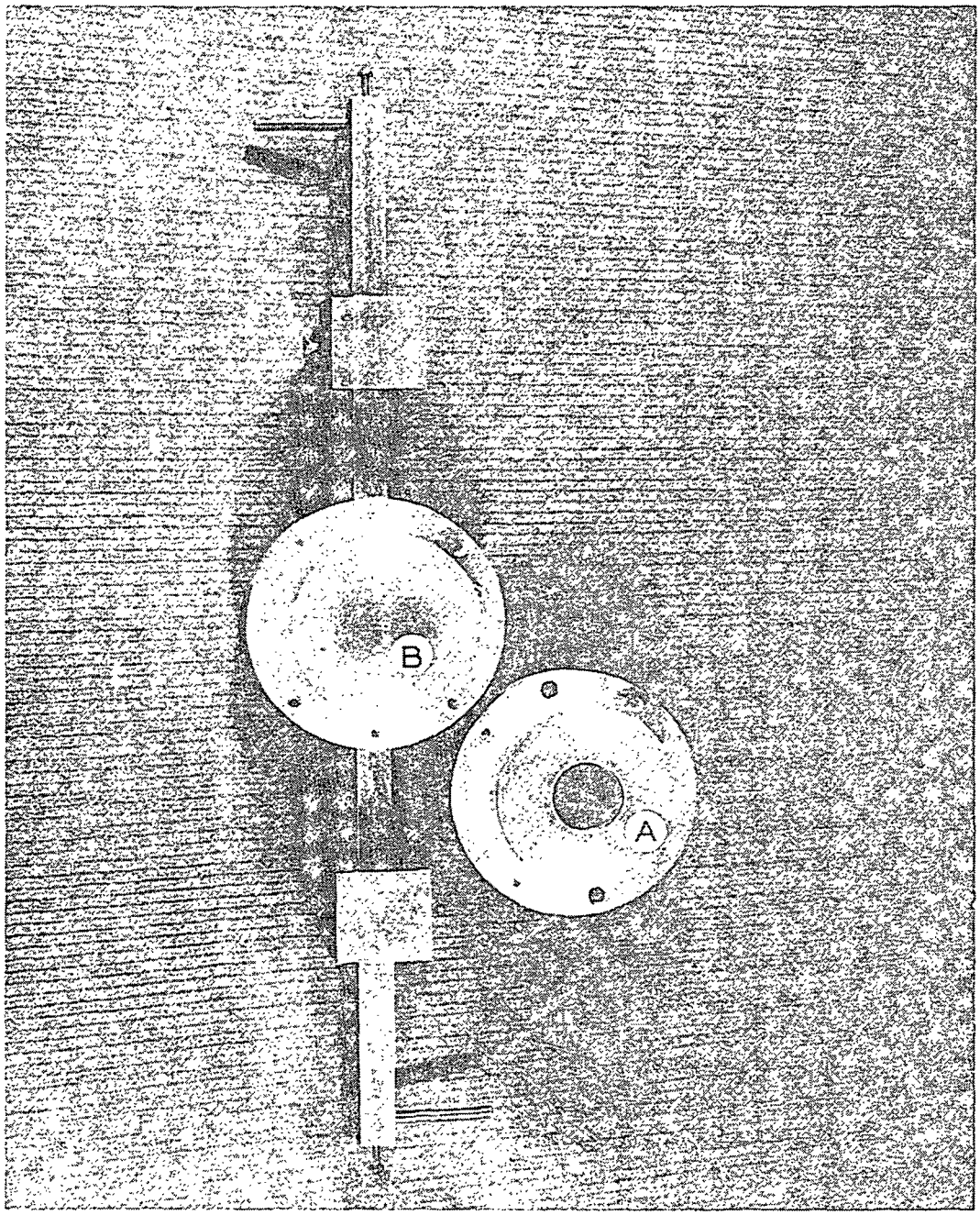

Figure 3. Lower Specimen Mount

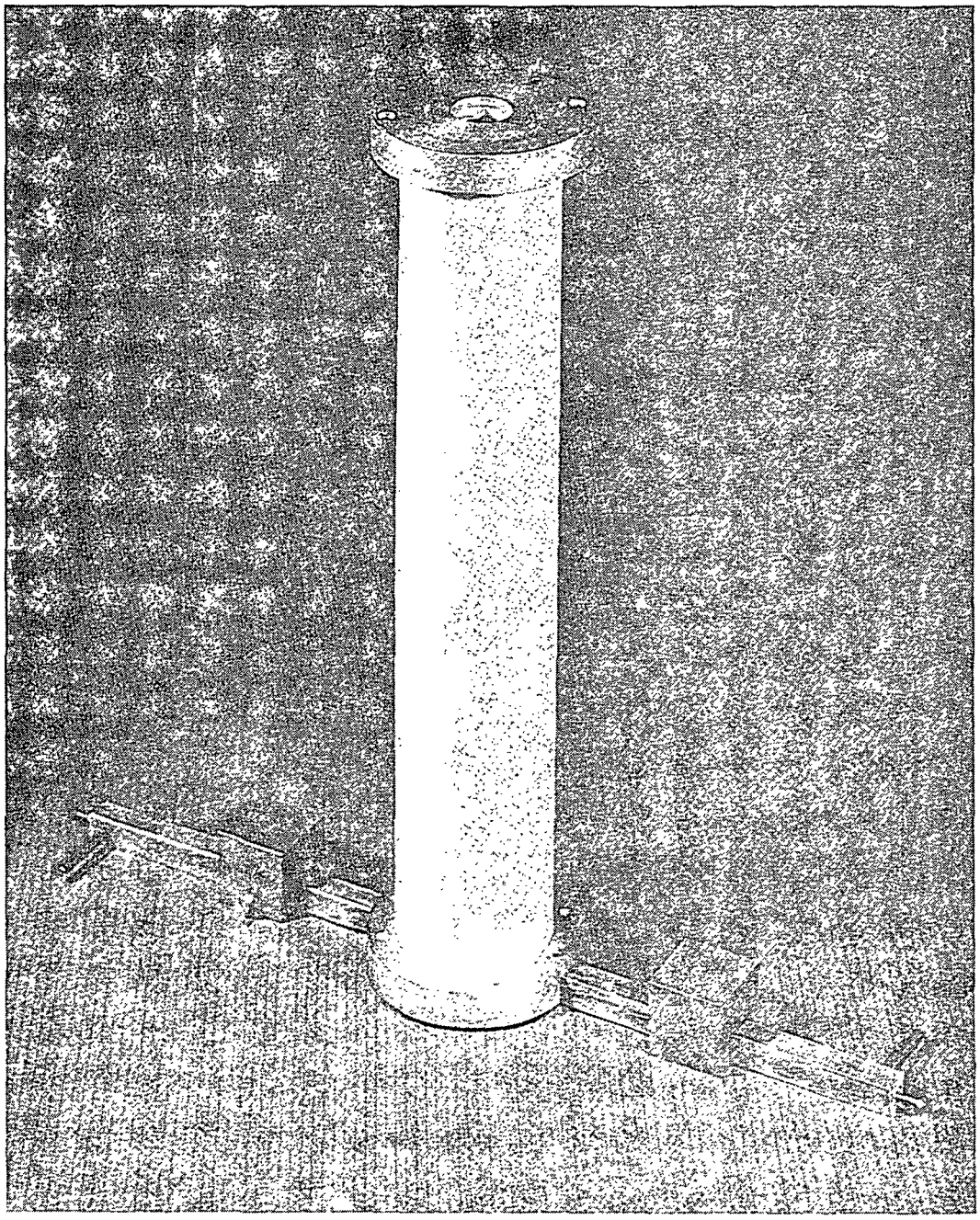

Figure 4. Mounted Specimen, Ready for Installation in Frame (See Fig. 2)

Each mount was machined from aluminum alloy. The base diameter was two and three-fourths inches and gluing area diameter was 1.997 inches. The base height was one-half inch and the length of the gluing area was one-half inch. The total height was one and three-sixteenth inches with the top three-sixteenths inch tapered to allow easy insertion of the mount into the cylinder.

The upper mount (A), contained two 1/4 inch-20 tapped holes located at either side of the base to allow the mount to be bolted to the lower side of the movable frame plate. A three-fourths inch diameter hole was bored through the center of the mount.

Lower Mount

A centered hole was turned out of the lower side of the lower mount to reduce the mass of the mount. The hole dimensions were one and five-eighth inches in diameter by one inch in depth. This left a three-sixteenths inch wall thickness in the gluing area of the mount.

A three-eighth inch channel was cut through the center of the mount base to accommodate a three-eighth inch square duralum bar, the moment arm. The moment arm was eleven and one-half inches in length extending equidistant from either side of the mount.

The moment arm served to carry two brass masses as well as to hold the bar magnets. The magnets were located one-fourth inch from either end of the moment arm and were oriented at 90° to the moment arm. Each magnet was held in place with a set screw.

The magnets were made from one-eighth inch diameter drill rod roughly one and one-half inches in length. The drill rod was hardened and magnetized after cutting.

The inertia masses were one-inch cubes of brass which could be positioned on the moment arm by means of set screws. By moving the masses away from the mount the moment of inertia of the system could be increased.

OSCILLATOR CALIBRATION

The advertised dial accuracy of the oscillator used is ± 1.0%. The dial accuracy of the instrument was checked under conditions of load and no load to determine the actual accuracy.

Frequency calibration was accomplished by feeding line current (60 cycles/second, 120 volts) to one axis of an oscilloscope while the oscillator output was fed to the other axis. Using line frequency as a reference, Lissajous figures were displayed on the oscilloscope screen by varying the oscillator output frequency.

Lissajous figures are the pattern seen when the ratio of line frequency to oscillator frequency is in the ratio of whole numbers, i.e., 5:4, 3:4, etc. (34). These figures are characteristic of the relative values of the two frequencies, and thus may be used to calibrate the oscillator behavior.

It was found that the dial reading of the oscillator was in error by no more than 0.5% in the range of frequency used in this thesis. The dial reading at a given frequency was found to be reproducible to within 0.3%.

Based on this study, the dial reading of the oscillator was taken to be the true frequency in all cylinder testing.

MOMENT OF INERTIA CALIBRATION

A precise estimate of the moment of inertia of the lower cylinder mount was required for an accurate estimate of the torsional stiffness of the paper cylinder. Two methods were used to estimate this value.

In the first method, the lower mount was suspended by a thin wire passed through the center of the mount. The period of torsional oscillation of this system was determined by timing several oscillatory cycles with a stopwatch. A known moment of inertia was then added to the lower mount, and the period of oscillation redetermined. The moment of inertia of the mount, $\underline{I}$, was then calculated from the relationship,

$$I = \Delta I / \left[(T_2/T_1)^2 - 1 \right] \quad , \tag{16}$$

where $\Delta\underline{I}$ is the added moment of inertia and $\underline{T}_1$ and $\underline{T}_2$ are the initial and final periods of oscillation, respectively.

The second method involved careful weighing and measuring of the parts of the lower mount, and then calculating the moment of inertia of the mount based on these measurements.

The inertia of the lower mount without the brass inertia masses or magnets was determined to be 6320 g.-cm.^{2} with a standard error of 45 g.-cm.^{2} using the first method. The inertia as calculated by the second method was 6290 g.-cm.^{2} with a standard error of 17 g.-cm.^{2}. With the magnets in place the moment of inertia was calculated to be 7170 g.-cm.^{2}. This value was used for all future experimental work.

The contribution of the brass inertia masses was calculated from the following equation:

$$I_b = 2I_{ob} + 2m_b r_b^2 = 85 + (225)\, r_b^2 \tag{17}$$

where $\underline{I}_b$ is the contribution of the inertia masses in g.-cm.^{2} and $\underline{r}_b$ is the distance in centimeters from the center of rotation to the center of mass of each brass mass.

TEST PROCEDURE

The movable plate in the apparatus frame was first placed at the elevation corresponding to the length of the cylinder to be tested. The plate surface was

then leveled using a 4-inch spirit level, by adjusting the nuts upon which the upper frame rested. The plate was leveled to within 0.003 inch per foot.

Cylinder Mounting

The cylinder was attached to the cylinder mounts by gluing. The adhesive used was Duco cement thinned with an equal volume of ethyl acetate. The adhesive was thinned to allow sufficient time to insert the mounts into the cylinder.

An excess of adhesive was wiped onto the gluing surface of the upper mount before the mount was bolted to the movable frame plate. The cylinder was slipped onto the mount and the excess glue, which was forced to the base of the mount, was wiped away. The upper mount with attached cylinder was then bolted to the movable plate in the torsion apparatus.

An excess of glue was then applied to the lower mount gluing surface. This mount was inserted into the end of the suspended cylinder being careful to align the moment arm with the driving coils. Again the excess adhesive was wiped from the base of the mount.

The fit between the cylinder and the mounts was such that the cylinder could be allowed to hang undisturbed while the adhesive set without noticeable movement at either mount. The adhesive was allowed to dry for thirty minutes before torque was applied.

Cylinder Length Measurement

The cylinder length was measured by means of a cathetometer which could be read to $\pm$ 0.005 cm. with a vernier scale. The length measured was the vertical distance between the base of each cylinder mount after the cylinder was placed in the torsion apparatus.

Oscillator

The oscillator was allowed at least a 60-minute warmup period before measurements were taken. Between tests the voltage across the oscillator terminals was shut off. During tests the output voltage was set at 15 volts r.m.s.

Microscope

The microscope used to observe the cylinder oscillations was a Bausch and Lomb stereo microscope with 60-power magnification. One eyepiece of the microscope was equipped with a micrometer scale.

A human hair was glued to one end of the lower mount moment arm. The microscope was focused on this hair.

During testing, the oscillator frequency was varied while observing the motion of the hair. When the amplitude of oscillation reached its maximum value, the dial reading of the oscillator was recorded as the cylinder resonance frequency. Two determinations of the resonance frequency were made by approaching the desired value from both lower and higher frequencies.

System Inertia

In actual testing the resonance frequencies of a given cylinder were determined with from four to seven different moments of inertia. One measurement was made without the brass masses on the moment arm, $\underline{I}$ = 7170 g.-cm.^{2}. The brass masses were then placed on the moment arm and the resonance frequency determined by locating the weights at several radial distances from the axis of rotation. The additional contribution to the moment of inertia was calculated using Equation (17).

PRELIMINARY OBSERVATIONS

Mode of Vibration

In all cylinders tested a maximum in the amplitude of oscillation was observed at two oscillator driving frequencies. The lower of the two frequencies was one-half the magnitude of the higher resonance frequency. Also, the amplitude of vibration at the lower frequency was approximately one-half the amplitude observed at the higher frequency.

A microscope with 400-power magnification was mounted so that the cylinder surface could be observed during oscillation. The microscope was translated vertically to observe the cylinder vibration as a function of cylinder length. The angular deformation of the cylinder at the higher resonance frequency was observed to decrease smoothly from the driven end of the cylinder to the fixed end. This indicates that this frequency was the primary mode of vibration of the cylinder (35).

A ceramic phonograph cartridge was rigidly mounted and forced against the lower mount. The output from this cartridge was connected to one axis of an oscilloscope. The oscillator output was wired to the other oscilloscope axis. When the cylinder was driven at the higher resonance frequency, an ellipse was traced on the oscilloscope screen. This is the Lissajous figure which occurs if two signals have the same frequency. When the cylinder was driven at the lower resonance frequency, a figure eight was traced by the oscilloscope. This pattern indicated that the frequency of vibration of the cylinder was twice as large as the oscillator driving frequency.

It was also observed that when the cylinder was driven at one-fourth the largest resonance frequency a Lissajous figure with four lobes was displayed on

the oscilloscope screen. This indicated that the cylinder was vibrating at a frequency four-times larger than the oscillator frequency.

These observations indicate that while the cylinder was being driven at one-half or one-fourth the "major" resonance frequency it was actually vibrating at this "major" frequency.

To confirm this conclusion, the moment arm was illuminated with a Strobotac, a variable frequency light source. While holding the oscillator frequency at either the greatest resonance frequency or one-half that value, the Strobotac frequency was varied. The illuminating frequencies at which an image or images of the arm appeared to stop were recorded as well as the number of images stopped.

Because the frequency of the Strobotac could not be determined precisely, it was not possible to determine the exact illuminating frequency at which the arm vibrated. However, the observations were identical whether the cylinder was driven at the higher or lower frequency.

An explanation for these subharmonic resonance frequencies is the presence of a nonlinear element in the vibrating system. That is, an element in which the response is not proportional to applied stimulus. The presence of such an element can produce frequencies other than the oscillator driving frequency.

The magnet-driving-coil interaction is the most likely point at which this could occur. First, the magnetization hysteresis of ferromagnetic materials is a nonlinear behavior. It is also possible that misalignments in the magnet-coil system could introduce nonlinear behavior.

Cylinder Alignment

Resonance behavior of cylinders with apparently perfect alignment was compared to the response of cylinders in which the lower mount was out of level by 1/16 inch per foot. No significant difference was found in the resonance frequency. Therefore, the cylinder mounting is apparently not a critical factor.

Elastic Stability of Cylinders

Gerard and Becker (36) discuss the torsional stability of tubes. A theoretical relationship has been derived for isotropic materials which relates the critical shear stress, τ_{cr}, at which buckling occurs to the mechanical properties and dimensions of the tube:

$$\tau_{cr} = 0.93(\pi^2/12)(1 - \upsilon^2)^{-(5/8)}E(t/r)^{(5/4)}(r/L)^{(1/2)} \quad , \qquad (18)$$

where υ is Poisson's ratio, E is Young's modulus, t is the wall thickness of the cylinder, r is the cylinder radius, and L is the cylinder length. The critical shear stress is related to the critical shear strain, γ_{cr}, by definition: $\tau_{cr} = G\gamma_{cr}$, where G is the shear modulus. Assuming that the ratio E/G is 2.5, and using a cylinder length of 15 inches, radius of 1.0 inch, and wall thickness of 0.005 inch, the critical shear strain, γ_{cr}, was calculated to be 9×10^{-4}. The maximum shear strain observed in practice was 1×10^{-4}. It was concluded that the cylinder was elastically stable under the test conditions used in this thesis.

Rate of Strain

The rate of strain in the cylinder depends upon the frequency and amplitude of vibration of the system. The highest rate of strain measured was 2.4×10^{-2}/second.

An experiment was performed in which the rate of strain was decreased by a factor of ten by lowering the amplitude of vibration. No difference in the resonance frequency of the cylinder was noted.

The rate of strain for Young's modulus determinations was 1.4×10^{-3}/second. The fact that the shear modulus was found to be insensitive to a one decade change in rate of strain indicates that this variable will not preclude comparisons of the Young's modulus and shear modulus results.

Sokolnikoff (37a) discusses the difference between elastic moduli measured by isothermal and adiabatic processes. These differences are dependent upon the thermal coefficients of expansivity among other things. Because of the relatively high rates of strain it is felt that the moduli measured in this thesis are, to good approximation, adiabatic elastic constants.

THEORETICAL VS. EXPERIMENTAL CONDITIONS

The earlier discussion of the torsion pendulum, Equations (13), (14), (15), is valid only for elastic cylinders of very great length. The paper cylinder presents several physical conditions which were not included in this simple analysis. These conditions include the seam in the cylinder structure, the stress distribution at the cylinder ends, the viscoelastic nature of paper, and the axial load applied to the cylinder by the weight of the lower mount.

Seam Width

The presence of a seam in the cylinder is the most obvious deviation from the theoretical model. The effect of this seam was investigated by measuring the stiffness of cylinders constructed from the same paper sample with different seam widths.

Data for two different paper samples are shown in Fig. 5. The cylinder seam width is plotted on the abscissa, and the stiffness, $\underline{K} = \underline{I}\ \omega_o^2 \underline{L}$, is plotted on the ordinate.

The slopes of the two regression lines were 0.130 and 0.123. The slope of the line indicates an increase in stiffness of 5.29% per centimeter of seam width relative to zero seam width.

For a thin-walled, circular cylinder the stiffness is nearly proportional to the wall thickness. If it is assumed that an increase in thickness of a small segment of the wall will obey this relation, then the expected increase in stiffness should be 6.26% per centimeter of seam width (cylinder diameter equal to 5.08 cm.).

It has been noted (37) that shear stresses are ineffectually transmitted in structures with sharp corners, such as the corners which exist at the seam boundary. It is believed, therefore, that the actual seam width overstates the effective width of the seam.

This fact is felt to explain the difference between the experimentally determined seam width correction (5.29%) and the theoretical value of 6.26% per cm.

In subsequent work all cylinders were constructed with 0.635 cm. seam widths. A correction factor of (0.635)(5.29) = 3.36% was applied to adjust cylinder stiffness for the effect of seam width.

Cylinder End Effect

Equation (13) is derived by presuming the shear stress in the cylinder may be expressed as follows (38):

$$\tau = Gr(\phi/L) \quad , \tag{19}$$

where τ is the shear stress at radius $\underline{r}$, ϕ is the angular deflection of the

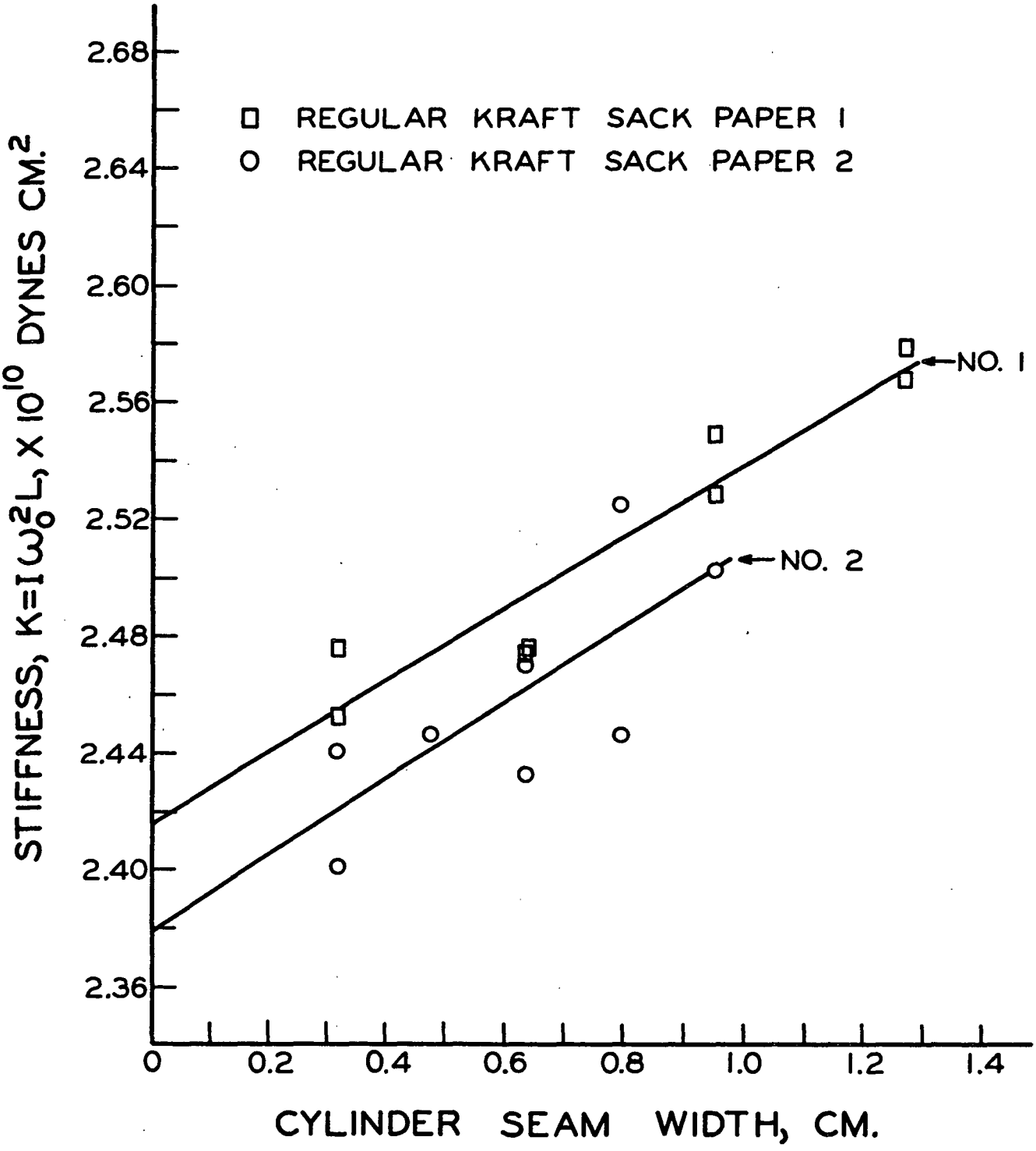

Figure 5. Effect of Seam Width on Cylinder Stiffness

cylinder, and $\underline{L}$ is the cylinder length. If the stress distribution at the cylinder ends does not comply with Equation (19), then the cylinder stiffness, $\underline{K}$,will not be adequately described by the relationship,

$$K = I\omega_o^2 L \quad . \tag{20}$$

In further discussion, the cylinder length, $\underline{L}$, will refer to the free cylinder length, i.e., the total length of the cylinder less the length which is glued to the cylinder mounts. This length is equal to the distance measured with the cathetometer minus 2.54 cm. since the glued length at each cylinder mount is one-half inch.

Van den Akker (39) has suggested a method for eliminating the effect of deviations from the simple theory at the cylinder ends. The compliance of the cylinder, $\underline{C}$, is defined as the reciprocal of the cylinder stiffness: $\underline{C} = 1/\underline{K}$.

An estimate of the actual compliance of the cylinder can be obtained in the following manner:

$$LC = \int_0^L c\,dl = \int_0^{L_e} c\,dl + \int_{L_e}^{L_e + L_o} c\,dl + \int_{L_e + L_o}^{L} c\,dl,$$

$$\text{or } LC = \int_{L_e}^{L_e + L_o} c\,dl + 2\int_0^{L_e} c\,dl,$$

$$LC = c_o L_e + 2 \langle C \rangle_{end} L_e \tag{21}$$

where $\underline{c}_o$ is the compliance of the length $\underline{L}_o$ along which the stress distribution corresponds to Equation (19), and $\langle \underline{C} \rangle_{\underline{end}}$ is the average compliance of the length $\underline{L}_e$ at either end of the cylinder.

The end effect, the term $2\langle C\rangle_{end} L_e$, should be independent of cylinder length if the free cylinder length, L, is greater than $2L_e$. This statement is based on the principle of Saint-Venant (40). The principle states that the strains produced by the localized application of a system of stresses and couples are negligible at distances relatively far removed from the point of application.

Thus, the compliance c_o should be equal to the slope of a linear regression of LC vs. L. The intercept of this line should be an estimate of the end-effect, $2\langle C\rangle_{end} L_e$.

Experimental results for two different paper samples are presented in Fig. 6. The cylinders were all constructed with 0.635 cm. seam width.

The cylinder compliance results were obtained by successively shortening a given cylinder. The cylinder length was decreased by carefully cutting a mounted cylinder from the cylinder mounts, using the top of the cylinder mount as a guide for the razor blade, and remounting the shortened cylinder.

The regression lines for both paper samples have negative intercepts. The negative intercept was characteristic of all of the paper samples tested for this thesis. The negative intercept indicates that the torsional stiffness at the ends of the cylinder is greater than the torsional stiffness away from the ends.

The estimate of the end effect can be used to evaluate the torsional stiffness, k, which was defined by Equation (15). By definition

$$c_o = 1/(I\omega_o^2 L_o) \tag{22}$$

Rearranging Equation (21)

$$c_o = \left[CL - (2\langle C\rangle_{end} L_e)\right] / L_o \quad .$$

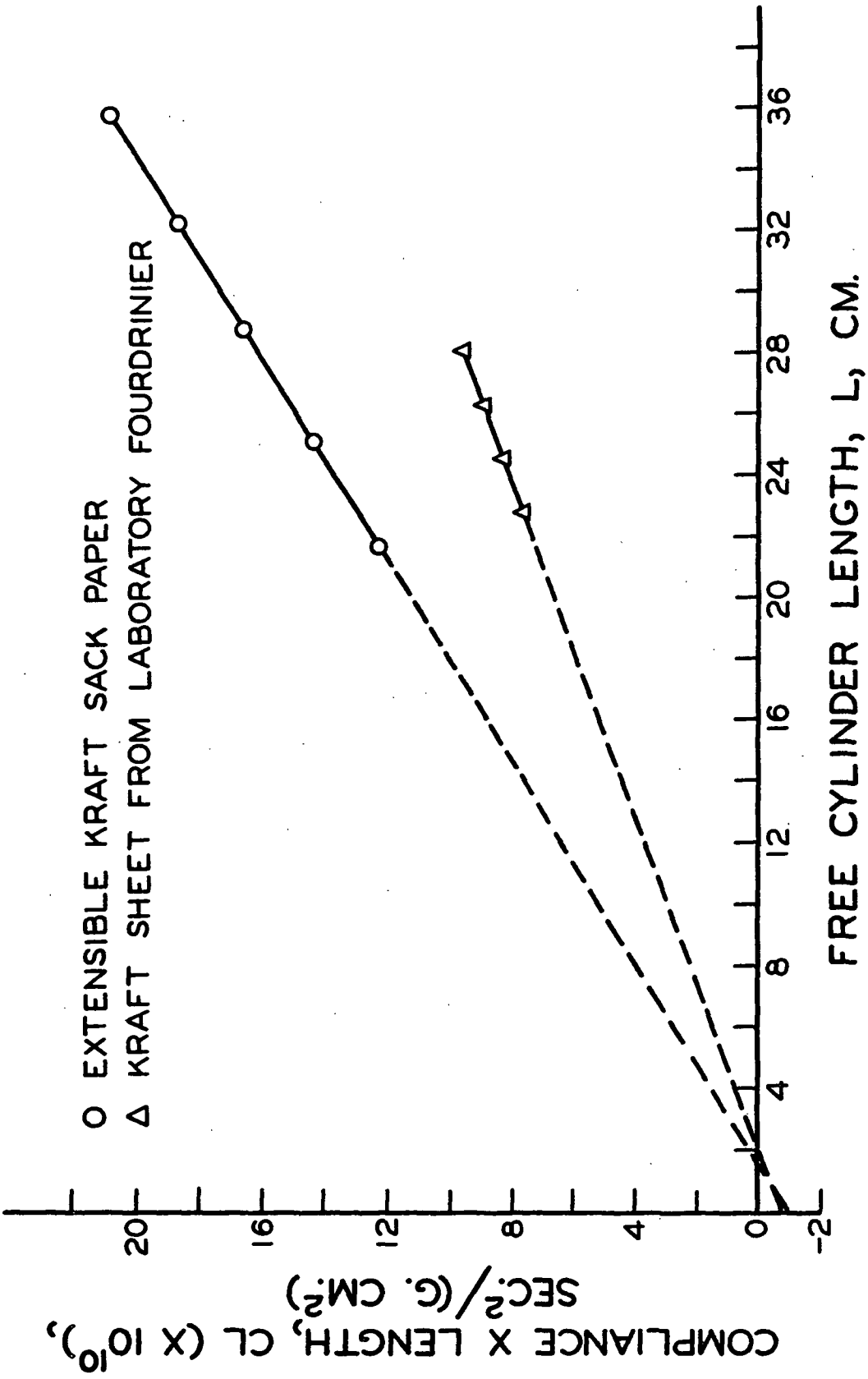

Figure 6. Regression Lines for End Effect

Therefore, the torsional stiffness may be expressed as follows:

$$k = 1/\left[CL - (2 \langle C \rangle_{end} L_e) \right] \qquad (23)$$

Note that the end effect is a negative quantity, and that this correction causes a reduction in the experimentally measured torsional stiffness.

Because of the locations of the microscope and the stationary moment arm, it was not possible to test cylinders of less than 20 cm. length. The relatively long extrapolations shown in Fig. 6 are not subject to the statistical uncertainty normally associated with such a procedure. The slope of the LC vs. L regression is the quantity of actual interest in making the end-effect correction.

For each paper sample tested an estimate of the end effect was made. Equation (23) was applied to obtain the torsional stiffness before the value of the shear modulus was calculated.

Viscoelastic Effects

There are two ways in which the viscoelastic nature of paper can affect the response of the torsion pendulum. One of these has been discussed previously. That is, the possible internal changes in paper structure due to stress relaxation phenomena caused by the bending stresses introduced in forming the cylinder. The other possible effect is related to the viscous dissipation of energy introduced into the sheet.

Cylinder Damping

The differential equation discussed earlier, Equation (13), describes the torsional oscillation of a perfectly elastic material. Paper does not conform to this model.

If it is assumed that the frictional torque developed in the cylinder is proportional to the angular velocity of the cylinder (viscous damping), the following differential equation describes the motion of the cylinder:

$$I(d^2\phi/dt^2) + q(d\phi/dt) + k\phi = N_o \sin(\omega t) \quad , \tag{24}$$

where I is the moment of inertia of the system, ϕ is the angular displacement of the free end of the cylinder, t is the time, q is the damping coefficient, and k is the torsional stiffness of the cylinder.

The solution of this equation can be expressed as follows:

$$\phi = A \cos(\beta t - \delta) \quad , \tag{25}$$

where A and δ are constants, and α and β are given by the following formulae:

$$\alpha = q/2I \tag{26}$$

and

$$A = \sqrt{(k/I) - 2\alpha^2} \tag{27}$$

If the terms k/I and $2\alpha^2$ are of the same order of magnitude, it is apparent that the observed resonance frequency will be lower than the frequency needed to predict the shear modulus.

Two experiments were performed to estimate the effect of damping on the magnitude of the resonance frequency. In the first experiment, a switch was placed in the coil-oscillator circuit so that the driving power could be shut off while the cylinder was at resonance. The time required for the amplitude of vibration to decay by a given amount was recorded.

It was found that the initial amplitude decayed to ten percent of the initial value in one second. Equation (25) was used to compute a value for the term α based on this information: $\alpha = 2.3$/second.

A recorder capable of responding to a 400-c.p.s. signal was wired across the driving coils through a double-pole, double-throw switch. When the switch was thrown, the oscillator-coil circuit was broken, and the coil-recorder circuit was closed. The motion of the magnets in the coils generated the recorded signal. As before, the cylinder was driven at resonance before breaking the coil-oscillator circuit.

A trace of the damped output is shown in Fig. 7. The frequency of oscillation of the cylinder was calculated from the recorder chart based on the chart speed of the recorder. The calculated frequency equaled the oscillator driving frequency. The shape of the damped oscillation curve indicates that the behavior is consistent with the assumption of viscous damping.

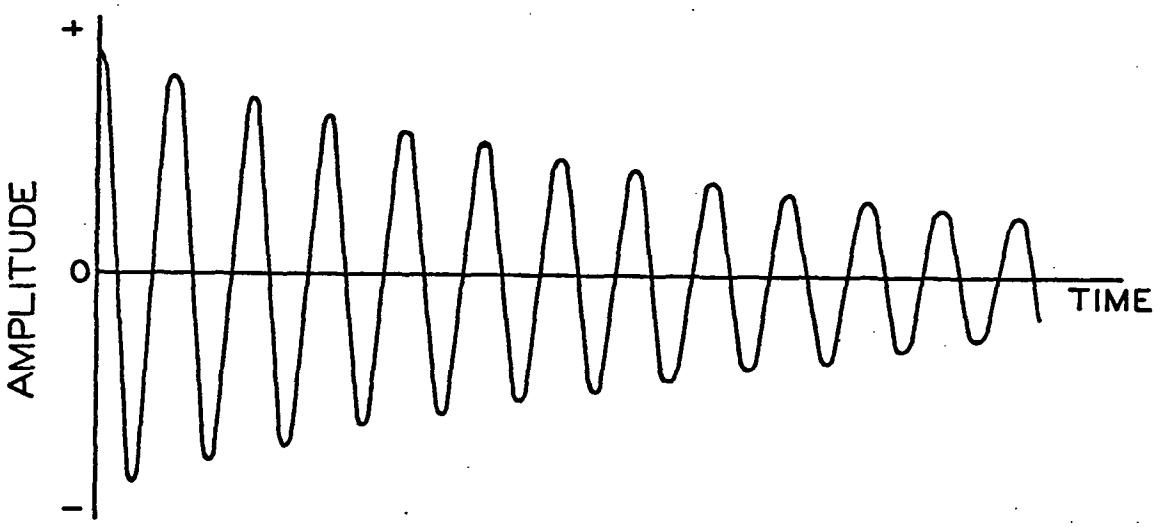

Figure 7. Damped Torsional Oscillation

The log of the ratio of succeeding amplitudes was used to calculate the damping term α = 2.6/second. The experimentally determined value of k/I for the cylinder tested was about 1 x 10^5/sec.^{2}. Therefore, the damping term, α, has a negligible effect on the resonance frequency of the cylinder as predicted by Equation (27).

Bending Stress Relaxation

For each of the paper samples tested a cylinder was tested 30 minutes after mounting and again after 24 hours. In all these tests no differences were found in the resonance frequencies before and after the 24-hour period. This indicates that relaxation due to the bending stresses in the cylinder wall has negligible effect on the mechanical behavior of the cylinder in shear.

Axial Load

Timoshenko (41) discusses the effect of axial stress on the torsional stiffness of cylinders due to longitudinal stresses introduced by torsion. He also indicates a method for treating the case of an external axial force applied to the cylinder.

Following his example, a relationship was derived to predict the effect of axial force on the torsional stiffness of a cylinder. This derivation is presented in Appendix II. The equation which compares the effect of axial force to the case of zero force is as follows:

$$(k-k_b)/k_b = [(4F/\pi G)/(d_o^2-d_i^2)\,]-(E\phi^2/132L^2G)(d_o^4 + 13d_o^2d_i^2 + d_i^4)/(d_o^2 + d_i^2) \quad , \qquad (28)$$

where k is the torsional stiffness of cylinder with axial force F acting, k_b is

the torsional stiffness of the cylinder with zero axial force, and all other symbols have been previously defined.

Apparatus

To relieve the axial load on the cylinder produced by the weight of the lower cylinder mount a knife-edge balance was constructed. The balance consisted of five parts: a brass knife-edge, a brass balance arm notched to ride on the knife-edge, a steel rod threaded into the balance arm, a brass counterweight, and a fine copper wire used to connect the mount to the balance. A diagram of the balance is given in Fig. 8.

A one-eighth inch diameter brass pin was soldered to one end of the support wire. This pin was held in position in the balance arm with a set-screw. This device was used to level the balance arm when counterweighting the lower cylinder mount.

The opposite end of the support wire was threaded through a small hole in the center of the mount. The wire was held in place with soft solder which was tamped into the hole.

The torque required to twist the support wire to the maximum deflection was calculated to be 2.9 dyne-cm. The corresponding torque to deflect the paper cylinder was 2×10^6 dyne-cm. Therefore, the support wire had no measurable influence on the torsional response of the cylinder.

Experimental

Three cylinders were tested with the axial load of the lower mount and again with this load relieved by the balance. The axial force contributed by the lower mount was 4.5×10^5 dynes.

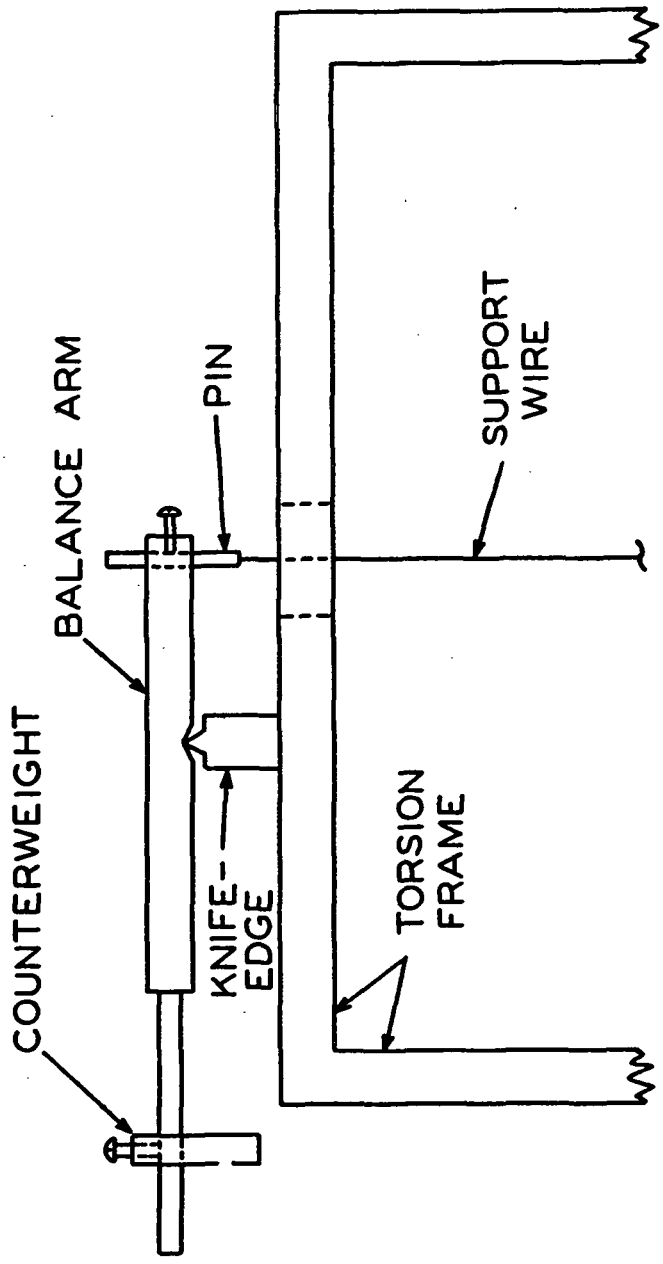

Figure 8. Knife-edge Balance

The average increase in torsional stiffness produced by the weight of the lower mount was found to be 0.26%. The theoretical value calculated from Equation (28) was 0.05%. For either increase the magnitude of the effect is negligible compared to other variations introduced by the material and testing procedures.

Longitudinal Modes of Vibration

The derivation given in Appendix II demonstrates the presence of longitudinal stresses acting in the direction parallel to the cylinder axis. The driving frequency of vibration in this direction is twice the torsional frequency of vibration. The longitudinal resonance frequency depends upon the Young's modulus of the cylinder material in the direction parallel to the cylinder axis and the cross-sectional area of the cylinder.

If the torsional resonance frequency is nearly one-half of the longitudinal resonance frequency, coupled oscillations will occur, and the torsional resonance frequency will not be that required by Equation (27). Calculated estimates of the longitudinal resonance frequency indicate that it is three to four times larger than the torsional resonance frequency. Also, measurements of the torsional resonance of each cylinder at several different moments of inertia indicate that the torsional response was not affected by coupled vibration with the longitudinal mode.

POISSON'S RATIO

Poisson's ratio is defined as the contraction strain, produced by a stress acting at 90° to the contraction, divided by the tensile strain which results from the applied force. For example, $\nu_{\underline{yx}} = \epsilon_{\underline{x}}/\epsilon_{\underline{y}}$, where $\nu_{\underline{yx}}$ is Poisson's ratio, $\epsilon_{\underline{x}}$ is the contraction strain in the $\underline{x}$-direction, and $\epsilon_{\underline{y}}$ is the tensile strain for force applied in the $\underline{y}$-direction. The contraction strain is taken to be a positive quantity in the convention used in this thesis.

Brecht and Wanka (42) discuss a method for measuring Poisson's ratio of paper. They measured the desired strains by mounting a microscope with two directions of travel above the straining device.

Their experimental results include test results on several machine-made papers as well as measurements on handsheets. They found that Poisson's ratio remains constant as a function of load until the tensile strain in the specimen exceeded 1.0%. At high strain, above 1%, the value of Poisson's ratio was found to increase slowly as the tensile strain increased. The maximum value of Poisson's ratio reported was 0.45. The minimum value was 0.1.

Ranger and Hopkins (43) report a method for measuring Poisson's ratios of paper in which the relative spacings between small glass beads glued to the paper surface are used to calculate the desired strains. The values of Poisson's ratio reported range from 0.4 to 0.95.

Lathrop (44) used the technique reported by Ranger and Hopkins (43) to measure local variations in the tensile strain of paper samples. In the procedure followed by Lathrop, glass beads 300 μm. in diameter were glued to the surface of a tensile strip. As this strip was strained using a Table Model Instron, a sequence of photographs was taken of the strip surface. The bead spacings on these photographs were subsequently measured with a microcomparator which could be read to the nearest 1/10,000 inch.

The procedures used by Lathrop were adopted for measurements made in this thesis with a few modifications. The requirements of the test specimen in this technique are twofold. The tensile specimen must have sufficient length-to-width ratio to preclude inhibition of Poisson's contractions due to the specimen clamps.

Also, the tensile specimen must present a flat surface area for photography which moves in a vertical plane as load is applied.

SPECIMEN PREPARATION

Tensile strips were cut with 6.35 cm. width and 31.75 cm. length to allow a 30.48 cm. span. Superbrite glass beads, type 090-5005, furnished by the Minnesota Mining and Manufacturing Company were glued to the strip surface with Epon 907, an epoxy resin.

The beads were arranged in four rows running along the strip length. Two rows were located 0.635 cm. in from the strip edges, and the other two rows were 1.27 cm. in from the edges. Each row was 5.08 cm. in length with beads spaced at 0.635 cm. intervals. This array of beads was located at the center of the strip length. A template was made from 0.002-inch aluminum shim stock with 1/32-inch holes located at each bead position to aid in mounting the beads.

Bead gluing was accomplished with the aid of a low-power stereo microscope. Epoxy adhesive was first applied to the paper at the center of each template hole using the tip of a sharpened dissecting needle as the applicator. The glue spot was approximately one-half the diameter of the glass beads which had diameters of 0.2-0.3 mm. A bead was then dropped onto the adhesive using jeweler's tweezers to manipulate the bead. The adhesive was allowed to set for 24 hours before testing proceeded.

STRAINING APPARATUS

A Table Model Instron was used to apply load to the Poisson's ratio specimens. Line-type clamps were used to grip the specimen. Instron operating conditions used were 0.2 inch/minute crosshead speed, and 20 inch/minute chart

speed. The full-scale load on the chart was adjusted according to the specimen tensile strength to produce an initial slope of the load-elongation curve of about 45°.

PHOTOGRAPHIC EQUIPMENT AND PROCEDURES

The camera used was a 4 x 5-inch Graflex which was fitted with a 5 x 7-inch auxiliary sliding back. The sliding back permitted three two-inch width exposures on a single glass photographic plate. The lens used was an 8-1/2-inch, f/9 Goertz Red Dot Artar process lens.

The camera was mounted on a rigid tripod. The tripod was constructed to permit translation of the camera in a horizontal plane. The camera was focused by moving the entire camera rather than moving the lens relative to the glass plate. This was done to maintain the same magnification for all work (slightly less than unity magnification).

The photographic emulsion used was Kodalith Ortho, type 3 on 5 x 7-inch glass plates. This is a high resolution emulsion. An f-stop of 9 was used for all exposures.

The camera was focused with the aid of a four-power hand magnifier. This lens has a very short focal length. The camera was moved in the horizontal plane until the reflected highlight from the glass bead surface was most intense when viewed with this lens through the camera optics. The camera was then secured in position.

Photographic illumination was obtained with a Strobotac, type 1531A manufactured by the General Radio Company, West Concord, Massachusetts. The flash rate was 360 flashes/minute. A five-second exposure time was used with this flash rate.

The Strobotac reflector was located two feet from the strip and twelve inches from the camera lens.

Due to the relatively long exposure time required it was necessary to stop the Instron while the photograph was taken. When this was done, the crosshead drive motor was also turned off to eliminate vibrations produced by it.

Three exposures were taken of each tensile specimen. The first exposure was made after the strip had been loaded to about five pounds. The second exposure was made when the load-direction strain had increased by about 0.15%. The third exposure was taken when the load-elongation curve first began to deviate from the initial straight line (approximately 0.25% strain in the direction of stress).

Photographic plates were developed for four minutes in Kodak D-76 developer at 68°F. These developing conditions provided good contrast between the bead image, the highlight of reflection from the bead surface, and the paper background.

PLATE MEASUREMENT

A modified Wilder microcomparator which provided an optically projected image of 45X magnification was used for measuring plates. This instrument was equipped with digital encoders mounted on each traversing screw. The stage location was displayed visually on a panel to the nearest 1/12,000 inch. This system was coupled to a card punch, and could be cued to punch the stage coordinates when the stage was in the desired position.

The operating characteristics of this instrument were determined. The reproducibility of a given measurement was found to be much less than $\pm$ 1/12,000 inch if the projected image had a sharp boundary.

In measuring the photographic plates for Poisson's ratio determinations the diameter of the reflected highlight was approximately 15 μm. (61 12,000 inch). It was found that the measurement of the center of the highlight image could be estimated to about ± 3 μm. (less than ± 2/12,000 inch).

Measurements of the coordinates of each highlight were made for all three exposures. When this was done, one of the 7-inch sides of the plate was chosen as the reference edge. This edge was butted against the alignment bar on the stage of the microcomparator. Measurements of successive exposures were then taken by sliding the plate along the alignment bar. This assured that the angular orientation of the plate with respect to the instrument travel did not change from exposure to exposure.

CALCULATION OF STRAIN

A diagram of the bead array is presented in Fig. 9. The bead spacings which were used in the calculation of the tensile and contraction strains are presented there.

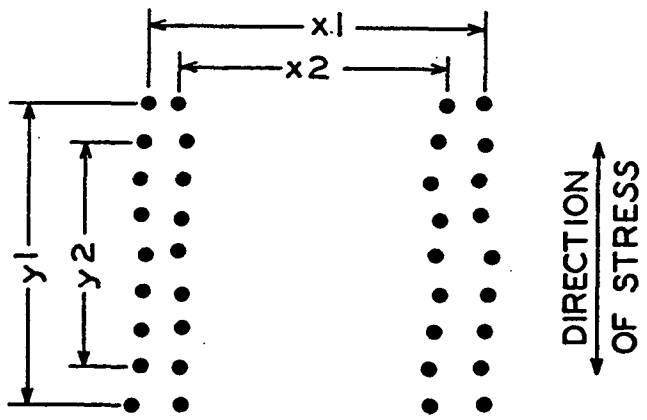

Figure 9. Bead Array

The bead spacings $\underline{x}1$ and $\underline{x}2$ were calculated for each row of each exposure. Contraction strains were then calculated based on the changes in these quantities with increasing stress. The average of all these individual strains was determined and used in calculating Poisson's ratio. An identical procedure was followed with the spacings $\underline{X}1$ and $\underline{Y}2$ to estimate the tensile strain. The standard error associated with strain measurements and the standard deviation of the estimate of Poisson's ratio were calculated.

LENS QUALITY

An experiment was made to determine the behavior of the Goertz lens used in this study. A piece of graph paper was glued to the surface of a 5 x 7-inch glass plate and then conditioned at 73°F. and 50% relative humidity for 48 hours.

A traveling microscope, which could be read to 0.0001 cm., was used to measure the line spacing of the graph paper in a 2 x 2-inch area. A photograph was then taken of this area, and the line spacing on the photograph was measured with the microscope.

The camera magnification was computed to be 0.92 from this data. A comparison of the line spacing data from the original grid and the photograph showed that no measurable distortion was produced by the lens.

ANGLE OF ILLUMINATION

As was mentioned earlier, the image of the highlight of reflection from the bead was used as the fiducial point when bead spacings were measured. Because of the geometry and location of the Strobotac, the angle of incident light is not the same for beads on opposite sides of the tensile strip. As the strip is strained, the angle of incidence changes, and as a result, the position of the reflected highlight on the bead surface, as viewed from the camera, changes.

It was not known whether this change would be the same for beads on either side of the strip, or whether the magnitude of a relative difference in this change would influence the measurement of bead position. Two exposures of a tensile strip were made. In the first the angle of illumination was 37° relative to the center of the strip; in the second this angle was 47°.

The bead spacings on these two photographs were measured using the image of the reflected highlight as the point of reference. No significant difference was found.

SPECIMEN CURL

Initial measurements of Poisson's ratio gave values which were much larger (υ = 0.5-1.2) than the values predicted assuming an orthotropic model. It was then noticed, while determining load-elongation curves for Young's modulus, that the tensile specimen appeared to curl about a vertical axis as the strip was loaded. This observation was confirmed by illuminating tensile specimens from the side and observing the shadow cast by the edge of the strip nearest to the light source.

The following observations were made: first, as the tensile stress in the specimen increased, the radius of curvature of the curl decreased; the strip was not curled near the line-type clamps, but in the central six inches of the ten-inch span curvature became very pronounced with increasing stress; second, the convex side of the curvature was always toward the wire side of the sheet; third, strips from some samples exhibited less curling tendency; however, at high stress a series of hills and valleys, somewhat similar in appearance to a pleated drapery, were observed.

Either the curl or the drapery effect could cause an overestimation of Poisson's ratio since the measured contraction strain would be overstated.

To correct for deviations of the strip from a flat surface a flattening jig was constructed.

FLATTENING JIG

A jig to aid in holding the tensile strip flat was constructed from 1/10-inch thick lucite. The jig was three inches in width by eight inches in length, and was designed to be supported by the tensile specimen. The jig was clamped to the tensile specimen by means of two 1/2 x 3-inch lucite bars which were bolted to either end of the eight-inch length. Counterweights were located at each clamp so that the jig exerted no bending moment on the tensile specimen. The jig is pictured in Fig. 10.

The jig surface away from the clamping area was sprayed with fluorocarbon aerosol to reduce the coefficient of friction. Estimates of the static and kinetic coefficients of friction of sack paper on lucite and of sack paper on the fluorocarbon sprayed surface were made by measuring the angles of inclination of the plate required to initiate and halt the motion of a piece of paper weighted with a cube of brass. For paper on lucite the static coefficient of friction was 0.384, and the kinetic coefficient was 0.314. For paper on the sprayed surface the static coefficient was 0.285, and the kinetic coefficient was 0.224.

The mass of the jig, including clamps and counterweights, was 67.5 grams. Based on the kinetic coefficient of friction of paper on lucite the normal force required to support the jig was estimated to be 5.25×10^4 dynes. The tensile load in the strip during the first photograph averaged about 1.5×10^6 dynes.

Observations of load-elongation samples were made with the jig positioned equidistant between the line-type clamps. As before, the strip was illuminated

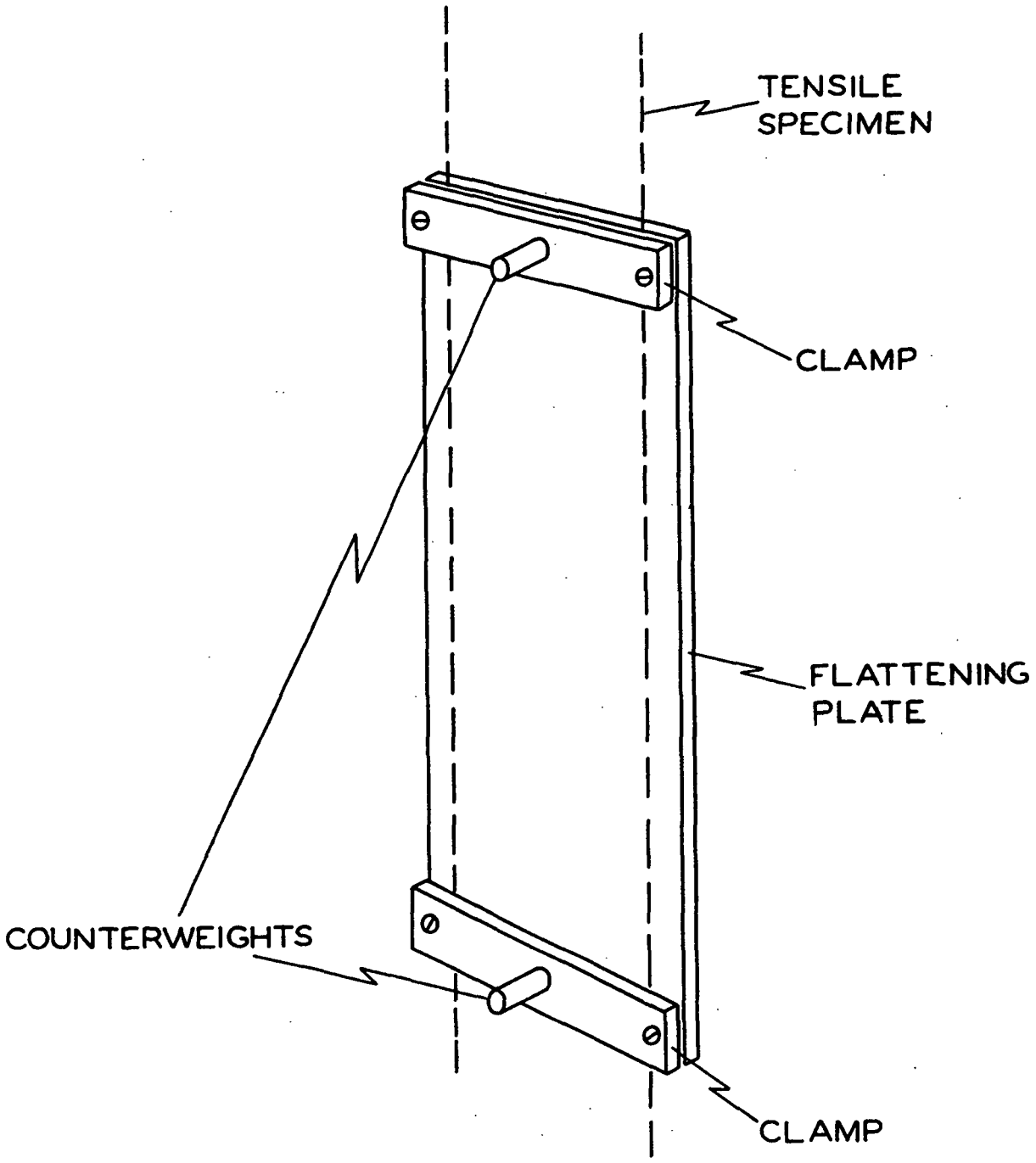

Figure 10. Tensile Strip Flattening Jig

from the side. The jig was found to eliminate the specimen curl. However, at high strain the drapery effect mentioned before was observed.

SHEET THICKNESS

Sheet thickness measurements were made with a Federal gage (45) using a platen pressure of 0.45 kg./cm.^{2}. The sheet thickness for a given paper sample was determined by finding the grand average of sets of twelve calipers on each of the shear modulus blanks.

It should be pointed out that in comparing test results to Equations (7), (8), (1), and (10) the product of the appropriate modulus times the sheet thickness can be substituted for the actual value of the modulus. This avoids the need for measuring sheet thickness.

SAMPLE PREPARATION

Four of the samples tested were commercial machine-made papers; another sample was formed on the experimental paper machine at the Forest Products Laboratory, Madison, Wisconsin.

The four commercial papers were obtained in 36-inch rolls. To prepare test specimens from a given sample approximately 20 sheets were clipped from the original roll. The seven interior sheets were taken for testing. Using the cut edge of the roll as a reference, test specimens for Young's modulus, shear modulus, and Poisson's ratios were cut at 0°, 15°, 30°, 45°, 60°, 75°, and 90° to the machine direction. Only one angular orientation was cut from each sheet. Guide lines for cutting the test specimens were laid out with a steel straight-edge and a beam compass. Test blanks were cut from the sheet with the straight-edge and a razor blade.

A similar procedure was followed with the sample formed on the experimental machine at Madison. However, because of insufficient paper, tests were made only at 0°, 45°, and 90° to the machine direction.

EXPERIMENTAL RESULTS

The hypothesis of this thesis was that the elastic behavior of paper for stresses parallel to the xy-plane of the sheet could be described by the orthotropic model. It was also desired to investigate the applicability of the relationships proposed by Campbell (10) for the elastic behavior of paper.

DATA TREATMENT

Equations (7), (8), and (9) predict the variation in elastic moduli with direction for an orthotropic material when stresses are parallel to the xy-plane of the material. Equations (1) and (10) were proposed by Campbell (10) to predict this variation in the moduli.

Using the trigonometric equality $\cos^2 \theta = 1 - \sin^2 \theta$, these equations may be written in the following form:

$$1/E_\theta = A_{eo} + B_{eo}X + C_{eo}X^2 \quad , \tag{29}$$

$$1/G_\theta = A_{go} + B_{go}X + C_{go}X^2 \quad , \tag{30}$$

and

$$1/E_\theta = A_{ec} + B_{ec}X \quad , \tag{31}$$

$$1/G_\theta = A_{gc} + B_{gc}X \quad , \tag{32}$$

where E_θ and G_θ are the Young's modulus and shear modulus, respectively, at angle θ to the x-direction, $X = \sin^2 \theta$, and the remaining quantities A_{mn}, B_{mn}, and C_{mn} are coefficients which will be defined later. Equations (29), (30), (31), and (32) are identical to Equations (7), (8), (1), and (10), respectively.

The coefficients A_{mn}, B_{mn}, and C_{mn} are functions of the principal planar moduli. They are defined as follows:

$$A_{eo} = 1/E_x \quad , \tag{33}$$

$$B_{eo} = (1/G_{xy}) - 2(\upsilon_{xy} + 1)/E_x \quad , \tag{34}$$

$$C_{eo} = (1 + 2\,\upsilon_{xy})/E_x + (1/E_y) - (1/G_{xy}) \quad , \tag{35}$$

$$A_{go} = 1/G_{xy} \quad , \tag{36}$$

$$B_{go} = 4(C_{eo}) \quad , \tag{37}$$

$$C_{go} = -(B_{go}) = -4(C_{eo}) \quad , \tag{38}$$

$$A_{ec} = 1/E_x \quad , \tag{39}$$

$$B_{ec} = (1/E_y) - (1/E_x) \quad , \tag{40}$$

$$A_{gc} = 1/G_{xy} = (1 + 2\upsilon_{xy})/E_x + (1/E_y) \quad , \tag{41}$$

$$B_{gc} = 0.0 \quad , \tag{42}$$

where E_x and E_y are Young's moduli in the x- and y-directions, respectively, G_{xy} is the shear modulus for stress in the x and y-directions and υ_{xy} is Poisson's ratio for stress in the x-direction and contraction in the y-direction.

The experimental data for the variation of modulus with angle were fitted to first- and second-order regression equations in which the independent variable was $\sin^2 \theta$ (46). The regression coefficients of the fitted equations were then equated to the appropriate coefficients A_{mn}, B_{mn}, and C_{mn}, of Equations (33) through (42).

Equations (33) through (38), the orthotropic model, and Equations (39) through (42), Campbell's proposal, were then available for calculating the principal moduli of elasticity. The equations for a given elasticity model were solved simultaneously to evaluate the moduli predicted by that model.

SHEAR MODULUS SYMMETRY

Both Equation (8) and Equation (10) predict that the variation of the shear modulus with angle will be symmetrical about the 45° axis as well as being symmetrical about the 0° and 90° axes. That is, the following pairs of moduli should be equal according to these equations: $\underline{G}_{30°} = \underline{G}_{60°}$, $\underline{G}_{15°} = \underline{G}_{75°}$, and $\underline{G}_{0°} = \underline{G}_{90°}$. If this is true, nonequality for a given pair should be attributable to experimental errors and sample variations.

When the shear modulus symmetry condition was applied, experimental values determined at both angle θ and angle $(\pi/2-\theta)$ were assigned the orientation θ. This modified set of data was used to calculate the shear modulus regression equations.

GRAPHICAL REPRESENTATION

Four polar graphs of modulus versus angular orientation were prepared for each machine-made sample. Each graph contained the data points for both the shear modulus and Young's modulus used in estimating the regression curve as well as the two regression curves and the 95% confidence limits about the regression.

The first two plots were constructed from the first- and second-order regression equations, respectively. In the latter two plots the shear modulus data were adjusted according to the statements of the previous section. First- and second-order regression equations were presented in those figures, respectively.

ANALYSIS OF VARIANCE

Two sources of error were recognized in estimating the experimental error. These errors were the test error associated with variations in making a given measurement and the sample error associated with variations in the material being tested.

In distinguishing between the test error and the sample error it was assumed that variations in results from adjacent test specimens were attributable to testing error while variations between tests made on specimens far removed relative to the specimen size were due to both testing and sample variation.

The goal of the analysis of variance is to provide a basis for deciding between the first- and second-order regression models. This was done by comparing the residual sum of squares about the regression to the experimental variance. This technique is discussed by Draper and Smith (47).

The concept involved in this analysis is that scatter about a regression curve should be attributable to experimental errors if the regression curve is of the proper form. That is, if the residual mean square about the regression curve is not significantly greater than the experimental error variance, the regression curve adequately describes the data.

Following the terminology of Draper and Smith (47), cases in which the residual mean square is significantly greater than the experimental error variance are referred to as having a significant lack of fit. The comparison between the residual mean square and the experimental error variance was made by using the F-test (46).

SAMPLE 30 (REGULAR KRAFT SACK PAPER)

This sample was a regular kraft sack paper produced on a commercial fourdrinier. The basis weight of the sample was 82.9 g./m.^{2}. The sample thickness was 0.01505 cm., and the density was 0.551 g./cm.^{3}.

Measurements of the shear modulus and Young's modulus were made in the machine and cross-machine directions, and at 15° intervals between these extremes.

Generally, ten load-elongation measurements were made at each interval and from one to four replicate cylinders were tested at each orientation. Each principal Poisson's ratio was determined four times.

DATA

Polar plots of the several regression curves and their corresponding experimental data are presented in Fig. 11, 12, 13, and 14. The outer two curves for each set of data are the 95% confidence limits on the regression. The principal moduli calculated from the coefficients of the regression lines are given in Table I. The actual experimental values for each point are given in Appendix III.

TABLE I

PRINCIPAL MODULI FOR SAMPLE 30

Order of Regression Equation	Shear Modulus Symmetry Applied	Young's Modulus, dynes/cm.^{2} E_x	E_y	Shear Modulus, dynes/cm.^{2} G_{xy}	Poisson's Ratio ν_{xy}	ν_{yx}
Campbell (1st order)	No	5.58×10^{10}	2.49×10^{10}	1.55×10^{10}	0.180	0.080
Orthotropic (2nd order)	No	5.26	2.42	1.55	0.385	0.177
Campbell (1st order)	Yes	5.58	2.49	1.54	0.191	0.085
Orthotropic (2nd order)	Yes	5.26	2.42	1.54	0.395	0.182

ANALYSIS OF VARIANCE

A comparison of the mean square residual with the error variance showed a significant lack of fit at the 0.01 level for both the first- and second-order regression predictions for Young's modulus. Only the test variance was available for this sample, and this is believed to be the cause of this result.

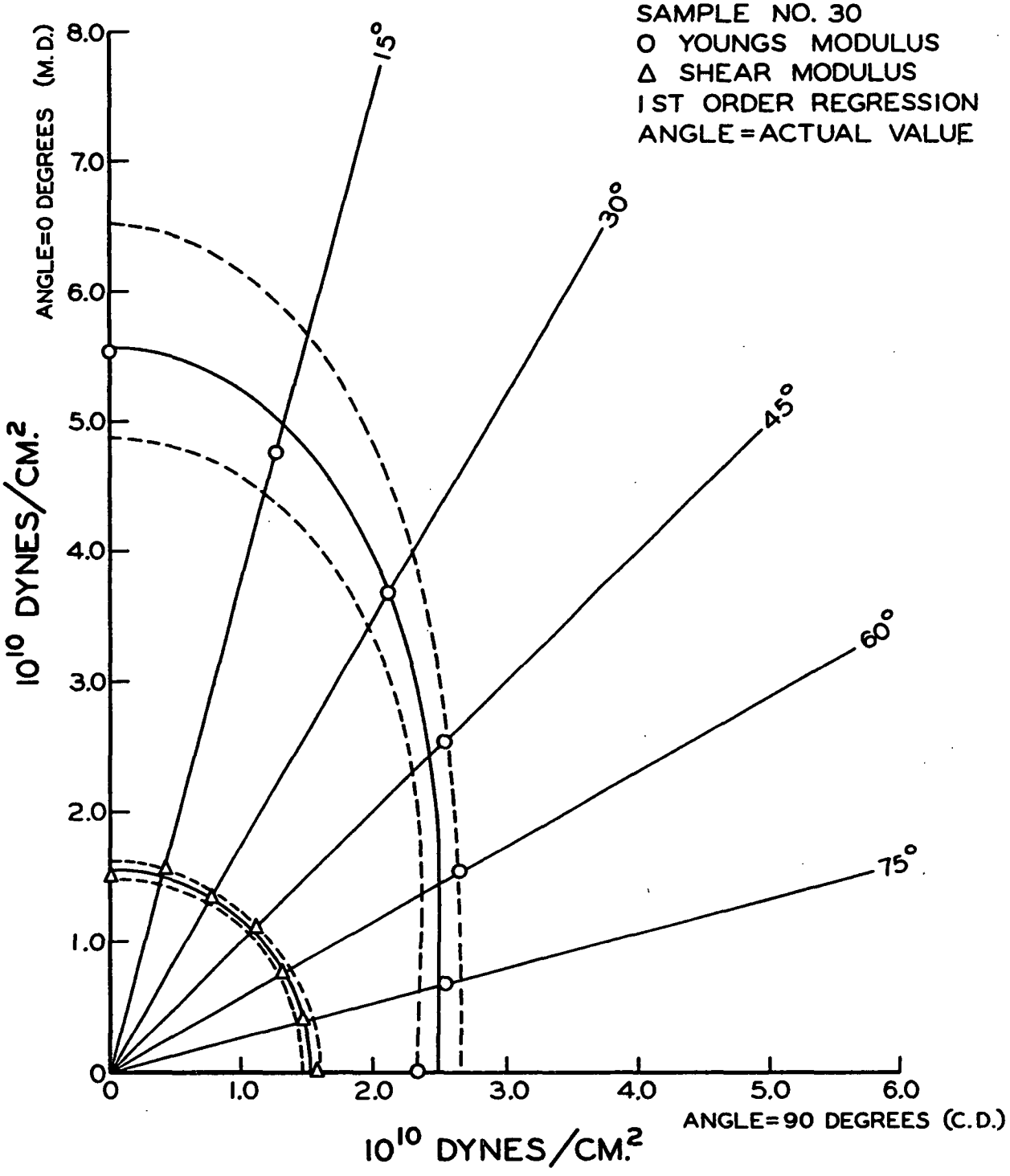

Figure 11. Modulus vs. Angle with 95% Confidence Limits

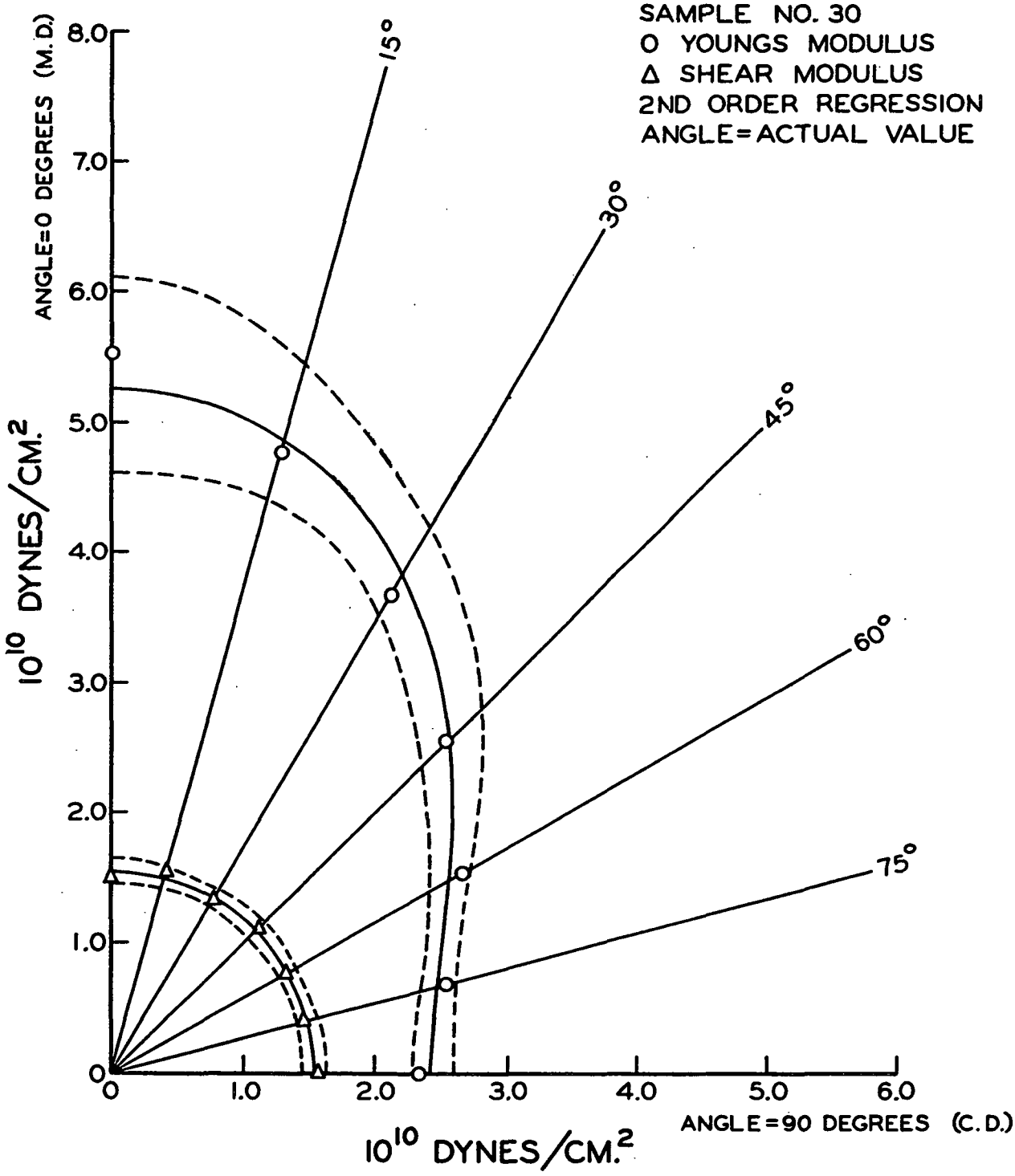

Figure 12. Modulus vs. Angle with 95% Confidence Limits

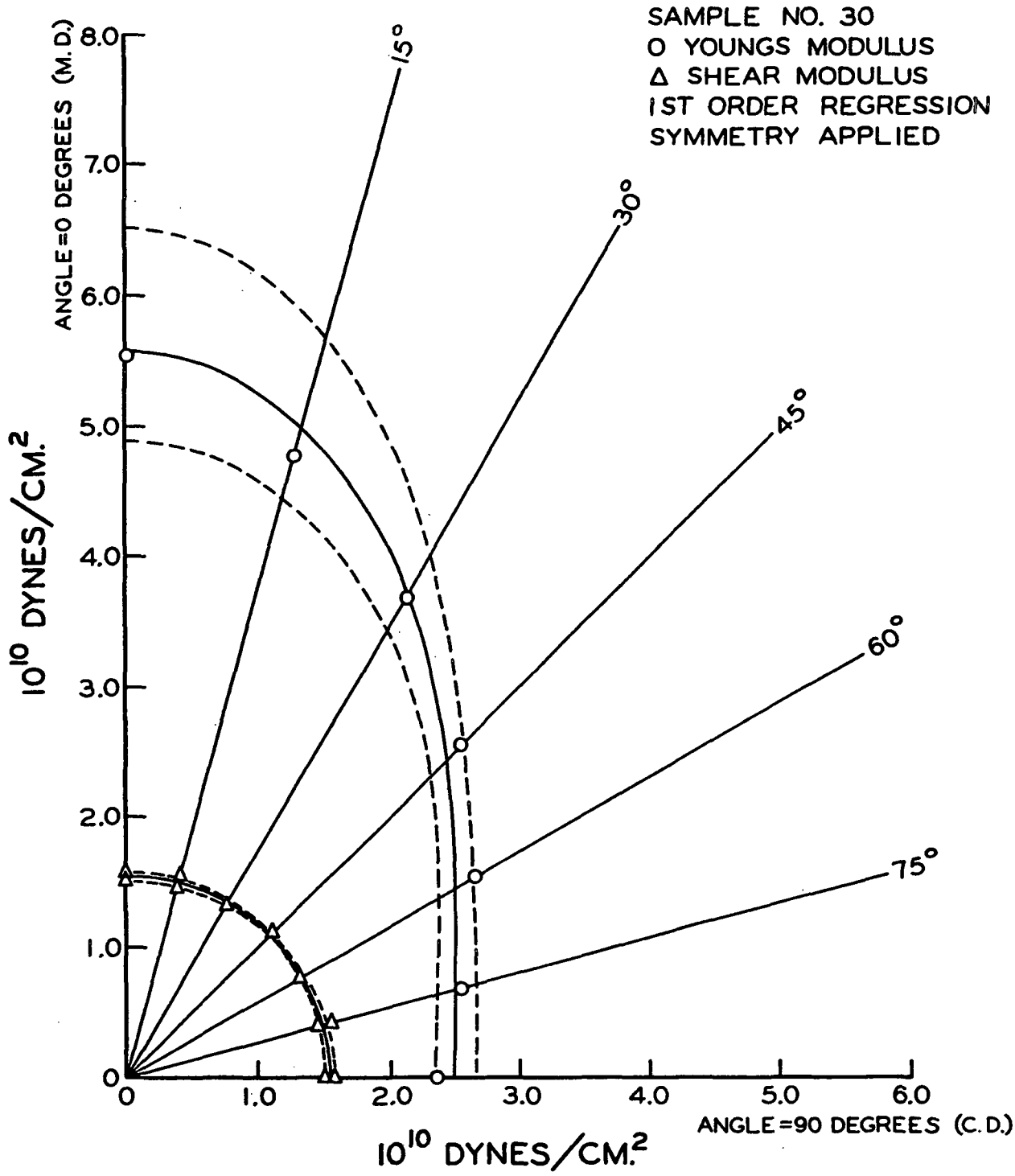

Figure 13. Modulus vs. Angle with 95% Confidence Limits

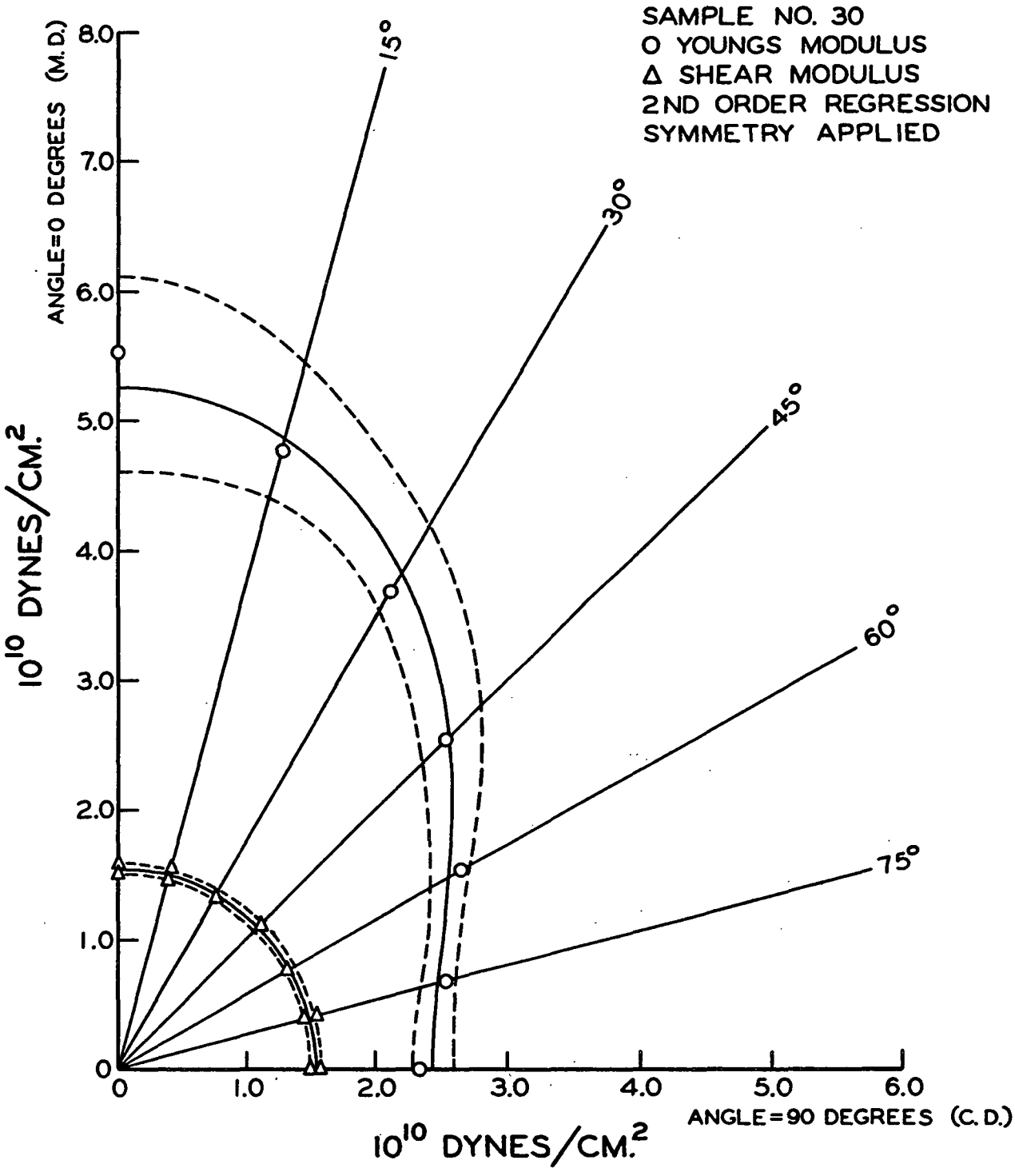

Figure 14. Modulus vs. Angle with 95% Confidence Limits

By the same test no significant differences at the 0.10 level were found when comparing first- and second-order regression equations for the shear modulus. It should be noted that there is apparently no variation of shear modulus with angle for this sample. An example calculation for this sample is given in Appendix IV.

POISSON'S RATIOS

Experimental and predicted values of Poisson's ratio are compared in Table II.

TABLE II

COMPARISON OF EXPERIMENTAL AND PREDICTED POISSON'S RATIOS FOR SAMPLE 30

Identification	Poisson's Ratio		Modulus Ratio, $cm.^2/dyne$	
	ν_{xy}	ν_{yx}	ν_{xy}/E_x	ν_{xy}/E_y
Experimental	0.476	0.207	8.34×10^{-12}	11.86×10^{-12}
Campbell (actual data)	0.180	0.080	3.22	3.22
Orthotropic (actual data)	0.385	0.177	7.32	7.32
Campbell (symmetry applied)	0.191	0.085	3.41	3.41
Orthotropic (symmetry applied)	0.395	0.182	7.52	7.52

The 95% confidence limits for the experimental values of Poisson's ratio are $\nu_{xy} = 0.476 \pm 0.076$ and $\nu_{yx} = 0.207 \pm 0.198$. On the basis of these limits, the experimentally measured Poisson's ratio for stress in the machine direction is significantly greater than any of the predicted values. There is no significant difference between the experimental and predicted values of Poisson's ratio for

stress in the cross-machine direction. Nor is there a significant difference between either experimental modulus ratio or between the experimental modulus ratio and the predicted values from the second-order regressions.

SAMPLE NUMBER 2 (KRAFT SHEET FROM LABORATORY FOURDRINIER)

A sample formed on the laboratory fourdrinier at the Forest Products Laboratory, Madison, Wisconsin was obtained from Mr. Vance Setterholm. The furnish for this sample was a commercial kraft pulp which had been refined at 27% consistency to a Canadian Standard Freeness of 600 ml.

The sheet had a good appearance. That is, the sample was flat, and the formation was quite good.

The basis weight of the sample was 100.3 g./m.^{2}. The sample caliper was 0.01481 cm., and its density was 0.677 g./cm.^{3}.

EXPERIMENTAL DETAILS

As received, the sample had a cross-machine width of fourteen inches. One inch was discarded from either edge of the sample. Because of a limited amount of material, modulus determinations were made only at 0°, 45°, and 90° to the machine direction.

In general, four replicate determinations of the shear modulus were made at each angle. Fifteen replicate measurements of Young's modulus were made at each angle, and four repeat measurements of each principal Poisson's ratio were made.

DATA

Polar graphs of the various regression curves and the corresponding experimental points are presented in Fig. 15, 16, 17, and 18. The principal moduli

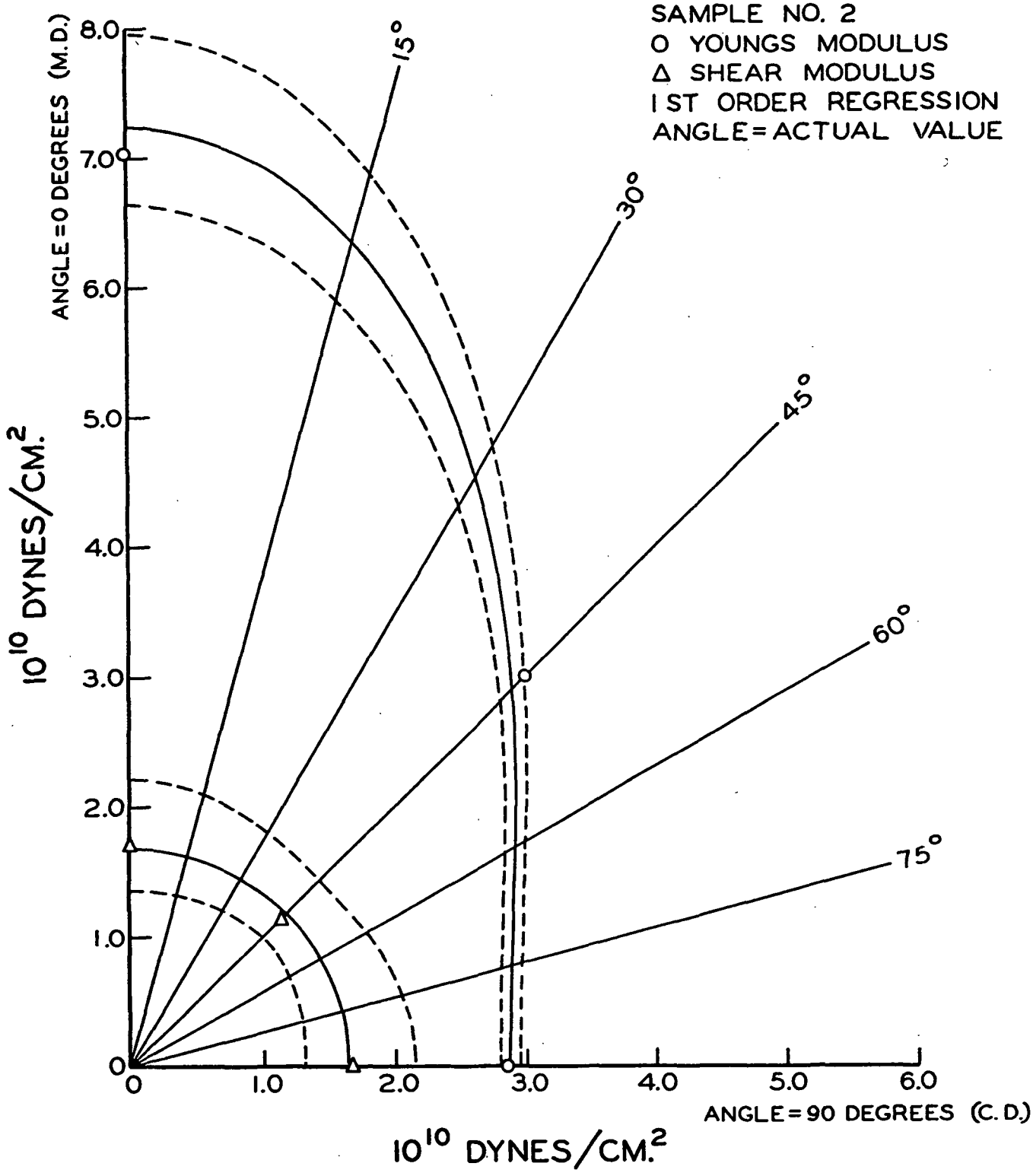

Figure 15. Modulus vs. Angle with 95% Confidence Limits

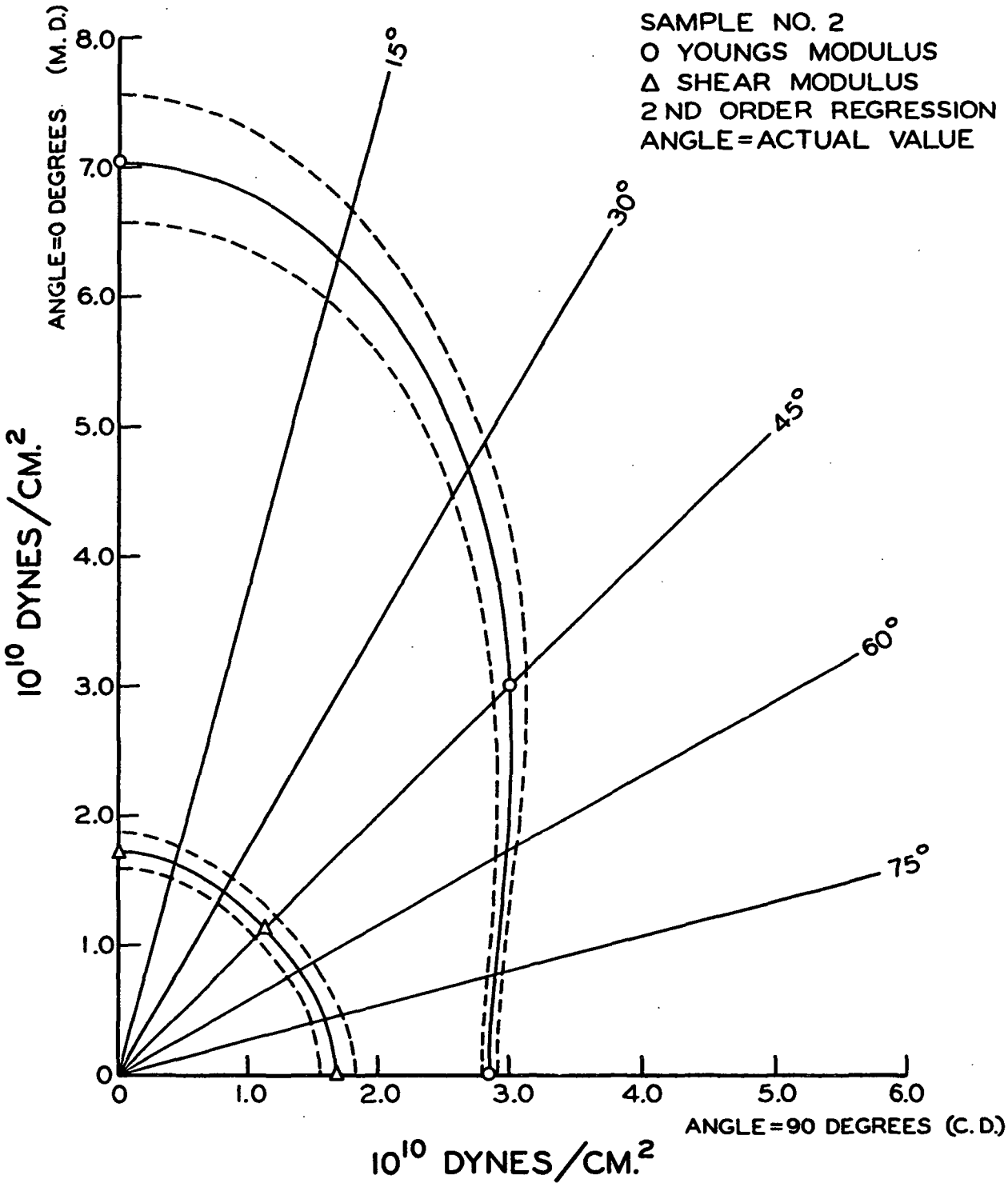

Figure 16. Modulus vs. Angle with 95% Confidence Limits

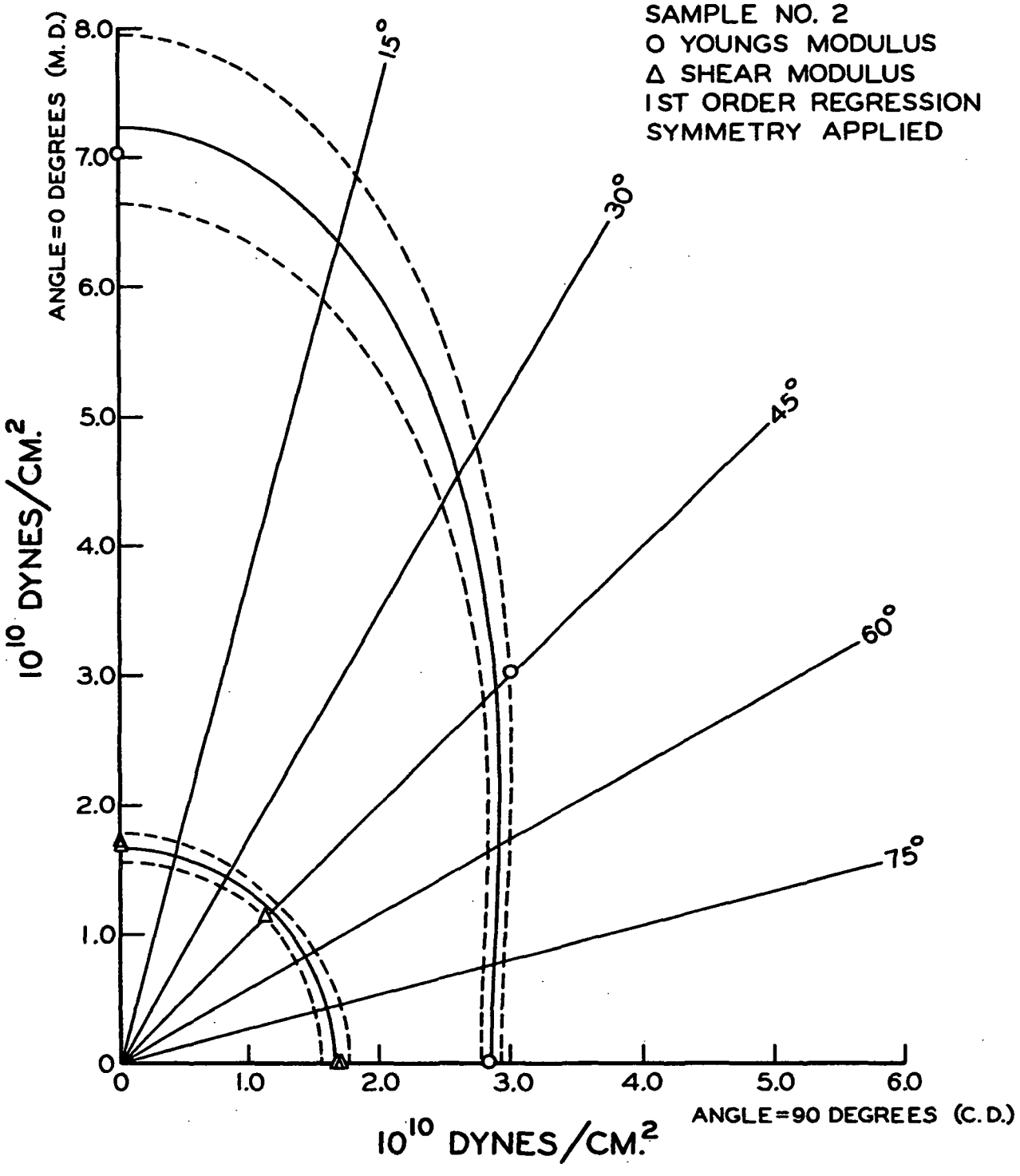

Figure 17. Modulus vs. Angle with 95% Confidence Limits

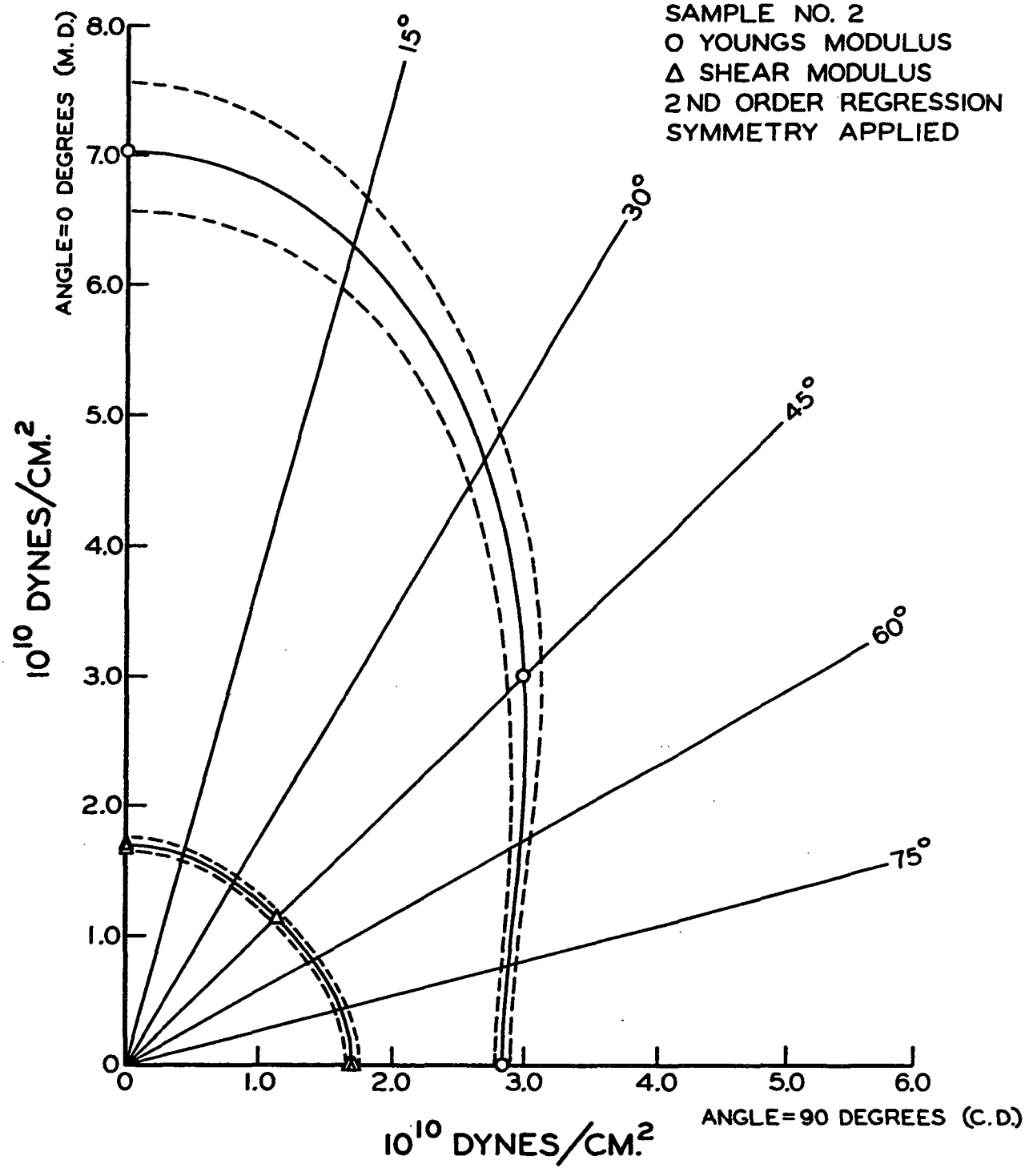

Figure 18. Modulus vs. Angle with 95% Confidence Limits

calculated from the coefficients of these regression curves are listed in Table III. The values for the data points in Fig. 15, 16, 17, and 18 are listed in Appendix III.

TABLE III

PRINCIPAL MODULI FOR SAMPLE 2

Order of Regression Equation	Shear Modulus Symmetry Applied	Young's Modulus dynes/cm.^{2} E_x	E_y	Shear Modulus dynes/cm.^{2} G_{xy}	Poisson's Ratio ν_{xy}	ν_{yx}
Campbell (1st order)	No	7.24×10^{10}	2.86×10^{10}	1.68×10^{10}	0.393	0.155
Orthotropic (2nd order)	No	7.03	2.84	1.71	0.477	0.193
Campbell (1st order)	Yes	7.24	2.86	1.66	0.412	0.163
Orthotropic (2nd order)	Yes	7.03	2.84	1.70	0.495	0.200

ANALYSIS OF VARIANCE

Using the F-test to compare the residual mean square with the experimental variance, a significant lack of fit at the 0.01 level was found for all first-order regression equations. No meaningful test was possible for the second-order regressions because data were available at only three orientations. The 95% confidence limits on the second-order regression curves are based on the testing error associated with each data point.

POISSON'S RATIOS

The experimentally determined values of Poisson's ratio are compared with the values predicted from the regression equation coefficients in Table IV. Experimental and predicted values of the ratio of Poisson's ratio to the corresponding Young's modulus are also presented.

TABLE IV

EXPERIMENTAL AND PREDICTED POISSON'S RATIOS
FOR SAMPLE 2

Identification	Poisson's Ratio		Modulus Ratio, $cm.^2/dyne$	
	ν_{xy}	ν_{yx}	ν_{xy}/E_x	ν_{yx}/E_y
Experimental	0.449	0.226	6.59×10^{-12}	8.92×10^{-12}
Campbell (actual data)	0.393	0.155	5.43	5.43
Orthotropic (actual data)	0.477	0.193	6.78	6.78
Campbell (symmetry applied)	0.412	0.163	5.70	5.70
Orthotropic (symmetry applied)	0.495	0.200	7.05	7.05

The 95% confidence limits on the experimental values of Poisson's ratio are $\nu_{xy} = 0.449 \pm 0.121$ and $\nu_{yx} = 0.226 \pm 0.069$. On the basis of these limits it is not possible to differentiate between the first-order or second-order regression models. There is no significant difference between the experimentally measured modulus ratios ν_{xy}/E_x and ν_{yx}/E_y.

SAMPLE 33 (REGULAR KRAFT SACK PAPER)

This sample was also a commercially produced regular kraft sack paper. The physical properties of Sample 33 were different in magnitude from those measured for Sample 30, but the two samples were very similar in appearance. The basis weight of this sample was 82.9 $g./m.^2$. The sample thickness was 0.01594 cm., and the density was 0.520 $g./cm.^3$.

Measurements of the shear modulus were made in the machine and cross-machine directions and at 15° intervals between these extremes. Two sets of Young's modulus determinations were made. In the first case tensile specimens were cut in a direction parallel to the shear modulus cylinder blanks. A second set of specimens was cut at right angles to the orientation of the shear modulus blanks. The second set of specimens corresponded to the direction $90°-\theta$. The two sets of data in a given direction were used to obtain an estimate of the sample variation as indicated in the section above describing the analysis of variance.

DATA

Polar diagrams of the various regression curves are presented in Fig. 19, 20, 21, and 22. The outer two curves for each set of data shown are the 95% confidence limits on the regression. The principal moduli calculated from the regression coefficients are presented in Table V. The experimental values for each data point are listed in Appendix III.

TABLE V

PRINCIPAL MODULI FOR SAMPLE 33

Order of Regression Equation	Shear Modulus Symmetry Applied	Young's Modulus, dynes/cm.^{2} $\underline{E}_x$	$\underline{E}_y$	Modulus, dynes/cm.^{2} $\underline{G}_{xy}$	Poisson's Ratio ν_{xy}	ν_{yx}
Campbell (1st order)	No	4.69×10^{10}	2.13×10^{10}	1.27×10^{10}	0.245	0.112
Orthotropic (2nd order)	No	4.73	2.14	1.34	0.364	0.165
Campbell (1st order)	Yes	4.69	2.13	1.30	0.211	0.096
Orthotropic (2nd order)	Yes	4.73	2.14	1.37	0.346	0.157

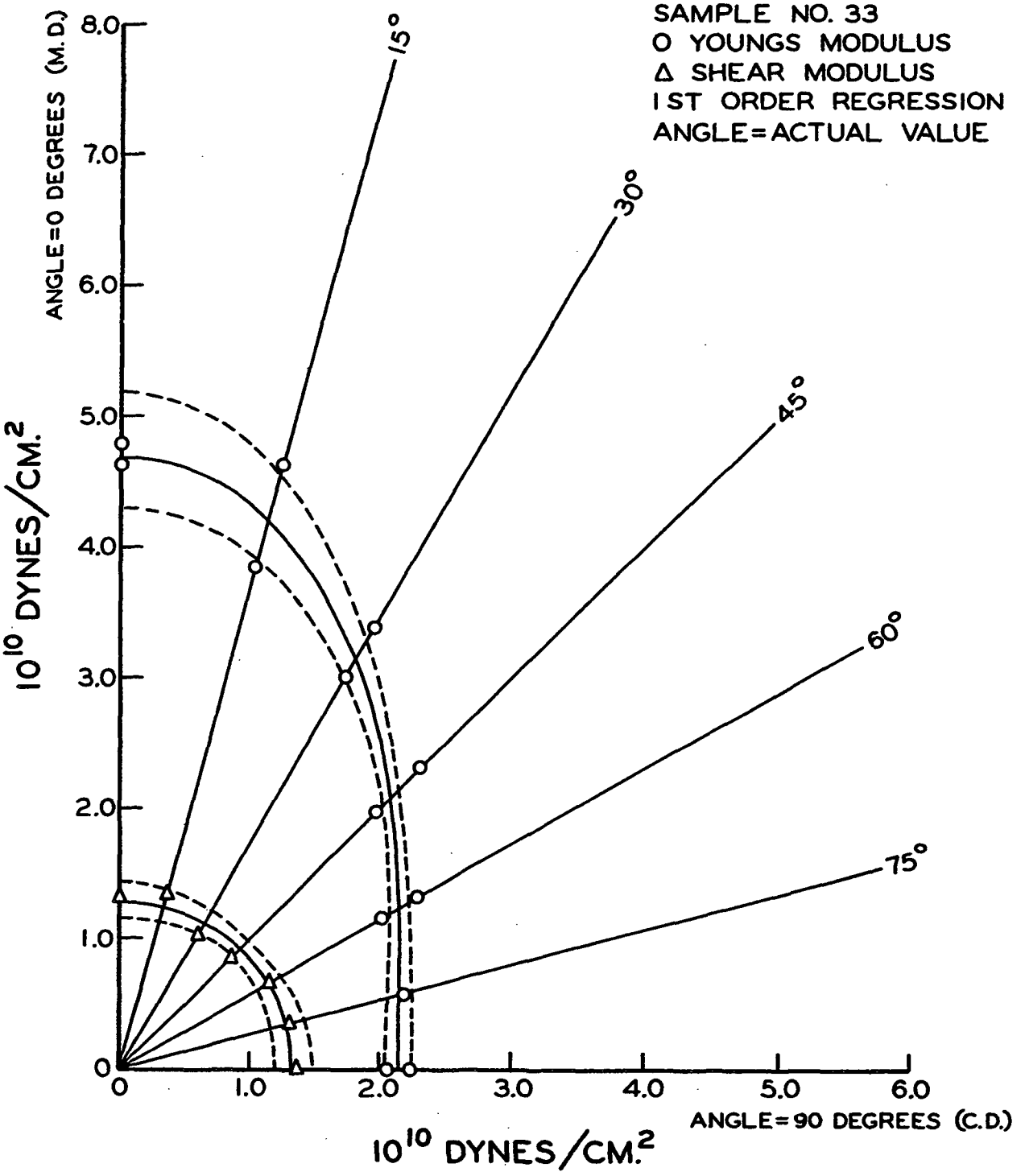

Figure 19. Modulus vs. Angle with 95% Confidence Limits

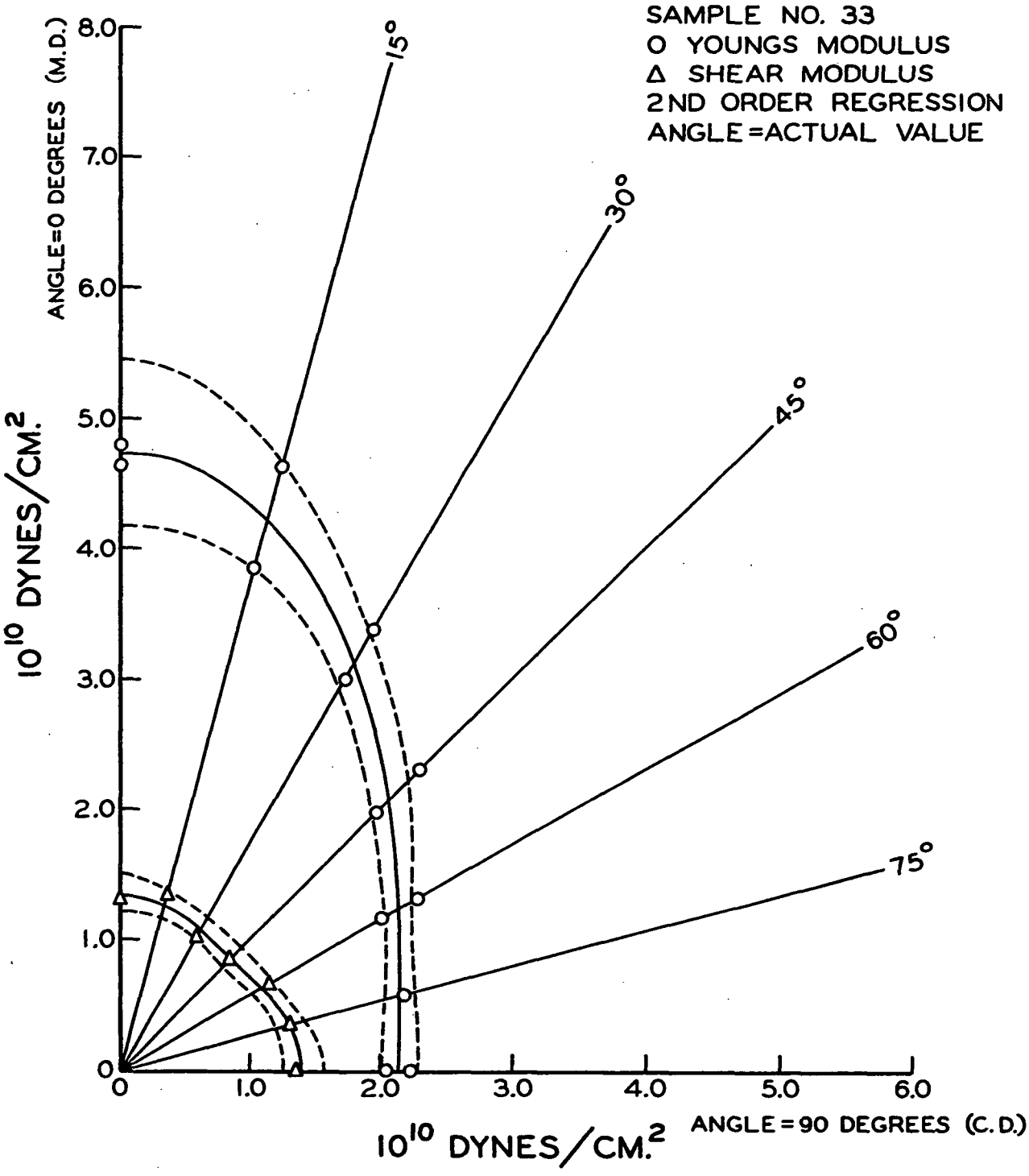

Figure 20. Modulus vs. Angle with 95% Confidence Limits

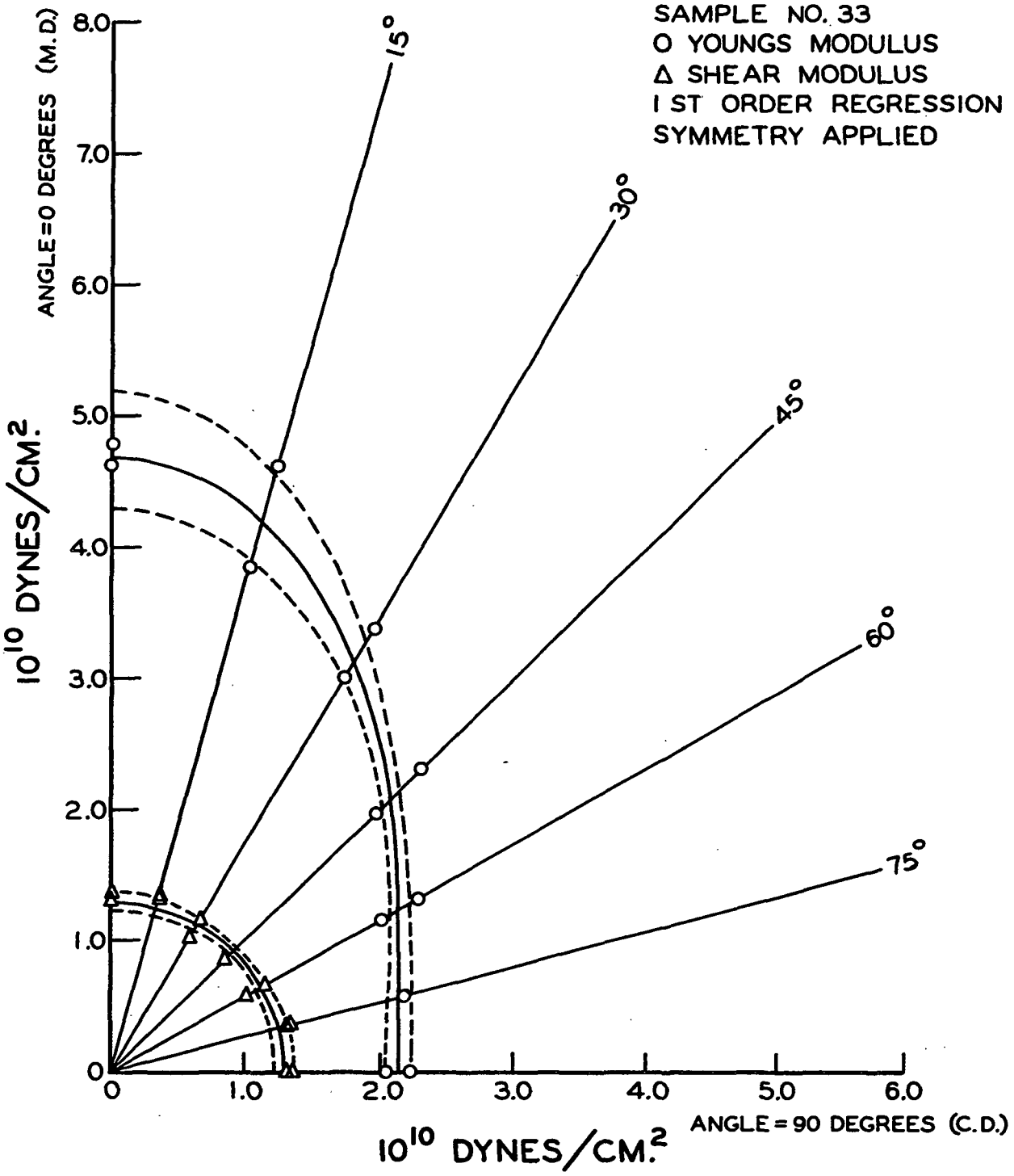

Figure 21. Modulus vs. Angle with 95% Confidence Limits

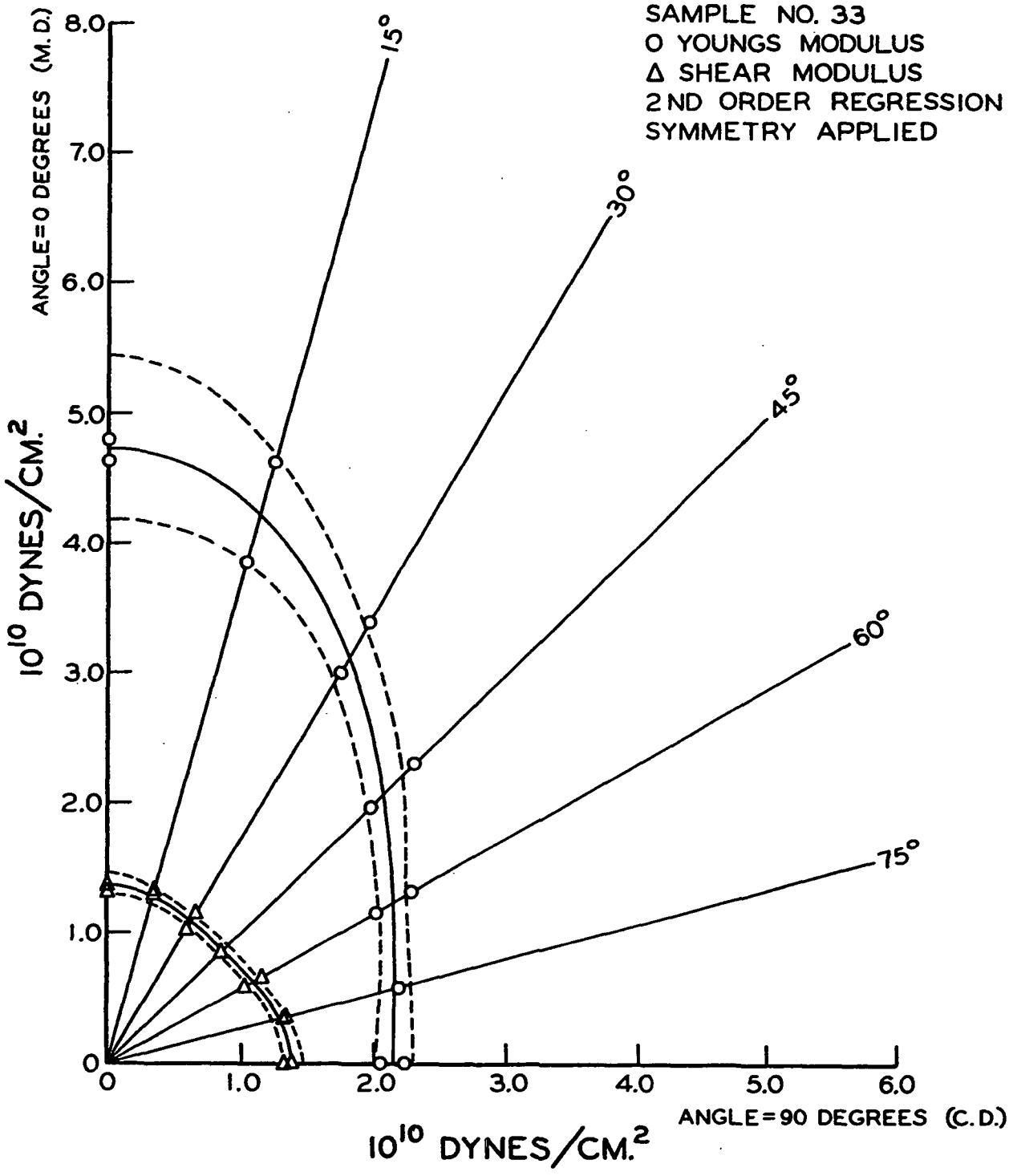

Figure 22. Modulus vs. Angle with 95% Confidence Limits

ANALYSIS OF VARIANCE

No significant lack of fit at the 0.10 level was found between either the first- or second-order regression mean square residual and experimental variance. This was true for both the shear modulus and Young's modulus predictions.

In all cases the lack of fit F-ratio for first-order regressions was larger than the corresponding F-ratio for the second-order regressions. However, this was a statistically nonsignificant trend.

POISSON'S RATIOS

Table VI contains both experimentally determined and predicted values of Poisson's ratios.

TABLE VI

COMPARISON OF EXPERIMENTAL AND PREDICTED POISSON'S RATIOS FOR SAMPLE 33

Identification	Poisson's Ratio		Modulus Ratio, $cm.^2/dyne$	
	ν_{xy}	ν_{yx}	ν_{xy}/E_x	ν_{yx}/E_y
Experimental	0.561	0.187	11.44×10^{-12}	11.15×10^{-12}
Campbell (actual data)	0.245	0.112	5.23	5.23
Orthotropic (actual data)	0.364	0.165	7.69	7.69
Campbell (symmetry applied)	0.211	0.096	4.49	4.49
Orthotropic (symmetry applied)	0.346	0.157	7.32	7.32

The 95% confidence limits for the two experimental values of Poisson's ratio are $\nu_{xy} = 0.561 \pm 0.128$ and $\nu_{yx} = 0.187 \pm 0.094$. There is no significant

difference between the experimental and any of the predicted values of $\nu_{\underline{yx}}$. However, the experimental value of $\nu_{\underline{xy}}$ is significantly larger than the predicted values of this quantity.

An estimate of $\nu_{\underline{xy}}$ was calculated considering measurements made at the lower of the two strain values. This value with its 95% confidence limits was $\nu_{\underline{xy}} = 0.474 \pm 0.107$. The lower end of this confidence range corresponds to the values predicted by the second-order regression equations.

There is no significant difference between the experimentally measured modulus ratios, and there is no significant difference between these values and the modulus ratios predicted by the second-order regression equations. However, the experimental modulus ratios are significantly larger at the 0.05 level than those predicted by the first-order regression equations.

SAMPLE 2440 (LINERBOARD)

This sample was a kraft linerboard produced in a Southern mill on a fourdrinier machine. The basis weight of the sample was 213.0 g./m.^{2}. The sheet thickness was 0.03056 cm., and the density was 0.697 g./cm.^{3}.

The sample was obtained as a 38-inch width roll. After sheets were lapped from the roll, they retained some of the curvature of the roll circumference.

Measurements of the shear modulus and Young's modulus were made at 15° intervals. As described for Sample 33, tensile specimens were cut at orientations both parallel and perpendicular to the shear modulus cylinder blanks. This was done to obtain an estimate of the sample variation.

DATA

Graphs in polar coordinates of the several regression curves are presented in Fig. 23, 24, 25, and 26. The two curves at the extremes of each set of data points are 95% confidence limits on the regression curve. The principal moduli calculated from the regression equation coefficients are given in Table VII. The experimental values of modulus variation with angle and their variances are presented in Appendix III.

TABLE VII

PRINCIPAL MODULI FOR SAMPLE 2440

Order of Regression Equation	Shear Modulus Symmetry Applied	Young's Modulus, dynes/cm.^{2} E_x	E_y	Shear Modulus, dynes/cm.^{2} G_{xy}	Poisson's Ratio ν_{xy}	ν_{yx}
Campbell (1st order)	No	6.44×10^{10}	2.44×10^{10}	1.64×10^{10}	0.147	0.056
Orthotropic (2nd order)	No	6.28	2.42	1.68	0.190	0.073
Campbell (1st order)	Yes	6.44	2.44	1.64	0.150	0.057
Orthotropic (2nd order)	Yes	6.28	2.42	1.68	0.191	0.074

ANALYSIS OF VARIANCE

For the Young's modulus regressions no significant lack of fit at the 0.10 level was found between the residual mean square and the experimental variance. However, the first-order regressions for shear modulus data showed a significant lack of fit at the 0.01 level. No significant lack of fit for the second-order shear modulus regression was found at the 0.10 level.

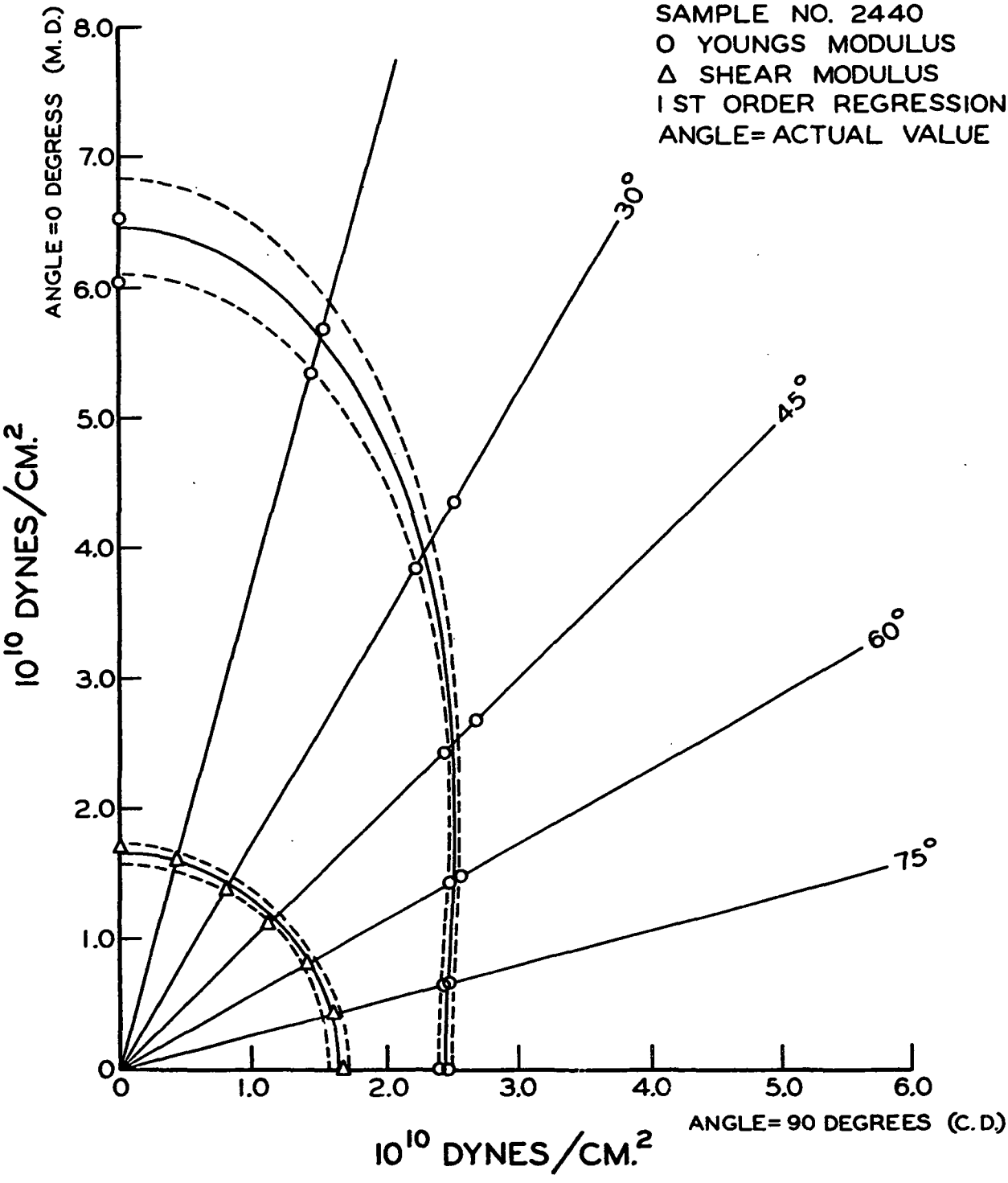

Figure 23. Modulus vs. Angle with 95% Confidence Limits

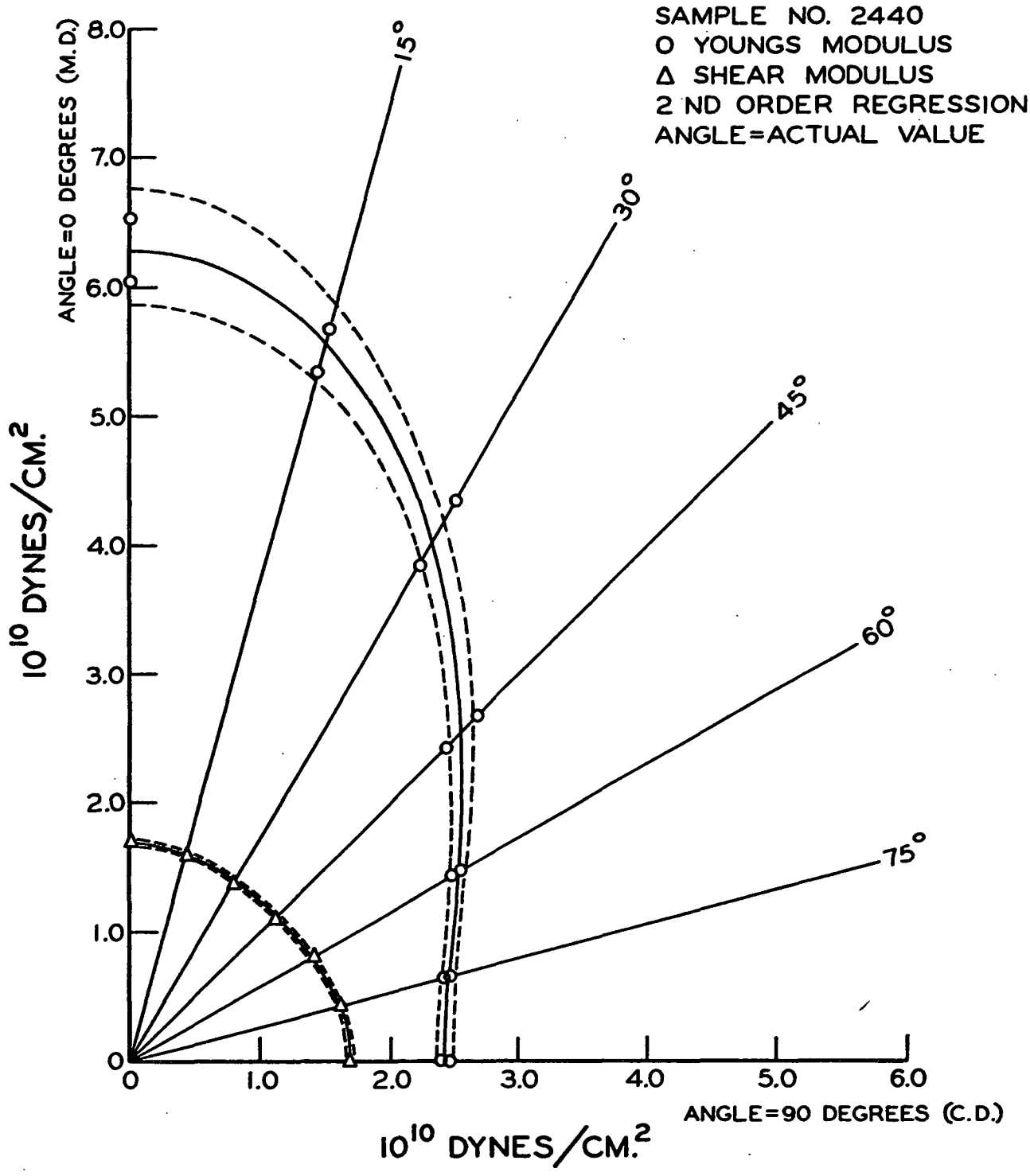

Figure 24. Modulus vs. Angle with 95% Confidence Limits

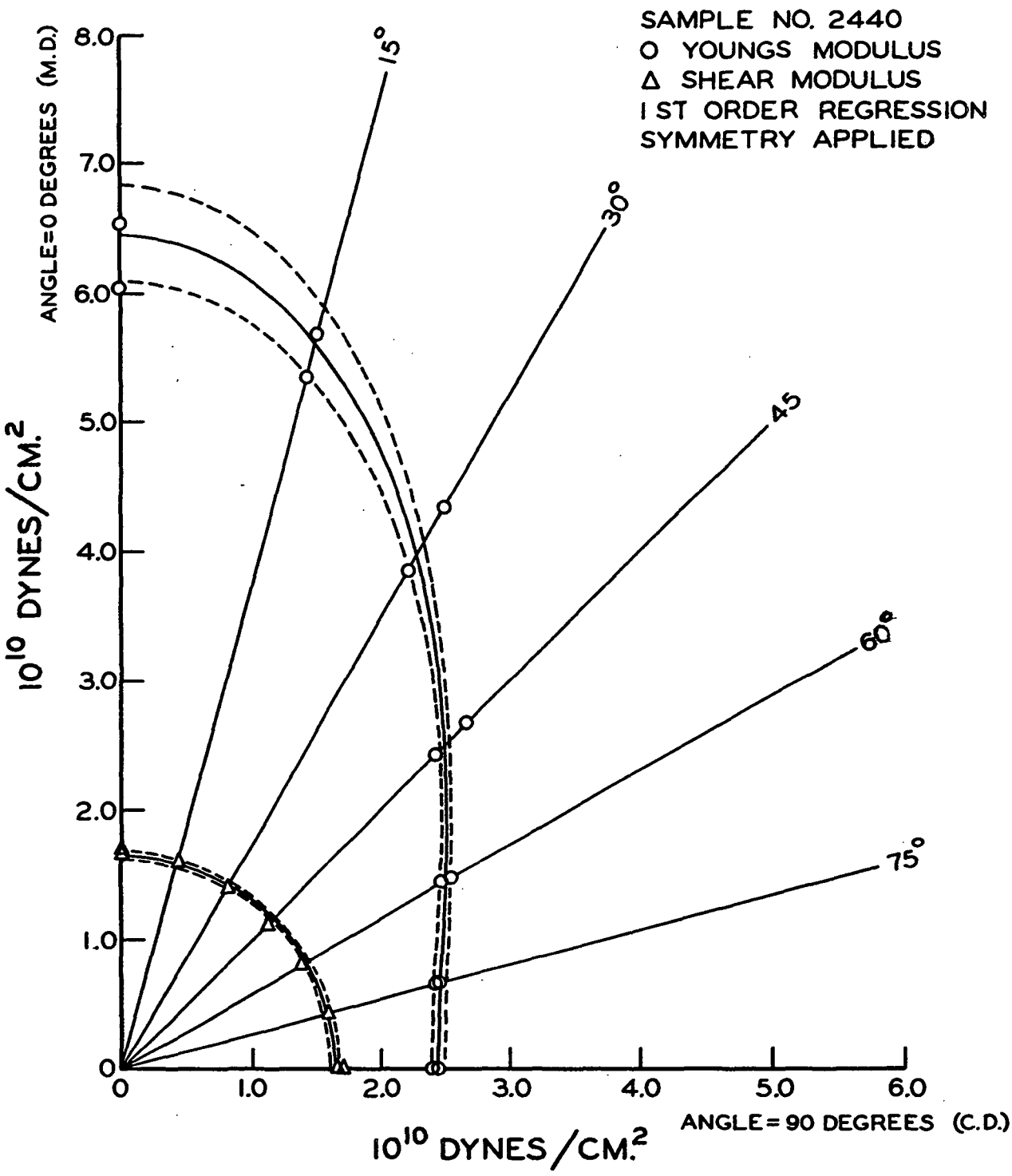

Figure 25. Modulus vs. Angle with 95% Confidence Limits

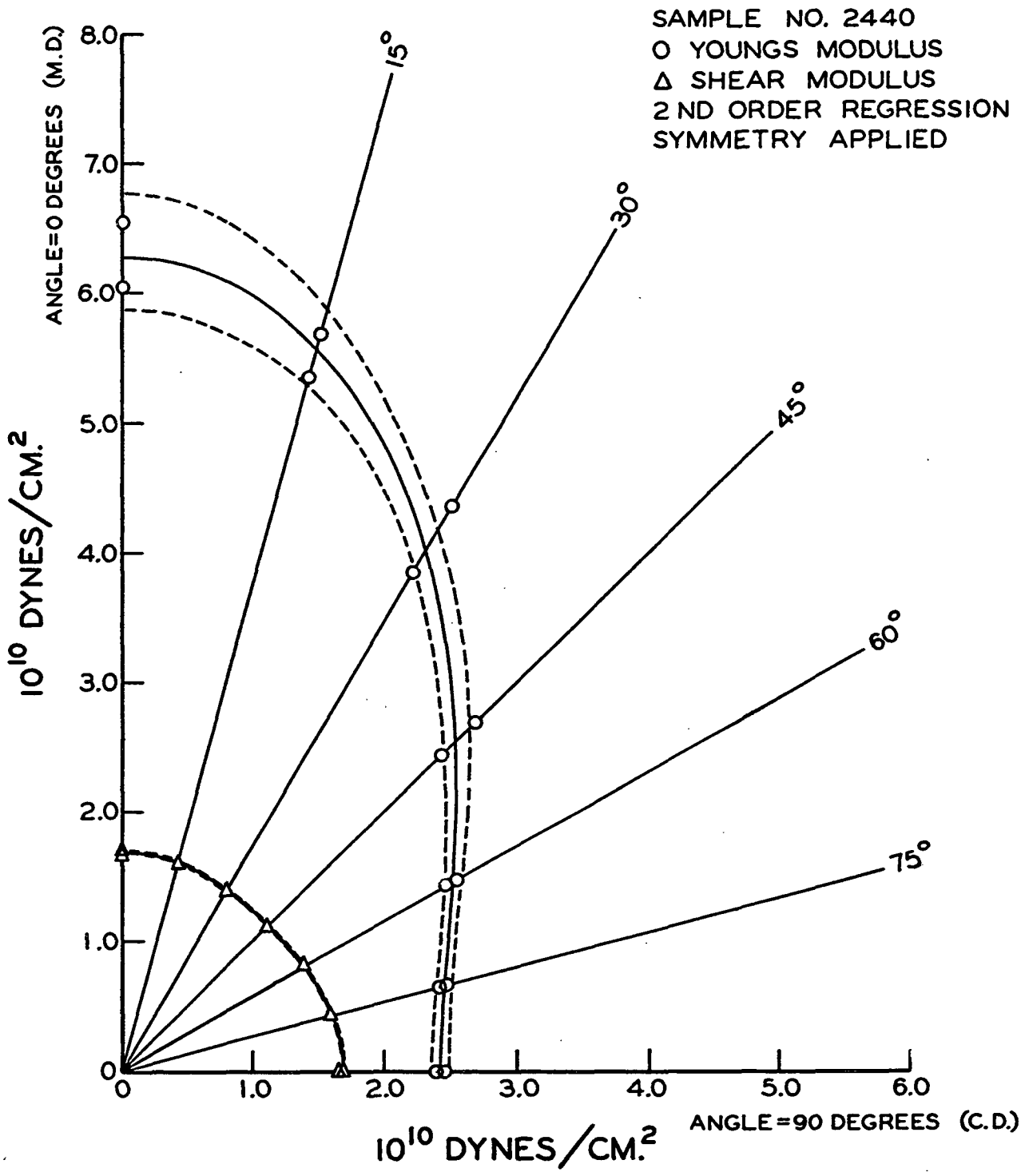

Figure 26. Modulus vs. Angle with 95% Confidence Limits

POISSON's RATIOS

Experimental and predicted values of Poisson's ratio are presented in Table VIII.

TABLE VIII

COMPARISON OF EXPERIMENTAL AND PREDICTED POISSON'S RATIOS FOR SAMPLE 2440

Identification	Poisson's Ratios		Modulus Ratio, $cm.^2/dyne$	
	ν_{xy}	ν_{yx}	ν_{xy}/E_x	ν_{yx}/E_y
Experimental	0.573	0.102	9.17×10^{-12}	4.67×10^{-12}
Campbell (actual data)	0.147	0.056	2.28	2.28
Orthotropic (actual data)	0.190	0.073	3.02	3.02
Campbell (symmetry applied)	0.150	0.057	2.32	2.23
Orthotropic (symmetry applied)	0.191	0.074	3.05	3.05

The 95% confidence limits for the two experimentally determined Poisson's ratios are $\nu_{xy} = 0.573 \pm 0.153$ and $\nu_{yx} = 0.102 \pm 0.048$. There is no significant difference between any of the predicted values of ν_{yx} and the experimental value. However, the values predicted by the second-order regression are more nearly equal to the experimental value.

The experimental value of ν_{xy} is significantly larger than any of the predicted values for this modulus.

The modulus ratio, ν_{yx}/E_y, is significantly larger than those predicted by the linear regressions, but is not significantly greater than the modulus ratio

predicted from the second-order regression coefficients. Also, the two experimentally determined modulus ratios are significantly different at the 0.05 level.

SAMPLE 72 (EXTENSIBLE KRAFT SACK PAPER)

This sample was an extensible kraft sack paper produced on a commercial fourdrinier at a Southern mill. The basis weight of this sample was 89.5 g./m.^{2}. The sample had a density of 0.646 g./cm.^{3}, and a thickness of 0.01330 cm.

Measurements of the shear modulus and Young's modulus were made at seven angular orientations as described for the previous sample.

DATA

Graphs of the several regression curves computed from these data are presented in Fig. 27, 28, 29, and 30. These figures are plotted in polar coordinates. The outer two curves for each set of data are the 95% confidence limits on the regression curve. The principal moduli calculated from the regression curve coefficients are given in Table IX. The values of the points shown on these figures are listed in Appendix III.

ANALYSIS OF VARIANCE

A comparison of the residual mean square with the experimental variance for each regression equation was made. A significant lack of fit at the 0.10 level was found for first-order regressions on both the Young's modulus and shear modulus data. No significant lack of fit at the 0.10 level was found for the second-order regression equations for the Young's modulus and shear modulus data.

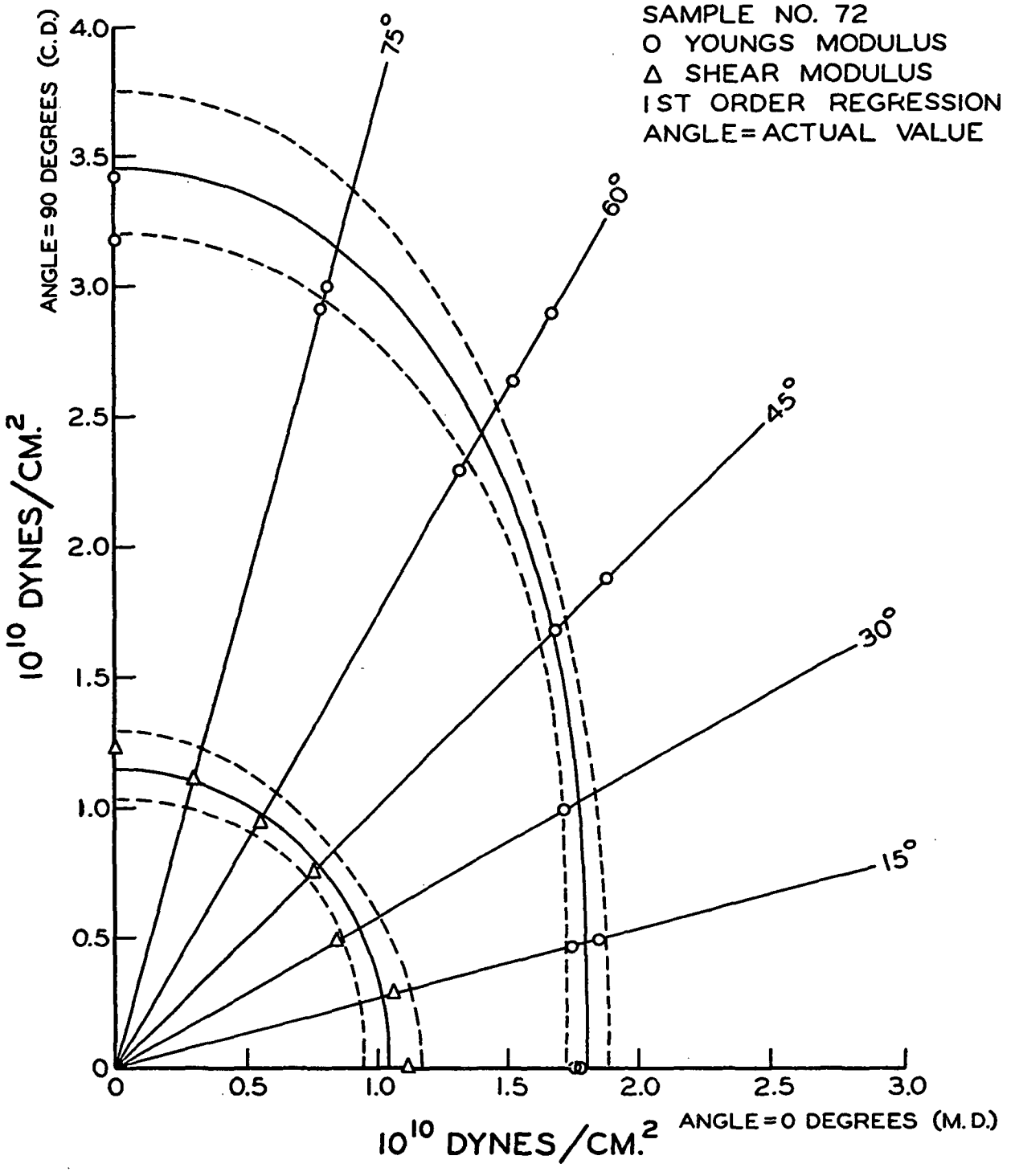

Figure 27. Modulus vs. Angle with 95% Confidence Limits

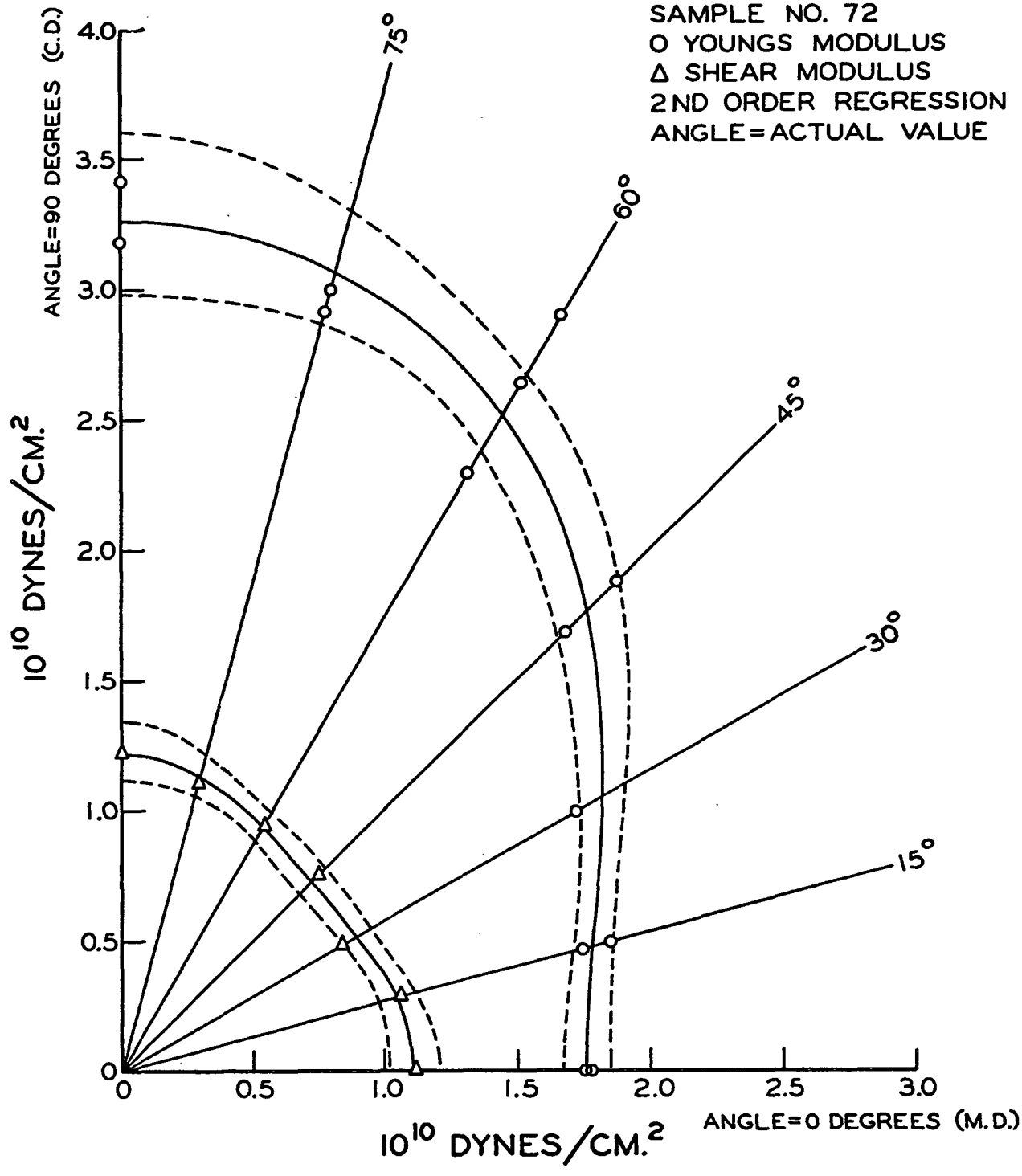

Figure 28. Modulus vs. Angle with 95% Confidence Limits

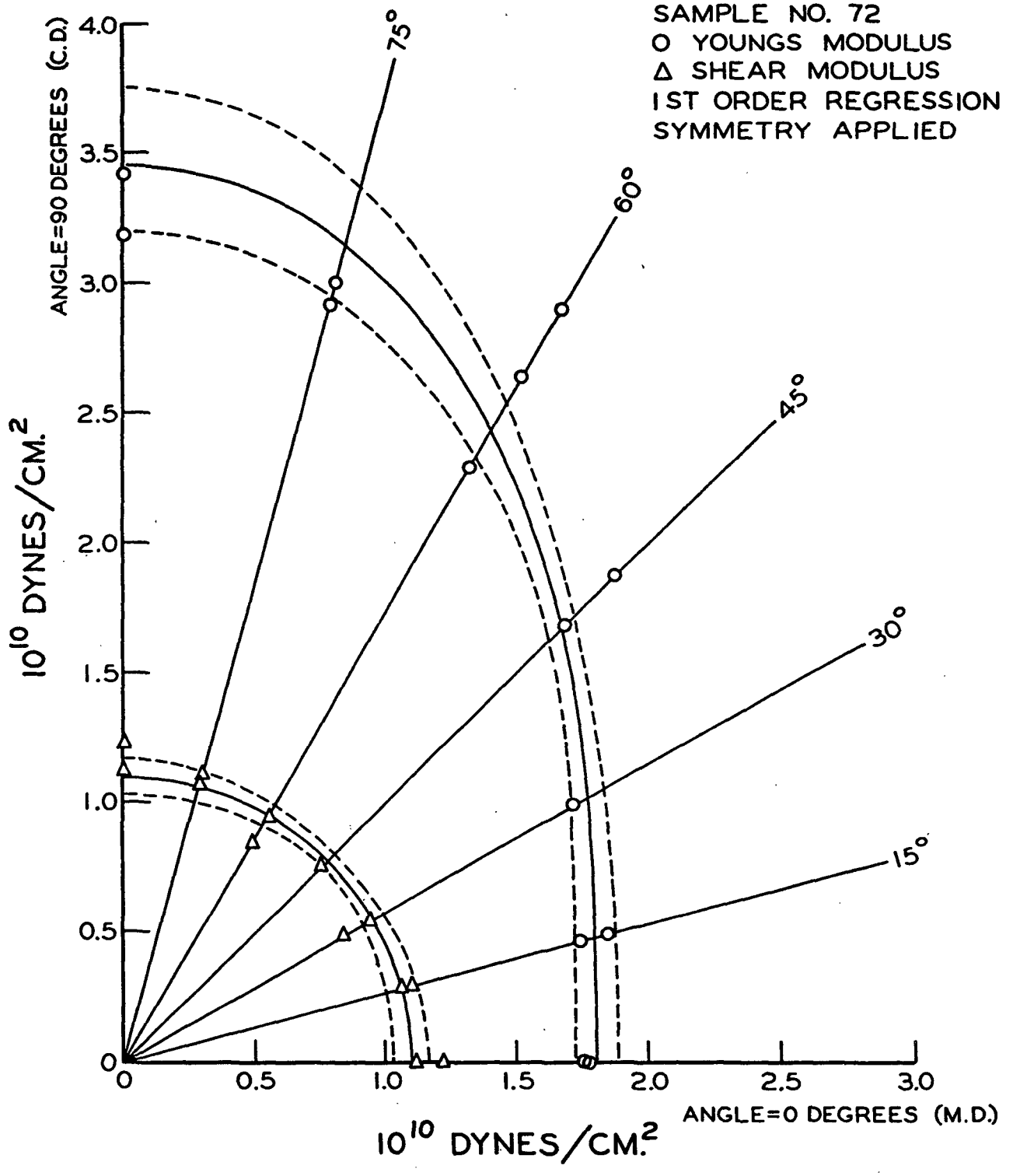

Figure 29. Modulus vs. Angle with 95% Confidence Limits

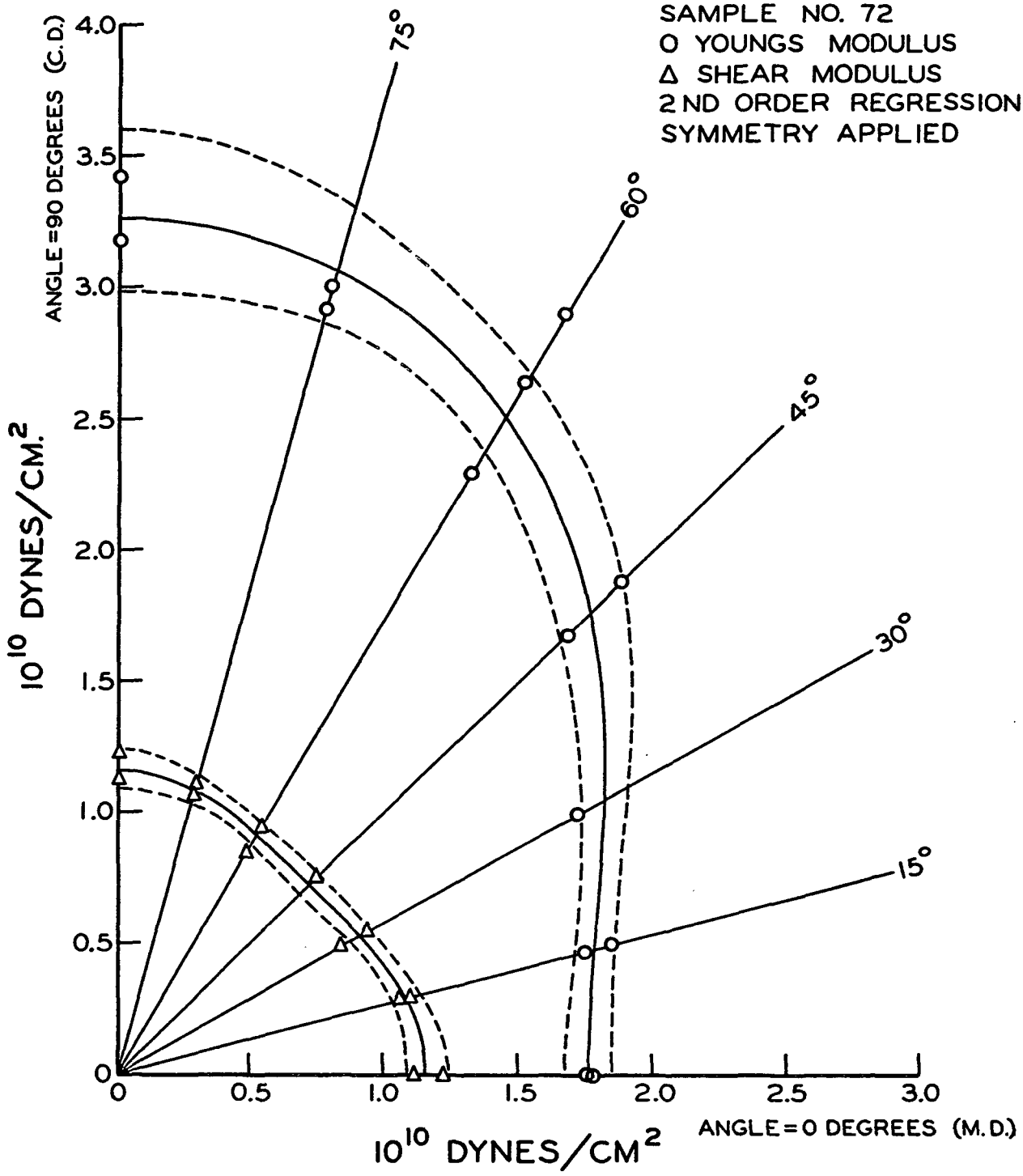

Figure 30. Modulus vs. Angle with 95% Confidence Limits

TABLE IX

PRINCIPAL MODULI FOR SAMPLE 72

Order of Regression Equation	Shear Modulus Symmetry Applied	Young's Modulus, dynes/cm.^{2} E_x	E_y	Shear Modulus, dynes/cm.^{2} G_{xy}	Poisson's Ratio ν_{xy}	ν_{yx}
Campbell (1st order)	No	1.80×10^{10}	3.46×10^{10}	1.05×10^{10}	0.097	0.187
Orthotropic (2nd order)	No	1.75	3.26	1.11	0.153	0.285
Campbell (1st order)	Yes	1.80	3.46	1.10	0.060	0.116
Orthotropic (2nd order)	Yes	1.75	3.26	1.16	0.117	0.218

POISSON'S RATIO

A comparison between experimentally measured and predicted values of Poisson's ratio is presented in Table X.

TABLE X

COMPARISON OF EXPERIMENTAL AND PREDICTED POISSON'S RATIOS FOR SAMPLE 72

Identification	Poisson's Ratio ν_{xy}	ν_{yx}	Modulus Ratio, cm.^{2}/dyne ν_{xy}/E_x	ν_{yx}/E_y
Experimental	0.350	0.240	21.11×10^{-12}	6.95×10^{-12}
Campbell (actual data)	0.097	0.187	5.41	5.41
Orthotropic (actual data)	0.153	0.285	8.73	8.73
Campbell (symmetry applied)	0.060	0.116	3.36	3.36
Orthotropic (symmetry applied)	0.117	0.218	6.68	6.68

The experimental value of Poisson's ratio for stress in the machine direction, $\nu_{\underline{xy}}$, is significantly larger than all of the predicted values of this quantity. There is no significant difference between the experimental value of $\nu_{\underline{yx}}$ and values predicted from the second-order regressions or the value predicted from the first-order regression in which the actual shear modulus data were used. The predicted value of $\nu_{\underline{yx}}$ from the first-order regression in which the shear modulus symmetry condition was adopted is significantly lower than the experimental value. The 95% confidence limits for the experimental Poisson's ratios are $\nu_{\underline{xy}} = 0.350 \pm 0.108$ and $\nu_{\underline{yx}} = 0.240 \pm 0.091$.

The experimental values of the modulus ratio are significantly different. There is no significant difference between the experimental modulus ratio $\nu_{\underline{yx}}/E_{\underline{y}}$ and the values predicted from the second-order regressions and the first-order regression in which the actual shear modulus data were used.

DISCUSSION OF RESULTS

To obtain experimental verification of a model for describing the elastic behavior of paper, predicted values of Poisson's ratio were compared to experimentally measured values. Statistical tests were made to determine how well the particular elasticity model conformed to the experimental Young's modulus and shear modulus data.

POISSON'S RATIO

For a valid comparison of experimental and predicted values of Poisson's ratio, an accurate estimate of the experimental value is required. An examination of the Poisson's ratio data shows only two experimental values to be less than the largest predicted value, the value ν_{xy} for Sample 2 and the value ν_{yx} for Sample 72. For all other samples the experimentally determined Poisson's ratios were larger than any of the corresponding predicted values. Experimental values for ν_{xy} for Samples 30, 2440, and 72 were significantly larger than the largest of the corresponding predicted values.

MODULUS RATIO

The modulus ratio is defined as the ratio of Poisson's ratio to Young's modulus when stress is applied in the same direction for each modulus, for example, ν_{xy}/E_x. For both the orthotropic model and the relationships proposed by Campbell (10), it is predicted that the modulus ratios are equal for two stresses applied at perpendicular directions. Equation (9) is a statement of this for stresses in the x- and y-directions. Love (48) demonstrates that this must be true for any anisotropic material.

This criterion provides a check on the validity of experimental measurements of Poisson's ratio. Of the measurements made, the modulus ratios, υ_{xy}/E_x and υ_{yx}/E_y, are significantly different for Samples 2440 and 72. This indicates that these measurements of Poisson's ratio are not accurate.

Since the experimental values for both Poisson's ratio and the modulus ratio tended to be larger than the predicted values for these quantities, it is possible that the experimental technique is biased in this direction. Such a bias could be introduced either by an overestimation of the contraction strain or an underestimation of the tensile strain.

An independent estimate of the tensile strain was available from the load-elongation output of the Instron. A comparison of the tensile strains calculated from glass bead displacement and the Instron tensile strains showed no significant difference.

CONTRACTION STRAIN

As was mentioned in the description of the Poisson's ratio technique, stress-induced dimensional changes were observed which resulted in curvature and waviness of the tensile strip surface. Two distinct phenomena were noticed, a curvature of the strip about a vertical axis, and wrinkling of the surface. The magnitudes of these effects increased with increasing tensile stress. Any deviation of the tensile strip from an initially flat surface will cause an overstatement of the contraction strain measured by the technique used in this thesis. For this reason, the flattening jig, described above, was adopted.

Observations of tensile strips with the flattening jig mounted were made using low-angle side illumination. It was found that strip curvature was inhibited

as was expected. At high tensile stress, however, a shadow pattern indicating surface wrinkles aligned in the direction of stress was observed.

Because of the physical location of the light-source, surface irregularities of less than 4° deviation from a flat surface were not detectable. A calculation of the effect of wrinkles of this size on the measured Poisson's ratio was made (see Appendix V). For a sample with an actual Poisson's ratio of 0.300 the measured value would be 0.50 according to this calculation.

SAMPLE STRESS

Since the tensile strip wrinkling was observed to increase with the tensile stress, it should be possible to observe an increase in the experimental value of Poisson's ratio with increasing stress. A comparison of this type was made for Samples 30, 33, 72, and 2440 by neglecting strain measurements made at the highest level of stress.

For Sample 30 the Poisson's ratio obtained from all the data was $\nu_{\underline{xy}} = 0.476 \pm 0.076$. The value calculated, when the high tensile strain measurements were neglected, was $\nu_{\underline{xy}} = 0.448 \pm 0.114$. For Sample 33 the Poisson's ratio from all measurements was $\nu_{\underline{xy}} = 0.561 \pm 0.128$. When the high strain measurements were omitted from this average, the value was $\nu_{\underline{xy}} = 0.474 \pm 0.107$. The 95% confidence limits are given with these averages.

For Sample 72 the comparison was $\nu_{\underline{xy}} = 0.350$ from all data and $\nu_{\underline{xy}} = 0.307$ from only the low tensile strain measurements. No differences were found for Sample 2440.

Measurements of $\nu_{\underline{xy}}$ for Samples 30, 33, and 72 were, therefore, reduced by considering only low tensile strain results. A similar recalculation was made for the experimentally determined values of $\nu_{\underline{yx}}$ for these samples with the same results.

The data obtained for Sample 2 did not exhibit increased contraction strain with increased tensile stress. This sample was the most uniform in appearance of all the samples tested in this thesis. That is, the formation of the sheet was exceptionally uniform, and the sheets were flat with no apparent cockle.

The data obtained for Sample 2440 also showed little improvement by neglecting the high tensile strain measurements. Test specimens cut from this sample showed a tendency to curl rather than remain flat. It is felt that this contributed to the value of the Poisson's ratio measurements made on the sample.

Based on visual comparisons of the samples tested, it is felt that the sheet formation and the flatness of the sample were related to the magnitude of the measured Poisson's ratios.

STRAIN CORRECTION

In the above comparisons between experimental Poisson's ratios at high and low tensile stress, the stress at the high strain was about 40% greater than the stress at the lower strain level. If it is assumed that the contribution to the contraction strain, as measured in the above comparisons, is linear with the tensile stress, the experimental values may be corrected to neglect this effect.

Such a correction was applied to the experimentally determined Poisson's ratios for Samples 30, 33, and 72. In Table XI the corrected and uncorrected experimental measurements of Poisson's ratio are compared to the Poisson's ratios predicted by the first-order and second-order regression equations. The predicted values of Poisson's ratio are from regressions in which the shear modulus symmetry condition was applied.

TABLE XI

COMPARISON OF CORRECTED AND PREDICTED POISSON'S RATIOS

Identification	Sample 30		Sample 33		Sample 72	
	$\nu_{\underline{xy}}$	$\nu_{\underline{yx}}$	$\nu_{\underline{xy}}$	$\nu_{\underline{yx}}$	$\nu_{\underline{xy}}$	$\nu_{\underline{yx}}$
Experimental (uncorrected)	0.476	0.207	0.561	0.187	0.350	0.240
Experimental (corrected)	0.406	0.210	0.344	0.140	0.211	0.211
Campbell's proposal	0.191	0.085	0.211	0.096	0.060	0.116
Orthotropic model	0.395	0.182	0.346	0.157	0.117	0.218

The above discussion points to inaccuracy in the experimentally determined Poisson's ratios. Based on the corrected experimental values, the orthotropic model appears to have adequately predicted the mechanical behavior of paper. However, as the tensile strain increases, the orthotropic model, as well as Campbell's proposal underestimated the values of Poisson's ratio.

It is possible that the effective contraction of paper or paperboard will be increased due to stress-induced wrinkling when tensile loading conditions other than those of the Instron are applied. Loading situations in which contraction is of importance should be examined in view of this possibility.

ELASTICITY MODELS

Analyses of variance were made to compare the form of the two elasticity models with the experimental data. With the exception of the Young's modulus prediction for Sample 30, the scatter about the orthotropic model predictions was not significantly greater than that expected due to experimental variation.

As was explained, the estimate of experimental variance was understated for Sample 30. This was felt to cause the significant difference noted.

On the other hand, the scatter, particularly for the shear modulus data, about the first-order regression equations was significantly larger than that expected based on the experimental variation. This lends strong evidence for the applicability of the orthotropic model.

COMPARISON OF THE TWO MODELS

Young's Modulus

It was found that the variation in Young's modulus with direction was often adequately described by either the first-order or second-order regression equations. The shapes of the two regression curves were found to be very nearly the same over the range of the data for all samples tested. Because of this similarity, it is easy to understand why Horio and Onogi (8) chose the simpler form of Equation (1) to describe their measurements.

Shear Modulus

The orthotropic model was found to describe the variation of the shear modulus with angle. However, the greatest variation in the magnitude of the shear modulus was found to be about 14% (Sample 72). For this reason, the value predicted by the linear model was in error at most by 7.5% for the samples tested in this thesis.

However, as was discussed in a previous section, Campbell's prediction for the shear modulus, Equation (10), implies that the shear modulus does not vary with direction in the plane of the sheet. In general, it was found that

shear modulus did vary with direction in the plane of the sheet. This fact demonstrates that Campbell's proposal is inadequate to describe paper elasticity.

ORTHOTROPIC MODEL

The equations for an orthotropic material relating the variation in Young's modulus and the shear modulus to direction in the xy-plane were examined in an attempt to compare them with Campbell's proposal (10). The derivatives of Equations (7) and (8) were taken with respect to angle. These derivatives were equated to zero to obtain the orientations at which the respective moduli were maximum or minimum values. The details of this calculation are presented in Appendix VI.

For the variation of Young's modulus with direction it was found that the machine and cross-machine directions ($\theta = 0°$ and $\theta = 90°$) were the only solutions of this calculation provided that the following inequality holds:

$$(1 + \upsilon_{yx})/E_y > 1/2G_{xy} > (1 + \upsilon_{xy})/E_x \quad . \tag{44}$$

Based on experimentally measured values for the parameters involved, this relation was found to hold for all of the samples tested in this thesis.

The minimum-maximum values for the Young's modulus prediction are another way of expressing the similarity between the orthotropic and first-order models, Equation (7) and Equation (1). In both cases the only minimum-maximum orientations are the machine and cross-machine directions.

For the variation of shear modulus with angle it was found that the minimum-maximum orientations were 0°, 45°, and 90° in the general case. A redundant solution corresponded to the shear modulus prediction of Campbell (10), Equation (10).

Poisson's Ratio

As was discussed in a previous section, the corrected Poisson's ratios agree with the predictions of the orthotropic model. Although the first-order regression equations provide reasonable approximations to the Young's modulus and shear modulus data, the Poisson's ratios predicted by these approximations were found to be low.

Based on the experimental evidence discussed above, it was concluded that the elastic behavior of paper for stresses parallel to the xy-plane of the sheet could be described by the orthotropic model, provided that the tensile strain is low.

Campbell's Proposal

The equation used by Horio and Onogi (8), Equation (1), is based on a derivation in which the tensile strain at an orientation θ is assumed to be a simple angular function of the tensile strains in the machine and cross-machine directions.

The derivation does not consider the Poisson's contractions associated with tensile strain in these two principal directions. It is likely that this fact accounts for the low predictions of Poisson's ratios by Campbell's proposal.

z-DIRECTION MODULI

The conclusion that the mechanical behavior of paper for stresses parallel to the xy-plane conforms to the orthotropic model is a necessary but not a sufficient condition for establishing whether or not paper behaves as an orthotropic material. Measurements of moduli in all principal planes of the sheet are required before sufficient evidence is available.

Data published with an instrumentation study on the compressibility of paper (49) were used to calculate estimates of the z-direction Young's modulus. These data included compressibility measurements on a book paper and a mimeograph paper.

The slopes of the stress-strain curves increased initially as the compressive stress increased. This was interpreted to be a stress concentration effect caused by the uneven mating of the paper surface and the platen of the compressibility gage. The z-direction Young's moduli were calculated from the slope at a compressive stress of 5.5×10^6 dynes/cm.^{2}. At this point the slopes of the stress-strain curves appeared to have reached a limiting value. The values calculated were 7×10^7 dynes/cm.^{2} for the mimeograph paper and 5×10^8 dynes/cm.^{2} for the book paper.

It is possible that these values understate the actual z-direction Young's modulus. Two factors could account for this. First, the testing method employed involved static loading of the sheet. For this reason compression creep response could cause a relatively slight overestimation of the desired compressive strain. A second possibility is that the compressive stress has been underestimated due to the uneven surface of the paper sheet. Even in the light of these two considerations, however, it is felt that the magnitude of the z-direction Young's modulus is much lower than the Young's moduli in the xy-plane of the sheet.

z-DIRECTION POISSON'S RATIO

Several observations have been published concerning the change in paper thickness during tensile loading. Observing the thickness of paper during straining, Maynard (50) reported the bulk of the sheet to increase. This indicates that

Poisson's ratio in the z-direction for stress in the xy-plane may be negative as defined in this thesis. Sanborn (51) measured the thickness of paper specimens after subjecting them to tensile stress. He found the thickness to decrease to a constant value as the nonrecoverable tensile strain increased. He attributed these observations to a removal of the specimen cockle with straining.

Ranger and Hopkins (43) report measurements of the thickness of tensile specimens while the specimen was subjected to loading. Using a caliper gage having 1/2-inch diameter anvils, they found the thickness of handsheets formed from pulp with little refining to increase as the tensile strain increased. Handsheets formed from highly refined pulp were found to exhibit first a decrease in thickness, at tensile strains less than 0.01, followed by an increase in thickness at high tensile strain.

Data reported (43) for a regular kraft sack paper with stress in the cross-machine direction show a decrease in thickness for tensile strains less than 0.01 followed by increase in specimen thickness with tensile strain. The Poisson's ratio for this sample, ν_{yz}, was about 0.3-0.4. Measurements of specimen thickness were made with 1/8-inch diameter anvils for this sack paper sample.

Ohrn (52) measured paper thickness while tensile load was applied to the sample. The thickness was measured between a 27-mm. diameter platen and a roller 25 mm. in length. He observed both increases and decreases in thickness at low tensile strain. Tracing paper samples showed decreased thickness with initial tensile strains. All samples increased in thickness before failure occurred.

The orthotropic model does not restrict z-direction Poisson's ratios to values greater than zero. That is, stress in the xy-plane could produce an expansion strain in the z-direction. However, none of the orthotropic materials discussed by Barkas (49) exhibit negative values for Poisson's ratios.

Based on the observation of stress-induced wrinkling made in this thesis, it is possible that increases in sample thickness at low tensile strain were influenced by this behavior, particularly when large diameter gage platens were used. It is felt that Poisson's ratios in the z-direction are positive quantities, involving contraction. Increases in the actual specimen thickness at high tensile strain can be attributed to fiber bond failure.

TENSILE INDUCED CURL

As discussed before, it was observed that tensile specimens curled about a vertical axis as the stress in the specimen increased. The convex side of this curl was observed to be toward the wire side of the sheet for the samples tested in this thesis.

The fact that this behavior was found to increase with tensile stress indicates that the structural nature of the samples was responsible. A sheet material composed of layers having different mechanical moduli would be expected to exhibit behavior of this type. Van den Akker (16) has suggested that a theoretical treatment of the mechanical behavior of paper may need to be adjusted to such a model.

There are several mechanisms whereby the structure of paper could conform to such a model. Due to the nature of the formation process, the density of the sheet is lower at the wire-side than at the felt-side of the sheet. Also, the wire mark indicates that the geometrical arrangement of fibers is different at the two surfaces of the sheet.

Danielsen and Steenberg (15) measured the angular orientation of fibers in machine-made papers. They found that the distribution of orientations was different on the wire-side than on the top-side of the sheet.

Lastly, the machine-made samples tested in this thesis were obtained in rolls. Paper in this type of storage is subjected to both tension and compression stresses due to bending. With the exception of Sample 2440, sheets lapped from the rolls appeared to be flat. However, it is possible that stress relaxation phenomena contributed to a mechanical two-sidedness of the samples.

If paper is, mechanically speaking, a layered structure, the moduli of elasticity measured at any orientation represent some average of the moduli for each particular layer. The question arises as to whether these average moduli may be described by the orthotropic model.

HANDSHEET

Test results were obtained for a handsheet formed from a kraft pulp. However, the exceptionally large standard error associated with the average value of Poisson's ratio precluded a meaningful discussion of these results. The sample was very cockled. This is felt to have contributed to the difficulty in measuring Poisson's ratio.

REGRESSION EQUATION COEFFICIENTS

The second-order regression coefficients, defined by Equations (33) through (38), provide two estimates of the quantity $(1 + 2\,\nu_{\underline{xy}})/\underline{E}_{\underline{x}} + (1/\underline{E}_{\underline{y}}) - (1/\underline{G}_{\underline{xy}})$. One of these estimates is from the Young's modulus regression, Equation (35), and the other is from the shear modulus regression coefficient defined by Equation (38). To calculate the values of Poisson's ratio listed in the Experimental Results section, the Young's modulus regression coefficient was used.

In general, the difference between Poisson's ratios calculated from either the Young's modulus coefficient or the shear modulus coefficient was less than ten percent. There was no trend in these differences which indicates that the data for both Young's modulus and the shear modulus were accurately measured.

However, for Sample 30 the second-order regression coefficients $\underline{\underline{B}}_{go}$ and $\underline{\underline{C}}_{go}$ were much lower than expected based on the Young's modulus regression. In addition, the arithmetic signs of $\underline{\underline{B}}_{go}$ and $\underline{\underline{C}}_{go}$ were opposite from what was expected. The Poisson's ratios computed using these coefficients were approximately one-third the magnitude of those calculated with the coefficient $\underline{\underline{C}}_{eo}$.

The shear modulus regression equation for Sample 30 predicts a <u>maximum</u> value at 45° to the machine direction. This is contradictory to the data gathered for all other samples. Since the variation with angle was found to be very small, it is possible that at least a part of the discrepancies noted are due to experimental errors. Since the Poisson's ratios predicted from the Young's modulus coefficient $\underline{\underline{C}}_{eo}$ are in good agreement with the experimentally determined values, the use of these predictions in this case is felt to be justified.

CONCLUSIONS

A method for the measurement of shear moduli in the xy-plane of the sheet has been developed. A cylinder formed from a sheet of the material to be tested is used as the elastic member in a torsion pendulum. After making corrections for the cylinder seam width and for nonideal behavior at the cylinder ends, the circular resonance frequency of the cylinder can be related to the shear modulus of the paper sample.

A method proposed by Ranger and Hopkins (43) and used by Lathrop (44) was modified to measure Poisson's ratios in the xy-plane of the sheet. It was found that by restraining tensile specimen curl with a flattening jig and by extrapolating Poisson's ratio averages to zero tensile stress an accurate estimate of Poisson's ratio was obtained.

The elastic model proposed by Campbell (10) for paper was found to approximately describe the variation of Young's modulus and the shear modulus with direction in the xy-plane of the sheet. The Poisson's ratios predicted by this model were understated by significant amounts.

Campbell's proposal predicts that the shear modulus does not vary with direction in the plane of the sheet. With the exception of one sample, the shear modulus was found to vary with direction in the plane of the sheet. Based on these findings it is concluded that the relationships proposed by Campbell do not adequately describe the elastic behavior of paper.

It has been shown that the orthotropic model describes the low-strain elastic behavior of paper for stresses parallel to the xy-plane of the sheet. The rigorous application of the orthotropic model was found to be limited to very low strains due to stress-induced dimensional aberrations which cause Poisson's contractions

to be overstated. These aberrations were found to be related to the formation of the sheet and were minimized with good sheet uniformity.

It was pointed out that for paper to behave as an orthotropic material it is necessary that the elastic behavior in the xy-plane conform to this model. However, measurements of elastic moduli in other planes are needed to confirm that paper behaves as an orthotropic material.

NOMENCLATURE

A	cylinder amplitude of vibration
A_{eo}	See Equation (33)
A_{go}	See Equation (36)
A_{ec}	See Equation (39)
A_{gc}	See Equation (41)
A_{mn}	general term for above four quantities
B_{eo}	See Equation (34)
B_{go}	See Equation (37)
B_{ec}	See Equation (40)
B_{gc}	See Equation (42)
B_{mn}	general term for above four quantities
C	total cylinder compliance
c	cylinder compliance
c_o	cylinder compliance for length L_o
$\langle c \rangle_{end}$	average cylinder compliance at cylinder ends
C_{eo}	See Equation (35)
C_{go}	See Equation (38)
C_{mn}	general term for above two quantities
d_o	outside cylinder diameter
d_i	inside cylinder diameter
E	Young's modulus
E_θ	Young's modulus in θ direction
E_x	Young's modulus in x direction
E_y	Young's modulus in y-direction
E_z	Young's modulus in z-direction
e	Instron chart length

F	axial force on cylinder
G	shear modulus
G_θ	shear modulus in θ-direction
G_{xy}	shear modulus in xy-plane
G_{xz}	shear modulus in xz-plane
G_{yz}	shear modulus in yz-plane
I	moment of inertia
I_b	moment of inertia of brass weights
k	torsional stiffness
k_b	torsional stiffness with no axial force applied
K	cylinder stiffness (= kL)
L	cylinder length
L_o	free cylinder length, see Equation (21)
L_e	cylinder length associated with end-effect
ℓ, ℓ_1	in Equations (2) and (3) direction parameters
ℓ	variable length for integration
m,m_1	direction parameters, See Equations (2) and (3)
n,n_1	direction parameters, See Equations (2) and (3)
N	torque on cylinder
P	Instron load, pounds
q	viscous damping coefficient
r	cylinder radius
r_b	radial dimension to center of mass of brass weights
t	sheet thickness, or
t	time in seconds
T	period of oscillation
X	independent regression variable equal to $\sin^2\theta$

$\underline{x}$	machine direction in sheet
$\underline{y}$	cross-machine direction in sheet
$\underline{z}$	direction perpendicular to $\underline{xy}$-plane of sheet
α	damping term equal to $\underline{q}/2\underline{I}$
β	resonance frequency of damped cylinder equal to $\sqrt{(\underline{k}/\underline{I}) - 2\alpha^2}$
γ	shear strain
δ	phase angle
ε	tensile strain
θ	angle in $\underline{xy}$-plane measured from $\underline{x}$-direction
κ	angular dimension of cylinder
υ	Poisson's ratio
$\upsilon_{\underline{ij}}$	Poisson's ratio for stress in the $\underline{i}$-direction and contraction strain in the $\underline{j}$-direction
σ	tensile stress
τ	shear stress
$\tau_{\underline{cr}}$	critical shear stress at buckling
ϕ	angle of twist of the cylinder
ω	frequency of vibration
ω_o	resonance frequency

ACKNOWLEDGMENTS

I wish to thank the many persons whose aid and advice made this thesis possible. I particularly want to acknowledge my thesis advisory committee, Dr. J. A. Van den Akker who suggested the dynamic rather than static torsion of cylinders, Mr. James W. Gander, and Mr. Harold H. Heller, whose advice was instrumental in making this thesis a reality.

I want to thank my wife, Susan, for her help in preparing the manuscript and for her continued encouragement.

LITERATURE CITED

1. Van den Akker, J. A. In The formation and structure of paper, Vol. I. p. 205-41, London, Clowes and Sons, 1962.

2. Onogi, S., and Sasaguri, K., Tappi 44, no. 12:874-80(Dec., 1961).

3. Litt, M., J. Colloid Sci. 16, no. 3:297-301(1961).

4. Ivarsson, B., and Steenberg, B., Svensk Papperstid. 50, no. 17:419-32(Sept. 30, 1947).

5. Brezinski, J. P. A study of the viscoelastic properties of paper by means of tensile creep tests. Doctor's Dissertation. Appleton, Wis., The Institute of Paper Chemistry, 1955. 242 p.

6. Hill, R. L. An investigation of the time-dependent structural and mechanical behavior of individual pulp fibers when subjected to an applied stress. Doctor's Dissertation. Appleton, Wis., The Institute of Paper Chemistry, 1966, 120 p.

7. Johanson, F., and Kubat, J., Svensk Papperstid. 67, no. 20:822-32(Oct. 31, 1964).

8. Horio, M., and Onogi, S., J. Appl. Phys. 22, no. 7:971-7(July, 1951).

9. Riemen, W. P., and Kurath, S. F., Tappi 47, no. 10:629-33(Oct., 1964).

10. Campbell, J. G., Australian J. Appl. Sci. 12, no. 3:356-7(1961).

11. Craver, J. K., and Taylor, D. L., Tappi 48, no. 3:142-7(March, 1965).

12. Craver, J. K., and Taylor, D. L. Preprint from Consolidation of the paper web, Cambridge Symposium. London, Clowes and Sons, Sept., 1965.

13. Kubat, J., and Lindbergson, B., Svensk Papperstid. 68, no. 21:743-56(Nov. 15, 1965).

14. Aaltio, E. A., Svensk Papperstid. 63, no. 3:58-61(Feb. 15, 1960).

15. Danielsen, R., and Steenberg, B., Svensk Papperstid. 50, no. 13:311-15(1947).

16. Van den Akker, J. A. Private communication, 1965.

17. Edge, S. R. H., Brit. Paper and Board Maker's Assoc., Proc. Tech. Sect. 25: 210-15(1944).

18. Edge, S. R. H., Chem. and Ind. (London) 67, no. 51:803-7(Dec., 1948).

19. Schulz, J. H., Tappi 44, no. 10:736-44(Oct., 1961).

20. Jentzen, C. A. The effects of stress during drying on some of the properties of individual pulp fibers. Doctor's Disseration. Appleton, Wis., The Institute of Paper Chemistry, 1964, 129 p.

21. Van den Akker, J. A., Tappi 33, no. 8:398-402(Aug., 1950).

22. Steenberg, B., Finnish Paper Timber J. 29, no. 7A:64-9(1947).

23. Kubat, J., Nyborg, L., and Steenberg, B., Svensk Papperstid. 66, no. 19: 754-64(Oct. 14, 1963).

24. Van den Akker, J. A. Unpublished material, 1963.

25. Love, A. E. H. Mathematical theory of elasticity, 4th ed. p. 160-2, New York, Dover Publications, 1944.

26. March, H. W. Stress-strain relations in wood and plywood considered as orthotropic materials, U.S.D.A., Forest Products Lab. Report No. R1503, 1944. 24 p.

27. Wink, W. A., Tappi 44, no. 6:171A-80A(June, 1961).

28. Crook, D. M. (Miss), and Bennett, W. E. The effect of humidity and temperature on the physical properties of paper, Kenley, Surry, The British Paper & Board Industry Research Association, St. Winifred's Laboratories.

29. Wink, W. A., Hardacker, K. W., and Van Eperen, R. H., Tappi 47, no. 1:13-15 (Jan., 1964).

30. Van den Akker, J. A., and Hardacker, K. W., Tappi 41, no. 8:224A-31A(Aug., 1958).

31. Wink, W. A., Hardacker, K. W., Van Eperen, R. H., and Van den Akker, J. A., Tappi 47, no. 1:47-54(Jan., 1964).

32. Constant, F. W. Theoretical physics. p. 209-11. Cambridge, Mass., Addison-Wesley Publishing Co. 1954.

33. Timoshenko, S., and Young, D. H. Strength of materials. 4th ed. p. 113. Princeton, N. J., D. Van Nostrand, 1962.

34. McGraw-Hill Encyclopedia of Science and Technology. Vol. 7. p. 541-3. New York, McGraw-Hill Book Co., 1960.

35. McCoy, E. E., Jr., Matl. Res. Std. 6, no. 4:238-41(May, 1966).

36. Gerard, G., and Becker, H. Handbook of structural stability. Part III. Buckling of curved plates and shells. N.A.C.A. Tech. Note 3783. p. 40-3. Wash., D. C., N.A.C.A., 1957.

37. Timoshenko, S. Strength of materials. Vol. II. Princeton, N. J., D. Van Nostrand Co., 1955.

37a. Sokolnikoff, I. S. Tensor analysis. 2nd ed. p. 336-40. New York, John Wiley & Sons, 1965.

38. Timoshenko, S., and Young, D. H. Strength of materials. 4th ed. p. 70-5. Princeton, N. J., D. Van Nostrand Co., 1962.

39. Van den Akker, J. A. Private communication, Feb., 1966.

40. Love, A. E. H. Mathematical theory of elasticity. 4th Ed. p. 131-2. New York, Dover Publications, 1944.

41. Timoshenko, S. Strength of materials, Vol. II, 3rd Ed. p. 286-91. Princeton, N. J., D. Van Nostrand Co., 1955.

42. Brecht, W., and Wanka, R., Papier 17, no. 4:141-7(April, 1963).

43. Ranger, A. E., and Hopkins, L. F. In The formation and structure of paper. p. 277-301. London, Clowes and Sons, Ltd., 1962.

44. Lathrop, A. Private communication, March, 1965.

45. Staff of The Institute of Paper Chemistry, Paper Trade J. 109, no. 13: 18-22(1939).

46. Davis, O. L. Statistical methods in research and production. 3rd Ed. Revised. p. 150-272. New York, Hafner Publishing Co., 1961.

47. Draper, N. R., and Smith, H. Applied regression analysis. p. 26-31. New York, John Wiley and Sons, 1966.

48. Love, A. E. H. Mathematical theory of elasticity. 4th Ed. p. 107-8. New York, Dover Publications, 1944.

49. Barkas, W. W. The mechanical properties of wood and paper. New York, Interscience Publishers, 1953.

50. Maynard, C. R. G., Paper Maker's Assoc. Brit. and Ireland, Proc. Tech. Sect. 29:470(1958).

51. Sanborn, I. B. A study of irreversible stress-induced changes in the macrostructure of paper. Doctor's Dissertation. Appleton, Wis., The Institute of Paper Chemistry, 1961. 105 p.

52. Ohrn, O. E., Svensk Papperstid. 68, no. 5:141-6(1965).

53. Nelson, R. Computer Program 911B. Appleton, Wis., The Institute of Paper Chemistry, 1964.

54. Davis, O. L. Statistical methods in research and production. 3rd Ed. Revised. p. 208-72. New York, Hafner Publishing Co., 1961.

55. Davies, O. L. Statistical methods in research and production. 3rd Ed. Revised. p. 368-72. New York, Hafner Publishing Co., 1961.

APPENDIX I

EFFECT OF BENDING STRESSES ON THE TORSIONAL RESPONSE OF A PAPER CYLINDER

Consider a sheet of paper wrapped into a cylindrical form with the machine direction, x-axis, along the cylinder circumference and the cross-machine direction, y-axis, parallel with the cylinder axis. Since Young's modulus is generally maximum in the x-direction, this case considers maximum bending stress. Figure 31 pictures a volume element in the cylinder wall:

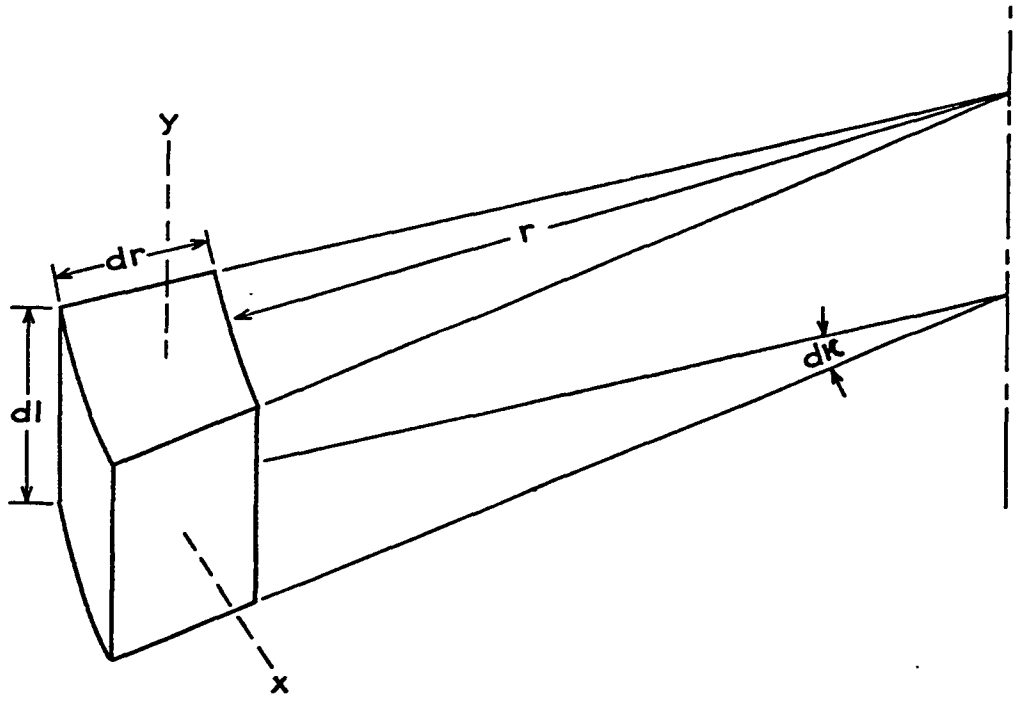

Figure 31. Cylinder Wall Volume Element

The strains in the two principal directions may be expressed as follows:

$$\epsilon_x = (\sigma_x/E_x) - (\sigma_y/E_y)\nu_{yx} \quad , \tag{49}$$

$$\epsilon_y = (\sigma_y/E_y) - (\sigma_x/E_x)\nu_{xy} \quad , \tag{50}$$

where σ_x and σ_y are the stresses in the x- and y-directions. If there is no axial load on the cylinder, and if the cylinder length is large compared to the radius, there is no tensile strain in the y-direction. This is due to inhibition of Poisson's contractions in bending wide plates.

Therefore, from Equation (50),

$$\sigma_y = (\nu_{xy})(E_y/E_x)\sigma_x = \nu_{yx}\sigma_x \quad , \tag{51}$$

and

$$\epsilon_x = (\sigma_x/E_x)(1 - \nu_{xy}\nu_{yx}) \quad .$$

Solving for σ_x,

$$\sigma_x = (E_x \epsilon_x)/(1 - \nu_{xy}\nu_{yx}) \quad . \tag{52}$$

The bending strain may be expressed in terms of the radius of curvature of the cylinder:

$$\epsilon_x = (r - r_m'/r_m) \quad , \tag{53}$$

where r_m is the mean radius of the cylinder wall,

$$r_m = (d_o + d_i)/4 \quad . \tag{54}$$

Expressing the principal stresses in terms of the cylinder radius:

$$\sigma_x = E_x[(r/r_m) - 1]/(1 - \nu_{xy}\nu_{yx}) \quad , \tag{55}$$

$$\sigma_y = E_x\nu_{yx}[(r/r_m) - 1]/(1 - \nu_{xy}\nu_{yx}) \quad . \tag{56}$$

SHEAR STRESSES CONTRIBUTED BY BENDING

If there is no change in the bending moment, there will be no shear stresses in the xz- or yz-planes. This condition is satisfied if the radius of curvature of the paper tube is constant.

Considering an element deformed by shear stress acting in the xy-plane, the bending stress will have the representation shown in Fig. 32.

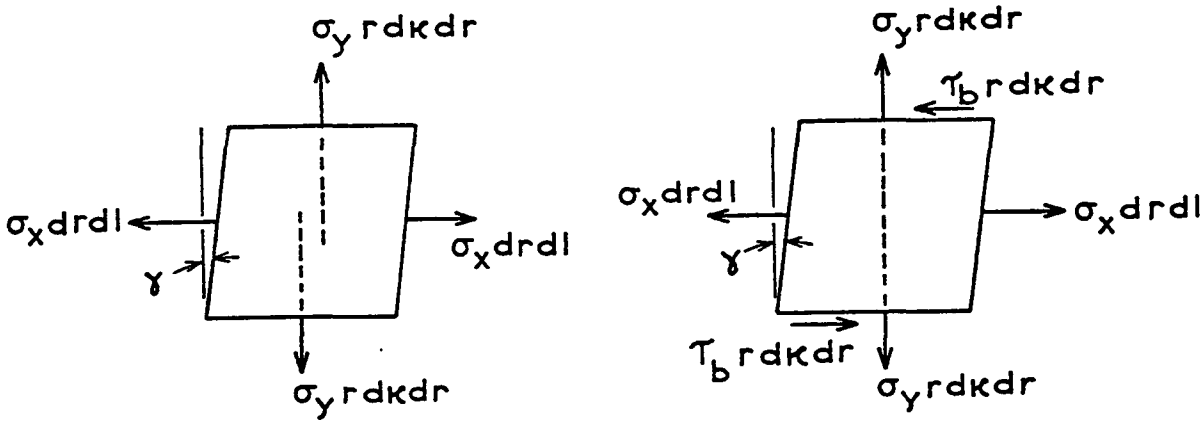

Figure 32. Free Body Diagrams of Volume Elements

These two free body diagrams are equivalent. Taking a sum of moments for each, the value of τ_b may be evaluated. For the left-hand diagram

$$\sum M = 2(\sigma_y r\, d\kappa\, dr)(d\ell/2) \tan \gamma$$

$$\cong \sigma_y r\, d\kappa\, dr\, d\ell\, (\gamma) \quad .$$

For the right-hand diagram

$$\sum M = \tau_b r\, d\kappa\, dr\, d\ell \quad .$$

Therefore,

$$\tau_b = \sigma_y \gamma \quad , \tag{57}$$

where γ is the shear strain and τ_b is the shear stress contribution due to bending. The stress, τ_b, opposes the applied shear stress when $r > r_m$.

TOTAL TORQUE ACTING

The torque acting on the paper cylinder must equal the sum of the shear stress due to bending and the shear stress contributed by conventional shear deformations. The total shear stress is expressed as

$$\tau_t = G_{xy}\gamma + \tau_b \quad . \tag{58}$$

The torque acting on the cylinder may be written as follows:

$$dN = [(G_{xy}\gamma + \sigma_y\gamma) r\, d\kappa\, dr]\, r \quad , \tag{59}$$

but the shear strain, γ, may be expressed in terms of the total angular deformation of the cylinder, ϕ

$$\gamma = r\phi / L \tag{60}$$

where L is the cylinder length.

$$N = \int_{d_i/2}^{d_o/2} \int_0^{2\pi} (G_{xy} + \sigma_y)(r\phi/L) r^2\, d\kappa\, dr$$

and simplifying,

$$N = \frac{G_{xy}\pi(d_o^4 - d_i^4)}{32L}\phi \left\{ 1 + \frac{E_x \nu_{yx}}{G_{xy}(1 - \nu_{xy}\nu_{yx})} \left[-1 + (8/5)\frac{(d_o^5 - d_i^5)}{(d_o + d_i)(d_o^4 - d_i^4)} \right] \right\} \quad (61)$$

The term in brackets is the change in torque due to the bending stresses. Evaluating this term, let

$$d_i = 2.00 \text{ inch}, \quad d_o - d_i = 0.010 \text{ inch}, \quad E_x/G_{xy} = 3.5$$

$$\nu_{yx} = 0.2, \quad \nu_{xy} = 0.4$$

$$\frac{E_x(\nu_{yx})}{G_{xy}(1 - \nu_{xy}\nu_{yx})} \left[-1 + (8/5)\frac{(d_o^5 - d_i^5)}{(d_o + d_i)(d_o^4 - d_i^4)} \right] = 4 \times 10^{-4} .$$

The magnitude of this term is negligible in comparison with the testing error and sample-to-sample variations of the test material.

APPENDIX II

EFFECT OF AXIAL STRESS ON THE TORSIONAL RESPONSE OF A PAPER CYLINDER

Timoshenko (41) indicates a method for treating the case of an axial force acting on a specimen subjected to torsion. Following his example a relationship is presented to describe the effect on the torsional stiffness of a cylinder.

In the elementary theory which relates the shear stresses in a cylinder to the shear strain it is assumed that sides of a volume element remain the same length while the corner angles of the element change. The assumption that cross sections perpendicular to the cylinder axis remain undistorted during torsion is also made. As will be shown, these assumptions are not rigorous.

Consider the volume element shown in Fig. 33.

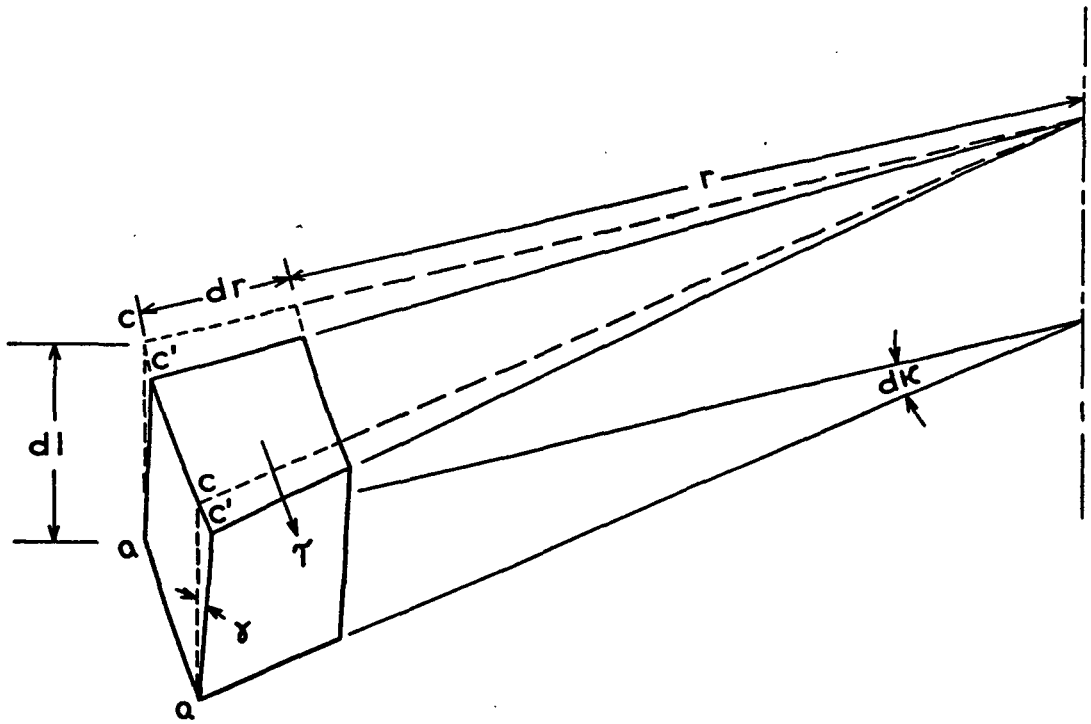

Figure 33. Cylinder Wall Volume Element

If there is no shortening of the cylinder during torsion, there must be a stress component acting along the segment $\overline{ac}$

$$\overline{ac} = \overline{ac}' \cos \gamma = \overline{ac}' \, (1 + 1/2\gamma^2 + \ldots.) \quad ,$$

where γ is the shear strain. The shear strain may be expressed

$$\gamma = r\phi \, L \quad ,$$

where r is the radius associated with the shear strain, ϕ is the angular deformation of the free end of the cylinder, and L is the cylinder length.

Combining the above two relations, the strain along the segment $\overline{ac}$ may be expressed as follows:

$$\varepsilon = (\overline{ac}' - \overline{ac})/(\overline{ac}') \cong 1/2 \, [r^2 \phi^2/L^2] \tag{62}$$

Let ε_o be the unit amount of shortening along the axis of the cylinder due to torsion; then, the axial stress acting on the cylinder is

$$\sigma = (E/2)(r^2\phi^2)/L^2 - E\varepsilon_o \tag{63}$$

where E is Young's modulus in the direction $\overline{ac}$. This states the condition that cross sections of the cylinder remain parallel and undistorted during torsion.

Integration of this stress across the cross section of the cylinder should yield the axial force acting on the cylinder. Performing this integration and solving for the unit amount of shortening:

$$\varepsilon_o = (\phi^2/16L^2)(d_o^2 + d_i^2) - (4F/\pi E)/(d_o^2 - d_i^2) \quad , \tag{64}$$

where F is the axial force acting on the cylinder. Equation (64) is then combined with Equation (63) to eliminate the term ε_o.

SHEAR STRESS

There will be a component of the axial stress, Equation (63), acting in the direction of the applied shear stress:

$$\tau' = \sigma \sin \gamma \cong \sigma \, r\phi/L \tag{65}$$

The total torque may then be expressed in differential form:

$$dN = \left[(Gr\phi/L + \tau')rd\kappa \, dr\right]r \quad .$$

Integrating,

$$N = (\pi G\theta/32L)(d_o^4 - d_i^4)\left[1 + (E\phi^2/12GL^2)(d_o^4 + d_o^2d_i^2 + d_i^2)/(d_o^2 + d_i^2) - (E\phi^2/11GL^2)(d_o^2 + d_i^2) + (4F/\pi G)/(d_o^2 - d_i^2)\right] \quad . \tag{66}$$

Using Equation (66), the following comparison between the cylinder torsional stiffness with axial force acting, k, and without axial force, k_b, can be made:

$$(k - k_b)/k_b = [(4F/\pi G)/(d_o^2 - d_i^2)] - (E\phi^2/132L^2G)(d_o^4 + 13d_o^2d_i^2 + d_i^2)/(d_o^2 + d_i^2) \quad . \tag{67}$$

Substituting maximum experimental values for these parameters into Equation (67) it is found that

$$(k - k_b)/k_b = 4.74 \times 10^{-4}$$

The magnitude of this difference indicates that the effect of axial load on the cylinder's response to torsion is negligible.

APPENDIX III

EXPERIMENTAL DATA

The values included in Tables XIII, XIV, XV, XVI, and XVII are the average Young's moduli and shear moduli determined for each machine-made paper tested for this thesis. The number of replicate measurements made and the standard error for the average modulus are presented with each value.

TABLE XIII

YOUNG'S MODULUS AND SHEAR MODULUS DATA
FOR SAMPLE 2

Angle[a], degrees	Young's Modulus, dynes/cm.^{2}	No. of Observations	Standard Error	Shear Modulus[b], dynes/cm.^{2}	No. of Observations	Standard Error
θ	$\underline{E}_\theta$			$\underline{G}_\theta$		
0	7.03×10^{10}	20	0.047×10^{10}	1.71×10^{10}	3	0.011×10^{10}
45	4.24	20	0.022	1.59	4	0.003
90	2.84	6	0.020	1.68	3	0.010
90	2.83	5	0.029	--	--	--

[a]Angle measured from the machine direction.
[b]End-effect and seam width correction totaled -10.48%.

TABLE XIV

Angle[a], degrees	Young's Modulus, dynes/cm.^{2}	No. of Observations	Standard Error	Shear Modulus[b], dynes/cm.^{2}	No. of Observations	Standard Error
θ	$\underline{E}_\theta$			$\underline{G}_\theta$		
0	5.52×10^{10}	14	0.042×10^{10}	1.50×10^{10}	1	--
15	4.92	10	0.036	1.60	4	0.009×10^{10}
30	4.24	9	0.042	1.54	4	0.018
45	3.59	12	0.033	1.56	4	0.019
60	3.06	11	0.042	1.51	1	--
75	2.62	11	0.017	1.50	1	--
90	2.34	8	0.017	1.56	4	0.025

[a]Angle measured from the machine direction.
[b]End-effect and seam width corrections totaled -3.2%.

TABLE XV

YOUNG'S MODULUS AND SHEAR MODULUS DATA
FOR SAMPLE 33

Angle[a], degrees	Young's Modulus, dynes/cm.^{2}	No. of Observations	Standard Error	Shear Modulus[b], dynes/cm.^{2}	No. of Observations	Standard Error
θ	E_θ			G_θ		
0	4.79×10^{10}	15	0.106×10^{10}	1.31×10^{10}	3	0.043×10^{10}
0	4.62	12	0.089	--	--	--
15	4.78	17	0.039	1.38	1	--
15	3.97	6	0.056	--	--	--
30	3.90	11	0.030	1.18	2	0.017
30	3.46	10	0.035	--	--	--
45	2.69	10	0.036	1.20	2	0.142
45	3.25	4	0.031	--	--	--
45	2.78	15	0.057	--	--	--
60	2.32	9	0.081	1.32	2	0.005
60	2.63	11	0.013	--	--	--
75	2.25	11	0.029	1.35	1	--
90	2.23	21	0.016	1.36	1	--
90	2.05	11	0.014	--	--	--

[a] Angle measured from the machine direction.

[b] End-effect and seam width corrections totaled -6.0%.

TABLE XVI

YOUNG'S MODULUS AND SHEAR MODULUS DATA
FOR SAMPLE 2440

Angle[a], degrees θ	Young's Modulus, dynes/cm.^{2} $\underline{E}_\theta$	No. of Observations	Standard Error	Shear Modulus[b], dynes/cm.^{2} $\underline{G}_\theta$	No. of Observations	Standard Error
0	6.53×10^{10}	8	0.086×10^{10}	1.70×10^{10}	2	0.001×10^{10}
0	6.04	10	0.043	--	--	--
15	5.53	8	0.044	1.64	2	0.009
15	5.87	6	0.048	--	--	--
30	4.43	8	0.040	1.60	2	0.008
30	5.01	7	0.021	--	--	--
45	3.44	8	0.021	1.57	3	0.013
45	3.80	9	0.023	--	--	--
60	2.85	10	0.011	1.62	2	0.013
60	2.94	8	0.025	--	--	--
75	2.51	11	0.013	1.65	2	0.012
75	2.54	9	0.011	--	--	--
90	2.46	11	0.013	1.67	2	0.005
90	2.40	10	0.006	--	--	--

[a]Angle measured from the machine direction.

[b]End-effect and seam width corrections totaled -3.2%.

TABLE XVII

YOUNG'S MODULUS AND SHEAR MODULUS DATA
FOR SAMPLE 72

Angle[a], degrees θ	Young's Modulus, dynes/cm.^{2} E_θ	No. of Observations	Standard Error	Shear Modulus[b], dynes/cm.^{2} G_θ	No. of Observations	Standard Error
0	1.76×10^{10}	6	0.049×10^{10}	1.12×10^{10}	2	0.011×10^{10}
0	1.75	6	0.068	--	--	--
15	1.80	8	0.034	1.09	2	0.025
15	1.90	7	0.024	--	--	--
30	1.97	6	0.044	0.97	2	0.011
45	2.37	3	0.054	1.05	2	0.007
45	2.65	10	0.038	--	--	--
60	2.64	5	0.047	1.09	2	0.015
60	3.34	9	0.027	--	--	--
75	3.01	5	0.025	1.15	2	0.008
75	3.10	8	0.021	--	--	--
90	3.41	6	0.036	1.22	2	0.010
90	3.19	6	0.039	--	--	--

[a] Angle measured from the machine direction.

[b] End-effect and seam width corrections totaled -8.24%.

APPENDIX IV

SAMPLE CALCULATION OF REGRESSION EQUATIONS AND THE ANALYSIS OF VARIANCE

The data used in this calculation is that reported in Table XIV of Appendix III for the variation of Young's modulus and the shear modulus with direction determined on Sample 30.

REGRESSION EQUATIONS

YOUNG'S MODULUS

The independent variable $\underline{X}$, for all regression analysis is the quantity $\underline{X} = \sin^2\theta$, where θ is the angle measured from the $\underline{x}$-direction (machine-direction). For Young's modulus regression equations the dependent variable, $\underline{Y}$, is the quantity $1/\underline{E}_\theta$ where $\underline{E}_\theta$ is Young's modulus at orientation θ.

Regression equations were determined using a computer program by Nelson (53) for multiple and curvilinear regression. The program was based on the technique of matrix inversion described by Davies (54).

For linear regression the equation calculated was

$$Y = (1.791 \times 10^{-11}) + (2.228 \times 10^{-11})X \quad .$$

The sum of squares removed by regression was 4.963×10^{-22}. The sum of squares present before the regression was made was 5.090×10^{-22}. The residual variance about the regression was 2.532×10^{-24}.

The test variance was calculated from the scatter of individual measurements at a given angular orientation about the average at that orientation. Based on 68 degrees of freedom the test variance was calculated to be 2.44×10^{-25}.

If the regression equation adequately fits the experimental data, the residual mean square, the residual variance, should be statistically identical with the experimental error variance. For this case only the test variance is available. The variance ratio is $(2.532 \times 10^{-24})/(2.44 \times 10^{-25}) = 10.4$. Based on 5 degrees of freedom for the numurator and 68 degrees of freedom for the denominator this ratio was found to be significant at the 0.01 level (55).

Similar calculations for a second-order regression on these data gave the following results:

$$Y = (1.902 \times 10^{-11}) + (1.200 \times 10^{-11})X + (1.028 \times 10^{-11})X^2 \quad ,$$

where the sum of squares removed by the regression was 5.027×10^{-22}, the sum of squares before the regression was 5.090×10^{-22}, and the residual variance about the regression was 1.573×10^{-24}. The variance ratio for lack of fit was $(1.573 \times 10^{-24})/(2.44 \times 10^{-25}) = 6.4$. Based on 4 degrees of freedom for the numerator and 68 degrees of freedom for the denominator, this ratio was found to be significant at the 0.01 level.

SHEAR MODULUS

Because of the similarity in calculation methods, the first- and second-order regressions in which the original data were used are omitted.

When the shear modulus symmetry condition was assumed, the shear modulus determinations were replicated at the angle $\theta_r = (\pi/2) - \theta$. Thus, all measurements made at angles other than 45° were used twice in the regression, once at the actual orientation of the measurement and once at the complementary angle for this orientation.

The pairs of measurements available at each orientation were then used to estimate the sample-to-sample variation and the total experimental variance. As was mentioned before, the variance calculated from these pairs of values was assumed to involve both testing errors and sample-to-sample variations and is, therefore, the total experimental error.

The first- and second-order regression equations calculated for the Sample 30 shear modulus data were

$$Y = (6.494 \times 10^{-11}) + (2.5 \times 10^{-17})X$$

and

$$Y = (6.507 \times 10^{-11}) - (1.259 \times 10^{-12})X + (1.259 \times 10^{-12})X^2 \quad ,$$

where $\underline{Y} = 1/\underline{G}_{\theta}$. The residual variances about the first- and second-order regressions were 2.722×10^{-24} and 2.953×10^{-24}, respectively.

The testing variance, based on 24 degrees of freedom, was calculated to be 2.343×10^{-24}. The total experimental variance, based on 7 degrees of freedom, was calculated to be 3.864×10^{-24}.

For both the first- and second-order regressions the ratio of the residual variance to the total experimental variance was less than one. Therefore, there is no significant lack of fit for either regression equation. That is, both the first- and the second-order regressions adequately fit the experimental data.

APPENDIX V

ERROR ANALYSIS FOR DEVIATIONS OF POISSON'S RATIO SAMPLE FROM A FLAT SURFACE

In the following calculations it is assumed that the actual specimen width in the loaded state corresponds to the initial specimen width less Poisson's contractions. The observed width in the loaded state corresponds to the initial specimen width less the Poisson's contractions and less the apparent contraction due to deviations of the initial specimen surface from flatness.

TENSILE SPECIMEN CURL

The three strip geometries of interest are pictured in Fig. 34. The lines shown represent the tensile specimen cross section with respect to the camera field of view.

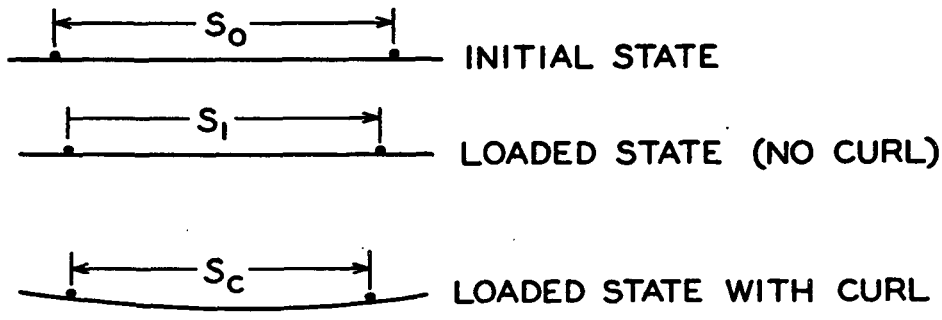

Figure 34. Tensile Strip Curl

For simplicity it is assumed that the curvature of the specimen is circular. The following relations may be presented:

$$s_1 = s_o (1 - \nu\epsilon) \quad , \tag{68}$$

where s_o is the initial bead spacing, s_1 is the bead spacing in the loaded state with no specimen curl;

$$s_c = 2R \sin (\theta/2) \quad , \tag{69}$$

where s_c is the bead spacing in the loaded state with specimen curl having a radius of curvature R. The angle θ is the angle subtended by the specimen and may be expressed $\theta = s_1/R$.

Based on these relationships, the apparent Poisson's ratio, ν_a, may be expressed

$$\nu_a = \left[(s_o - s_c)/s_o\right] /\epsilon \quad . \tag{70}$$

For an order of magnitude calculation let $\nu = 0.300$, $\epsilon = 0.002$, and assume R = 10 inches ($\theta/2 = 5.7°$). The apparent Poisson's ratio under these conditions was calculated to be $\nu_a = 0.950$.

The radius of curvature chosen for this calculation was realistic based on the observations made during the course of the thesis.

STRESS-INDUCED WAVINESS

The strip geometries of interest are pictured in Fig. 35. As before, the lines shown represent the tensile specimen cross section with respect to the camera field of view.

In this calculation it is assumed that each lobe of a surface wave is the arc of a circle of radius R. The chord length, T, of this arc is assumed to be 0.750 inch based on experimental observations. The angular deviations from the initial surface, $\theta/2$, is assumed to be 4°.

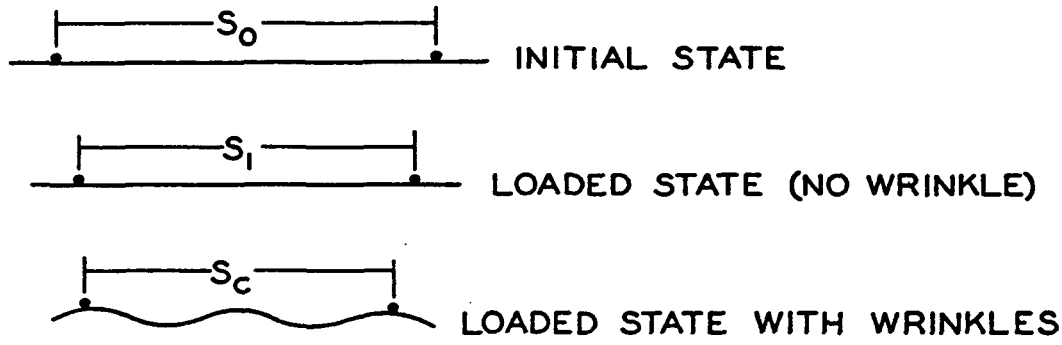

Figure 35. Tensile Strip Wrinkling

The radius of curvature of the lobe may be calculated from Equation (69). In turn, the arc length, $\underline{a}$, of the lobe is related as follows:

$$a = \theta/R \quad .$$

The actual measured length of the loaded specimen is given by

$$s_c = T(s_1/a) \quad , \tag{71}$$

where $\underline{s_1}$ is given by Equation (68). The apparent Poisson's ratio can then be calculated from Equation (70).

For an actual Poisson's ratio of $\nu = 0.300$, and specimen strain $\varepsilon = 0.002$, the apparent Poisson's ratio $\nu_a = 0.500$.

APPENDIX VI

MINIMUM-MAXIMUM CALCULATION FOR ORTHOTROPIC MODEL

YOUNG'S MODULUS

Starting with Equation (7),

$$1/E_\theta = \cos^4\theta/E_x + \sin^4\theta/E_y + 2\sin^2\theta\cos^2\theta/F \quad ,$$

where

$$1/F = 1/G_{xy} - 2\nu_{xy}/E_x \quad ,$$

$$d(1/E_\theta)/d\theta = 4\sin\theta\cos\theta(-1/E_x) + \sin^2\theta/E_x + \sin^2\theta/E_y + (1/F) - 2(\sin^2\theta/F) \; .$$

When this derivative is equal to zero, the roots of the resulting equation are found to be

$$\theta = 0° \quad ,$$

$$\theta = 90° \quad ,$$

and
$$\theta = \sin^{-1}[(1/E_x - 1/F)/(1/E_x + 1/E_y - 2/F)]^{1/2} \; . \qquad (72)$$

If the expression in brackets is less than zero, there are only two minimum-maximum directions for Equation (7). This quantity will be zero if the following inequality holds

$$(1 + \nu_{yx})/E_y > (1/2G_{xy}) > (1 + \nu_{xy})/E_x \; .$$

SHEAR MODULUS

Starting with Equation (8), and following the same procedure as was outlined in the previous section:

$$d(1/G_{xy})/d\theta = (8\sin\theta\cos\theta)(1 - 2\sin^2\theta)[(1 + 2\nu_{xy})/E_x + (1/E_y) - (1/G_{xy})] \; .$$

Equating this derivative to zero, the following minimum-maximum orientations are found:

$$\theta = 0°, 90°, 45° \quad .$$

If the quantity

$$(1 + 2\,\nu_{xy})/E_x + (1/E_y) - (1/G_{xy})$$

equals zero, the minimum-maximum calculation is also satisfied.